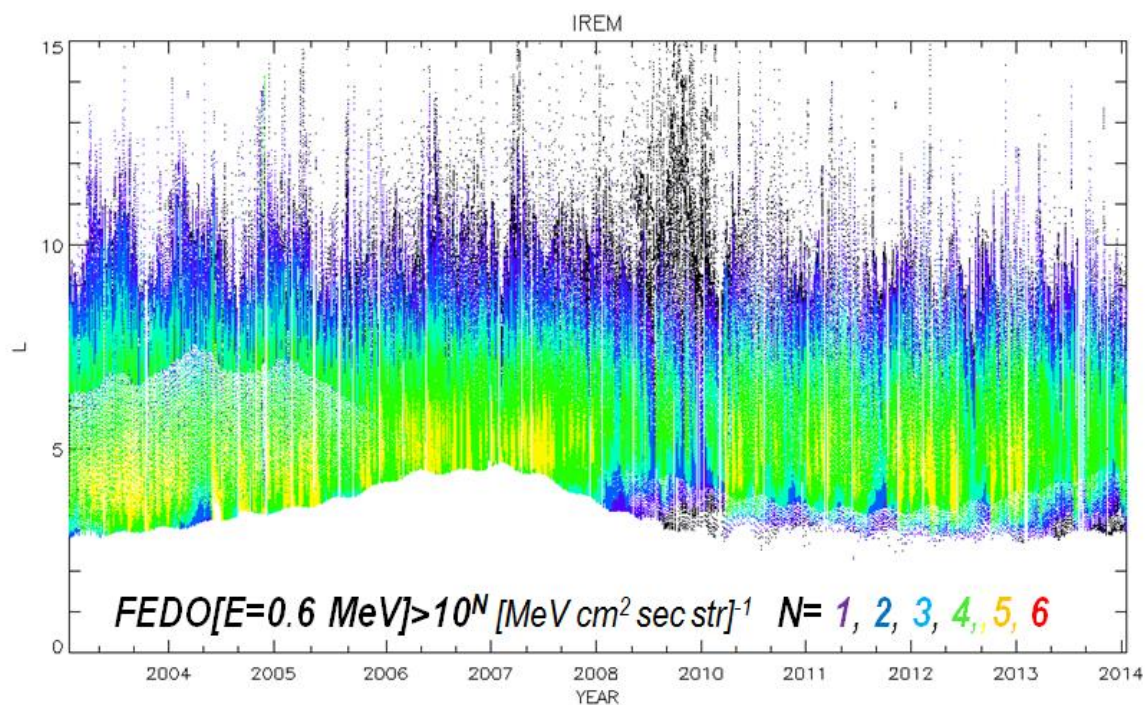


(S)REM-DC

SREM and REM Data Consolidation

FINAL REPORT

July 2017



Institute of Accelerating Systems and Applications

University of Athens, Department of Physics, Panepistimioupoli Zografou, 15784 Athens, Greece

Tel: +30-2108109114 • Fax: +30-2106138343 • <http://www.iasa.gr>

DOCUMENT INFO

	Name	Date
Prepared by	Ingmar Sandberg Paul Bühler	20.07.2017
Approved by	I.A. Daglis (Project Manager)	26.06.2017
Reference	SREMDC_Final_Report	

DISTRIBUTION

Name	Organisation
Hugh Evans	ESTEC/ESA

CHANGE LOG

Date	Issue	Rev.	Reason for change
29.11.2016	0.	0.	Submission of Draft
26.06.2017	1.	0.	Minor Updates in response of Hugh Evans comments

Contents

Description of Final Report Contents	4
CONSOLIDATION OF SREM DATA.....	5
PROCESSING CHAIN.....	5
Design and development of a processing chain to handle various different raw data providers.....	6
Integration of SVD unfolding process.....	7
Description of SREM CDF files	8
Description of unfolding process	9
References	12
APPENDIX A: Signal Extraction Algorithm.....	13
Signal extraction from SREM data	14
Appendix B: Characterization of SREM data.....	18
Characterisation of SREM measurements	19
Classification scheme A: Signal extraction from S15, S25, C1, C2 and TC3	19
Classification scheme B: Relative response of S12 and S13 SREM channels	20
Summary Results.....	23
Appendix C.....	28
Technical Note 1: Cross-Calibration of SREM data.....	28
Cross-calibration of ESA SREM SVD fluxes	29
Cross-calibration of ESA SREM proton fluxes.....	29
Cross-calibration of SREM SVD electron fluxes	47
Appendix D.....	77
Technical Note 2: Lessons learned in the processing and calibration of the SREM	77
Strengths/weakness of the SREM design with respect to the final production of particle flux data for various species	78
Recommendations for future radiation monitoring activities in the magnetosphere and heliosphere	79

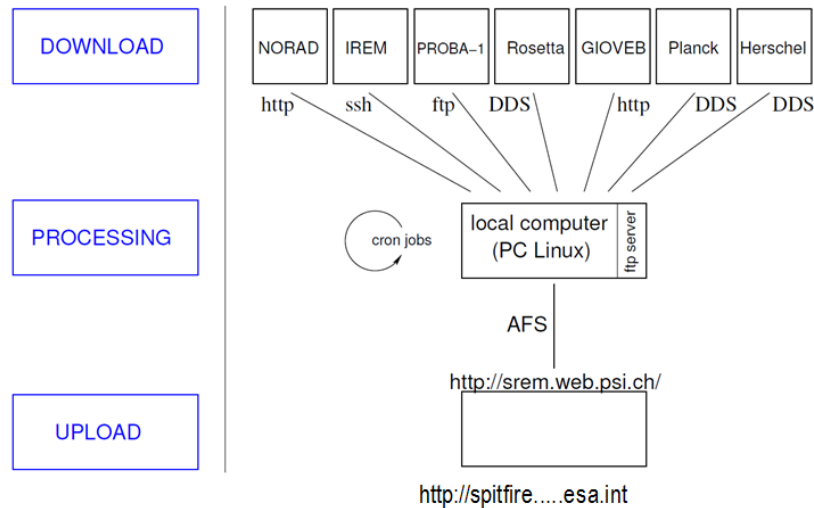
Description of Final Report Contents

This document reports the work carried out during the (S)REM-DC project and includes the Technical Notes/Deliverables of the project. The Final Report includes:

- Documentation for the consolidated processing chain (WP1000 output)
 - o APPENDIX A: Signal Extraction method
 - o APPENDIX B: Characterization of SREM data
- APPENDIX C: Cross-calibration analysis (Technical Note 1)
- APPENDIX D: Lessons learned in the processing and calibration of SREM (Technical Note 2)

**CONSOLIDATION OF SREM DATA
PROCESSING CHAIN**

Design and development of a processing chain to handle various different raw data providers



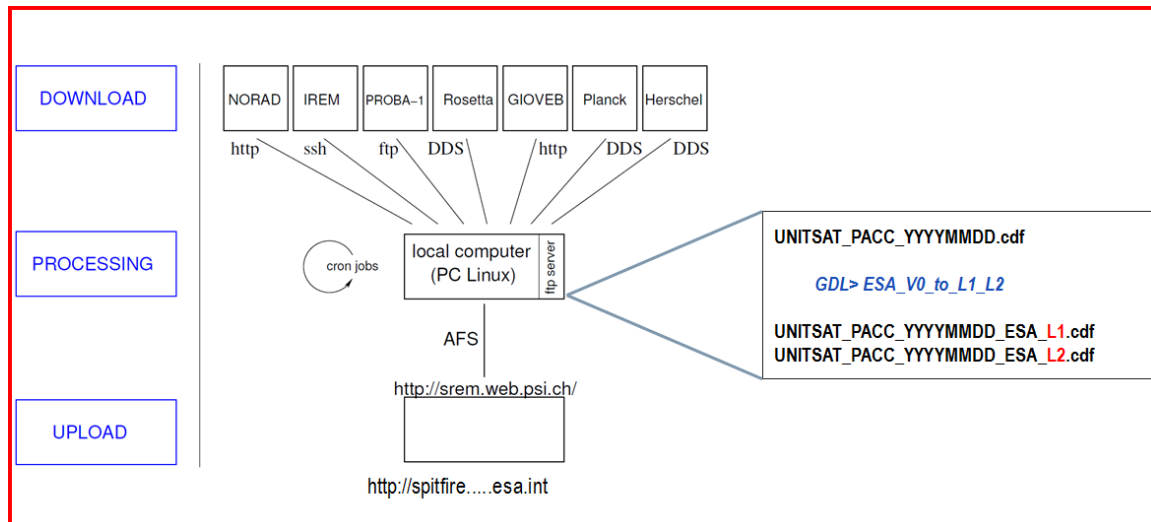
Flowchart 1: Schematic drawing of a data processing chain

The data processing chain for the SREM data consists of three main blocks, which are illustrated in Flowchart 1. When the telemetry of an SREM unit is received on ground it is usually kept on site or transferred to a data center, where it is made accessible to the data owner(s). The first step in data processing is to download this raw data to a local computer, where it can be further processed. The sites have their specific methods to provide the data and correspondingly the methods to retrieve the data have to be tailored. The purpose of the first block in Figure 1, denoted with *DOWNLOAD* is hence to copy the raw data from the data providers site to a local data processing computer. Once the raw data is locally available, it is processed – second block in Figure 1, denoted with *PROCESSING*. There is no common format for the raw SREM data. The formats are mission specific and generally optimized to minimize the data volume. The raw data are therefore first run through a decoding procedure, which extracts the SREM information and converts it to a standard format - in this case the Common Data Format CDF (<http://cdf.gsfc.nasa.gov/>) is used. The data is sorted according to time and written to one file per calendar day. Data quality checks are carried out as well and alerts are riced when the data is found to be inconsistent with the data format prescription. At this point of the data processing the data of all SREM units are saved in a common data format, which allows to use a largely unified framework for the further processing steps. These include the conversion of the SREM counts to count rates, conversion of the count rates to particle fluxes, and computation of auxiliary data, like orbit and Earth magnetic field parameters. The final product of this processing block is a file with processed data per calendar day and SREM unit. The last block in this scheme is denoted as *UPLOAD* and includes the dissemination of the processed data files. In case of SREM the data is uploaded for public access to a website and is ingested into the ODI database at ESTEC. A more detailed technical description of the system has been given in the technical report to WP 10 in [1] of which an updated version is attached to this report.

The main parts of the processing chain are written in PV-WAVE (<http://www.roguewave.com/products-services/pv-wave>). PV-WAVE is a commercial software and a rather costly license is needed to use it. This makes it difficult to distribute the software and run it on other sites. In order to improve this situation the processing chain has been translated within this project to the open source version of PV-WAVE/IDL, the GNU Data Language GDL (<http://gnudatalanguage.sourceforge.net/>). However for new developments similar in kind, I would propose to use a freely available programming language to avoid such problems. Python (<https://www.python.org/>) might be a good option. It does not only provide the core functionalities of any programming language, but comes with a large number of additional packages for scientific and numerical computing, production of graphics, and also interfaces to many data formats, including e.g. CDF. Nowadays it is widely used in science communities.

Integration of SVD unfolding process

Within work package WP1000 we performed an update of the SREM/SVD unfolding IDL processing algorithm and integrated the unfolding process in the chain of SREM data processing.



Flowchart 2: Integration of unfolding process in SREM data processing chain

The wrapper procedure of the processing chain from the count-rate cdf files (denoted here as V0 files), leads to the production of cdf files that contain the SREM SVD unfolded proton/electron fluxes (LEVEL 1 files) and to the production of cdf files that contain the cross-calibrated SREM proton/electron flux products (LEVEL 2 files).

The wrapper procedure is compiled and executed in IDL (GDL) environment:

```
IDL> ESA_V0_to_L1_L2
```

and requires as input the directory path and the filename of the count-rate SREM CDF file:

```
UNITSAT_PACC_YYYYMMDD.cdf
```

Where UNITSAT stands for:

- SREMPROBA1 for PROBA1/SREM
- IREM for INTEGRAL/IREM
- SREMRosetta for Rosetta/SREM
- SREMHerschel for Herschel/SREM
- SREMPPlanck for Planck/SREM
- SREMGIOVEB for GIOVEB/SREM

and YYYYMMDD stands for the day of the year (e.g. 20080226). Validation of the functionality of the IDL wrapper procedure was performed by executing several tests for all missions of interest (INTEGRAL, Planck, Herschel, PROBA1 and Rosetta).

The procedure file [ESA_V0_to_L1_L2.pro](#) which includes all the necessary functions - was initially written for IDL environment. However, additional modifications were applied to ensure compatibility with GDL. The file was uploaded, compiled and tested on a virtual machine that was set up on external server at www.buehler-paschen.at.

Description of SREM CDF files

In what follows, we present brief information regarding the content of the products of the updated SREM data processing chain as resulted from ESA SREM-DC project. This information is also included in the updated SREM websites hosted in PSI servers.

SREM CDF Files	
Description	Contents extracted using Autoplot
V0 files: Contain ephemeris and SREM count-rate data.	Select CDF Variable (of 5) <ul style="list-style-type: none"> ● COUNTRATE ● ORBIT ● MAGFIELD ● LSHELL ● EPOCH
Level 1 files: Contain ephemeris data and secondary products of SREM count-rate data: proton differential fluxes FPDO at proton energies FPDO_Energy, electron differential fluxes FEDO at electron energies FEDO_Energy, quality variables FPDO_Quality and FEDO_Quality. The differential fluxes have been derived using a dedicated unfolding technique over pre-defined energies. The unfolding technique is based on the regularized Singular Value Decomposition (SVD) method. More details can be found in [3]	Select CDF Variable (of 10) <ul style="list-style-type: none"> ● Position ● B_Calc ● L ● FPDO_Quality ● FPDO ● FEDO_Quality ● FEDO ● EPOCH ● FPDO_Energy ● FEDO_Energy
Level 2 files: Contain the same variables as in Level 1 files. The values in the FPDO_Energy and FEDO variables have been rescaled according to cross-calibration studies between Level 1 data and selected reference datasets. SEPEM Reference Dataset v2.0 (i.e. GOES/EPS fluxes cross-calibrated with IMP-8/GME) has been selected as reference dataset for proton fluxes, while RBSP/MAGEIS spin averaged datasets has been selected as reference dataset for electron fluxes.	Select CDF Variable (of 10) <ul style="list-style-type: none"> ● Position ● B_Calc ● L ● FPDO_Quality ● FPDO ● FEDO_Quality ● FEDO ● EPOCH ● FPDO_Energy ● FEDO_Energy

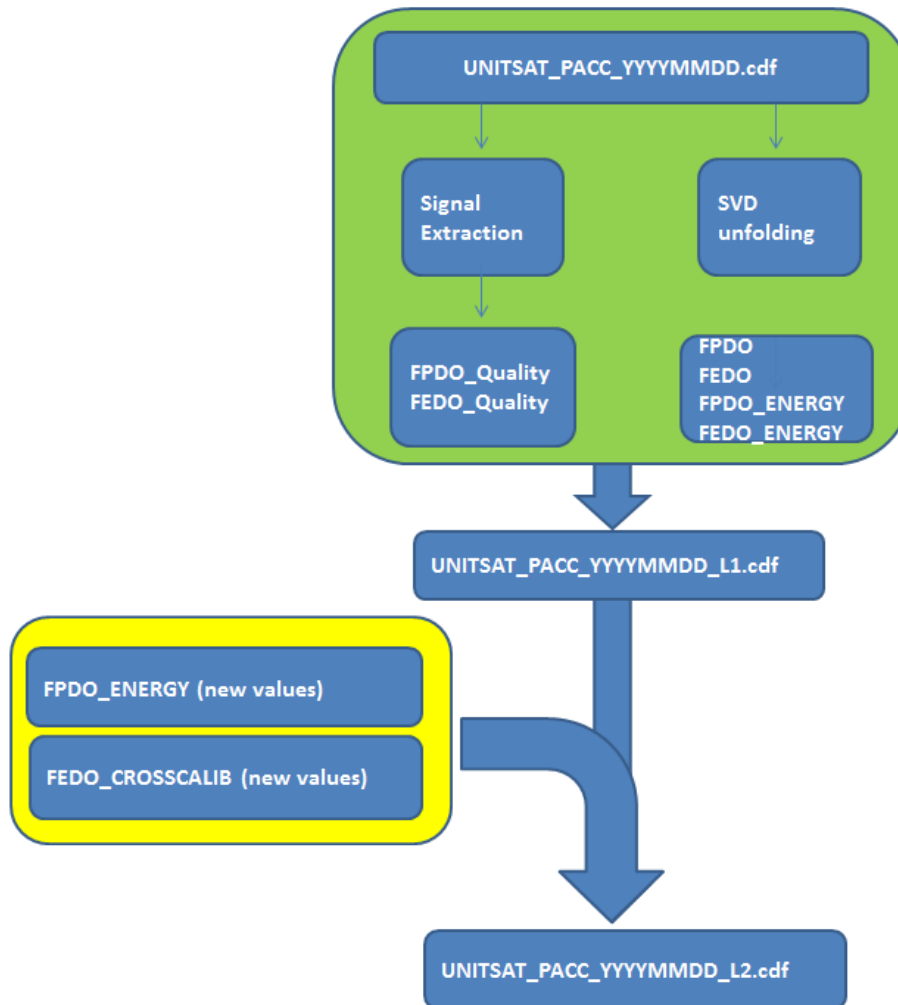
The values in the flux quality variables FQDO_Quality provide recommendations on the use of the values stored in the FQDO variables according to the table below (Q=P,E).

FQDO_Quality variables

Case	Comment	Recommendation
FQDO_Quality=0	SREM count-rate data determined by charged particle fluxes Q.	Use FQDO
FQDO_Quality=1	SREM count-rate data most likely determined by charged particle fluxes Q.	Use FQDO with some caution
FQDO_Quality=2	SREM count-rate contaminated by various sources. None criterion is satisfied	Do not use FQDO
FQDO_Quality=3	SREM count-rate dominated by fluxes of non-Q particles.	Do not use FQDO
FQDO_Quality=5	SREM count-rate data dominated by background (cosmic, detector electronics)	Do not use FQDO

Description of unfolding process

The wrapper procedure `ESA_V0_to_L1_L2` calls the main procedure `SREM_SVD_FLUXES.PRO` which calculates the differential fluxes FQDO (proton and/or the electron: Q=P,E) and the corresponding `FQDO_Quality` indices. The unfolding method has been described in detail in [2] and comprehensively in [3]. Modifications were introduced to calculate proton and electron fluxes automatically using the count-rate SREM CDF files (i.e. V0) that come from different SREM missions and contain variables with different names. In addition, a novel method was developed and integrated for the characterisation of SREM measurements as background, proton-dominated, electron-dominated and the subsequent definition of `FQDO_QUALITY` variables.



Flowchart 3: `ESA_V0_to_L1_L2` wrapper procedure

The procedure leads to the production of Level 1 and Level 2 cdf files. Level 1 files include products derived by the unfolding of SREM count-rate data, while Level 2 files include updated products resulted from the proton and electron cross-calibration studies.

The main procedure `SREM_SVD_FLUXES` is used for the:

- **Calculation of SREM SVD fluxes:** the code extracts the count-rates from the `UNITSAT_PACC_YYYYMMDD.cdf` file and calculates the proton FPDO and the electron FEDO fluxes.

NOTE: Proton fluxes are calculated for each case. Electron fluxes are calculated ONLY for the cases where the CDF file includes the 'L' or the 'LSHELL' variable.

- **Calculation of quality values:** The calculation of the proton and electron quality flags, `FEDO_Quality`, `FPDO_Quality`, was developed in the framework of SREM-DC project and adopts an entirely new approach based on the development and combination of two independent classification schemes for SREM data.
 - **The signal extraction from measurements of selected SREM counters.** This is achieved by estimating the background level using a time window of 90 days centered around the day of reference. In order to reduce the repetition of the background calculations, we consider that the background is constant at least over a month and perform the calculation of the background only once for each calendar month. The resulted background levels are stored and are used for the signal extraction on each of the daily files of the month. The method we use for the signal extraction is described in detailed in APPENDIX A.
 - **The behaviour of S12 & S13 measurements,** which is consistent with the numerically defined response functions and permit us to refine the characterisation of SREM measurements as proton or electron dominated.

For the derivation of the `FQDO_Quality` variables, we apply the limit of detection (LOD) algorithm in selected channels and we initially characterize SREM measurements based on the existence of "signal" measurements in the `TC3` channel and in of the pure proton channels `S15`, `S25`, `C1`, `C2`. The main uncertainty regards the measurements that accompanied by `TC3` signal and do not have any signature in the pure-proton channels. Such cases may be attributed either to electron or to low energy proton fluxes. We initially assume that for regions where L cannot be defined (outside the magnetosphere) the signal is likely attributed to protons and that for regions where the L can be defined to electrons. Then, we refine the characterization of SREM data by using the properties arising by the comparisons of S13 and S12 measurements. In what follows, we present S12 and S13 data (for the cases of `TC3` signal data) plotted together with simulated count-rates.

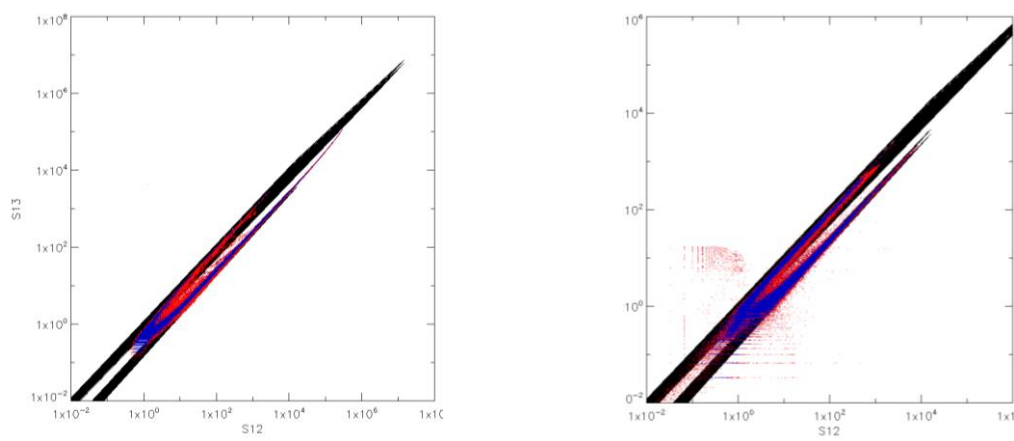
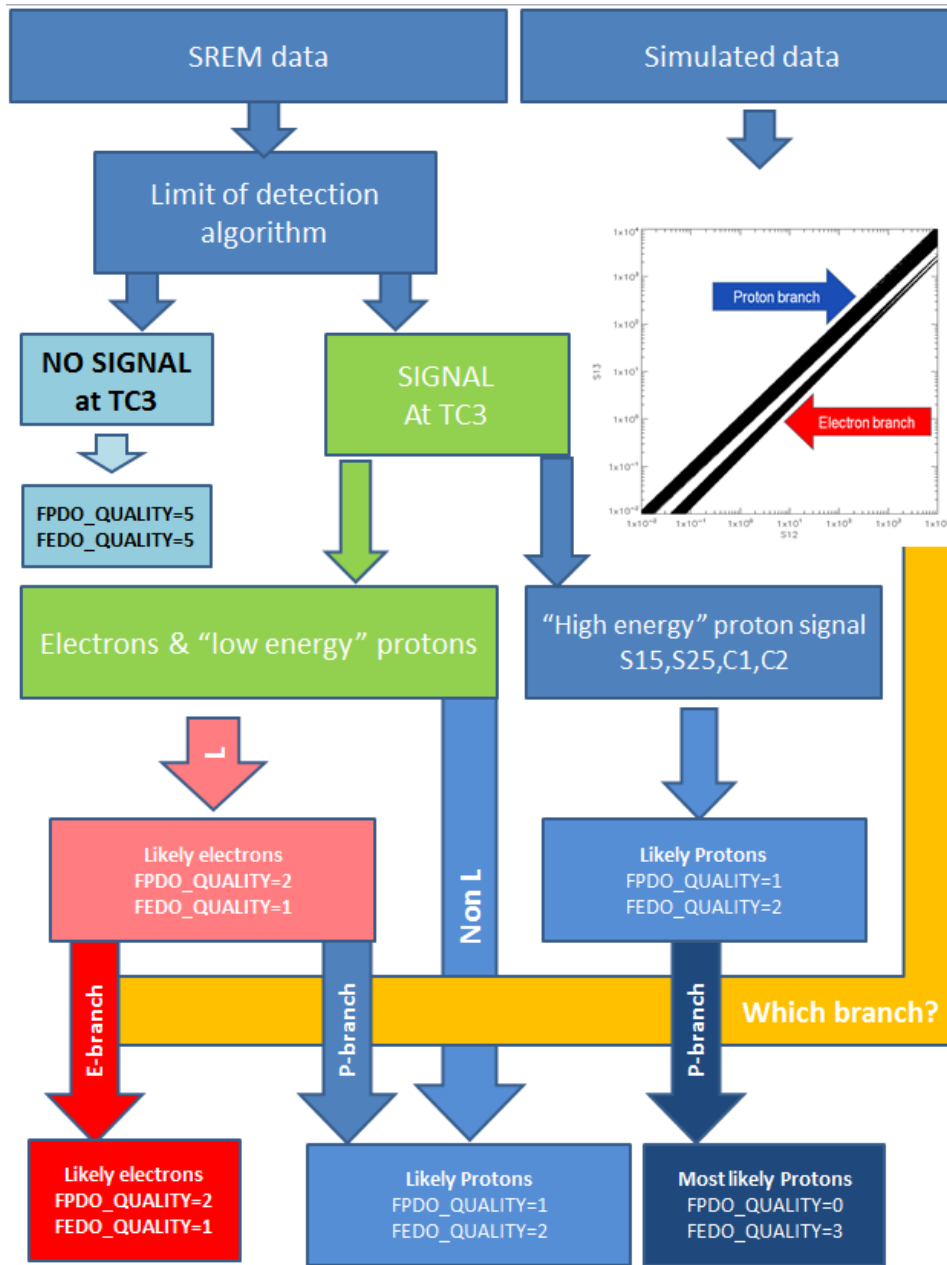


Figure: S13 versus S12 measurements for INTEGRAL (left plot) and PROBA1 (right plot). The red dots represent all the data, while the blue ones the data for the local maxima of `TC3` data. The black stripes represent simulated count-rates when only protons (upper stripe) and only electrons (lower stripe) are considered.

After we tested several different schemes for the derivation of **FQDO_QUALITY** variables, we apply that described in flowchart 4.



Flowchart 4: The applied scheme for the characterization of SREM data

APPENDIX B presents in detail all the parts of the characterization scheme together with summary plots.

References

- [1] P. Bühler, SREM automated data processing, Report within ESTEC contract No. 19336/05/NL/Ja/pg, (2007)
- [2] Final Report of *SREM Solar Particle Event Scientific Analysis Extension (ESA/ESTEC Contract No. 21480/08/NL/NR)* ESA project
- [3] I. Sandberg et al, IEEE Transactions on Nuclear Science 59 (4), 1105 (2012).
- [4] I. Sandberg et al, Geophysical Research Letters, DOI: 10.1002/2014GL060469, (2014)
- [5] Final Report of SEPCALIB *project (ESA/ESTEC Contract No. 4000108377/13/NL/AK)* ESA project
- [6] P. Bühler et al., Nucl. Instr. and Meth. in Phys. Res. A **386** (1996) 825.
- [7] P. Bühler et al, ESA Symposium on Environment Modeling for Space-based Applications SP-392 (1996) 87).
- [8] M. Siegl et al., IEEE Trans. Nucl. Sci. **57** (2010)

APPENDIX A: Signal Extraction Algorithm

Signal extraction from SREM data

In what follows, we consider as signal the part of the data attributed to proton or to electron fluxes that lead to enhancements above the “background”. As “background” we define the part of measurements attributed to cosmic rays and vary depending on the magnetospheric shielding and the solar cycle phase. We have developed an algorithm that permits us to determine the limit of detection (**LOD**) which enables us to extract the signal from SREM data. The method is based on the properties of the distribution of “clumps”. A *clump* is defined as the group of consecutive data below or above a given threshold.

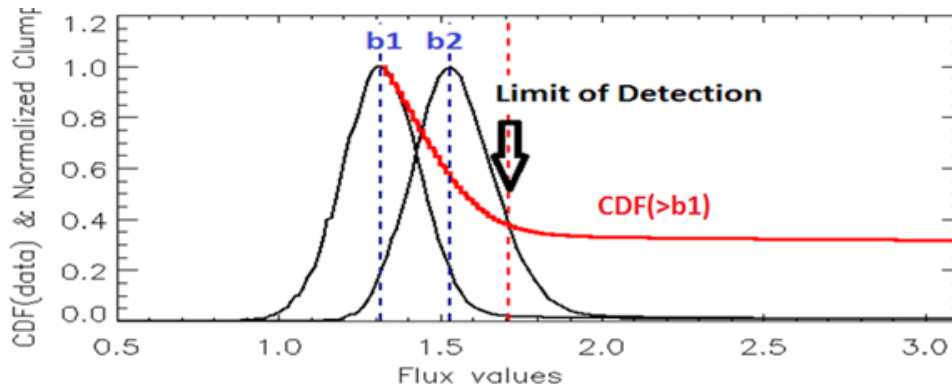


Figure A1: Determination of LOD: Normalized distribution(s) of clumps (below and above the flux values) over-plotted with the CDF (using data above b_1).

In the figure below, we use 10^5 continuous data of an ESA INTEGRAL/SREM channel and calculate the (normalized) number of clumps above/below continuous thresholds (left/right of the black curve). Their local maxima b_1 , b_2 (blue lines) define a well localized area within the “background fluctuations”, while the intersection of the *Cumulative Distribution Function* (calculated using only data $> b_1$) with the right hand side “distribution” defines the **LOD** and permits us to separate the “signal” and the “background” from the measurements. Characteristic examples are presented below.

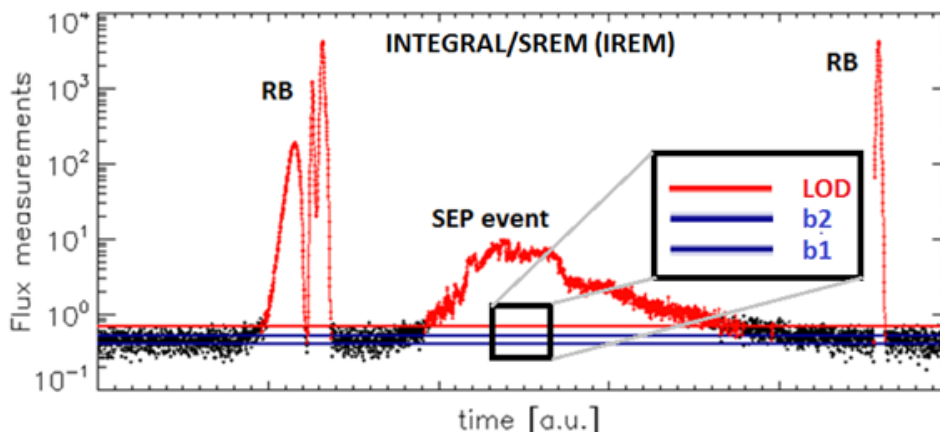


Figure A2: Separation of signal and background INTEGRAL/SREM data using the LOD method.

In Fig. A2 we demonstrate application of the LOD method using ESA SREM measurements from the unit on board INTEGRAL. The particular time-range was selected in order to focus on measurements about RB crossings and SEP occurrence. In Fig. A3 we demonstrate application of the LOD method using ESA SREM measurements from the unit on board PROBA1. The particular time-range was selected in order to focus on measurements about RB crossings and SEP occurrence. Moreover, measurements of a SREM channel with characteristic low signal to noise ratio was selected. It is shown that LOD can operate sufficiently well for such cases as well.

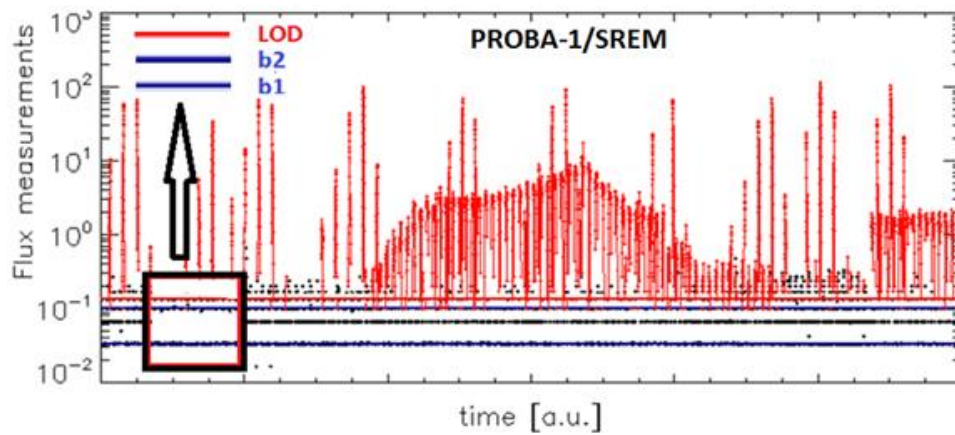


Figure A3: Separation of signal and background PROBA1/SREM data using the LOD method.

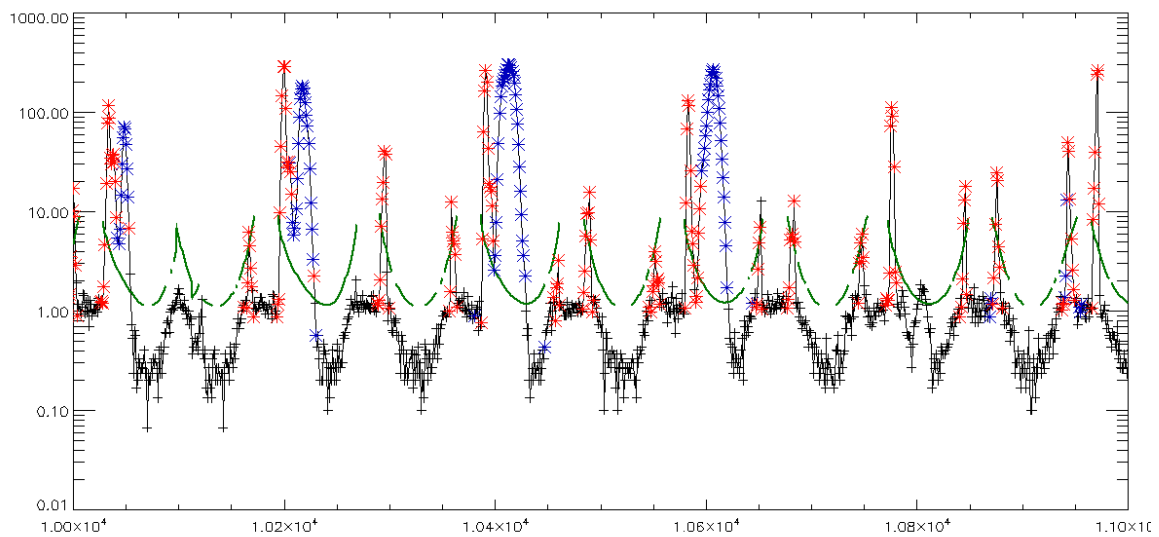


Figure A4: Profile of PROBA1/SREM/TC3 measurements. Blue color represents the part of measurements determined by protons (i.e. signal in SREM proton counters), while red color the part attributed – most likely to – to electrons (i.e. absence of signal in SREM proton counters). The green line corresponds to L values defined by UNILIB library.

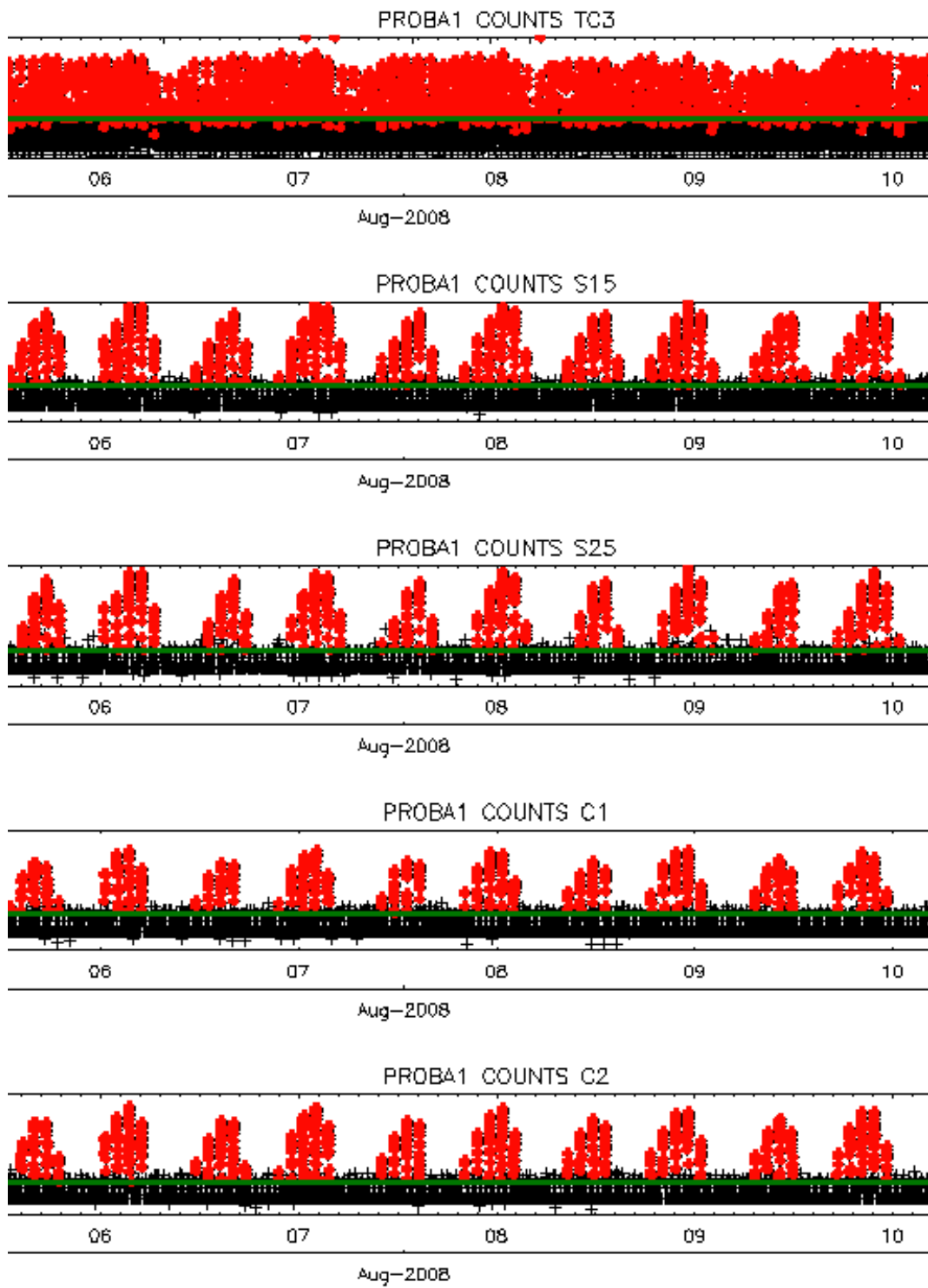


Figure A5: Extract of signal data from selected PROBA1/SREM counters.

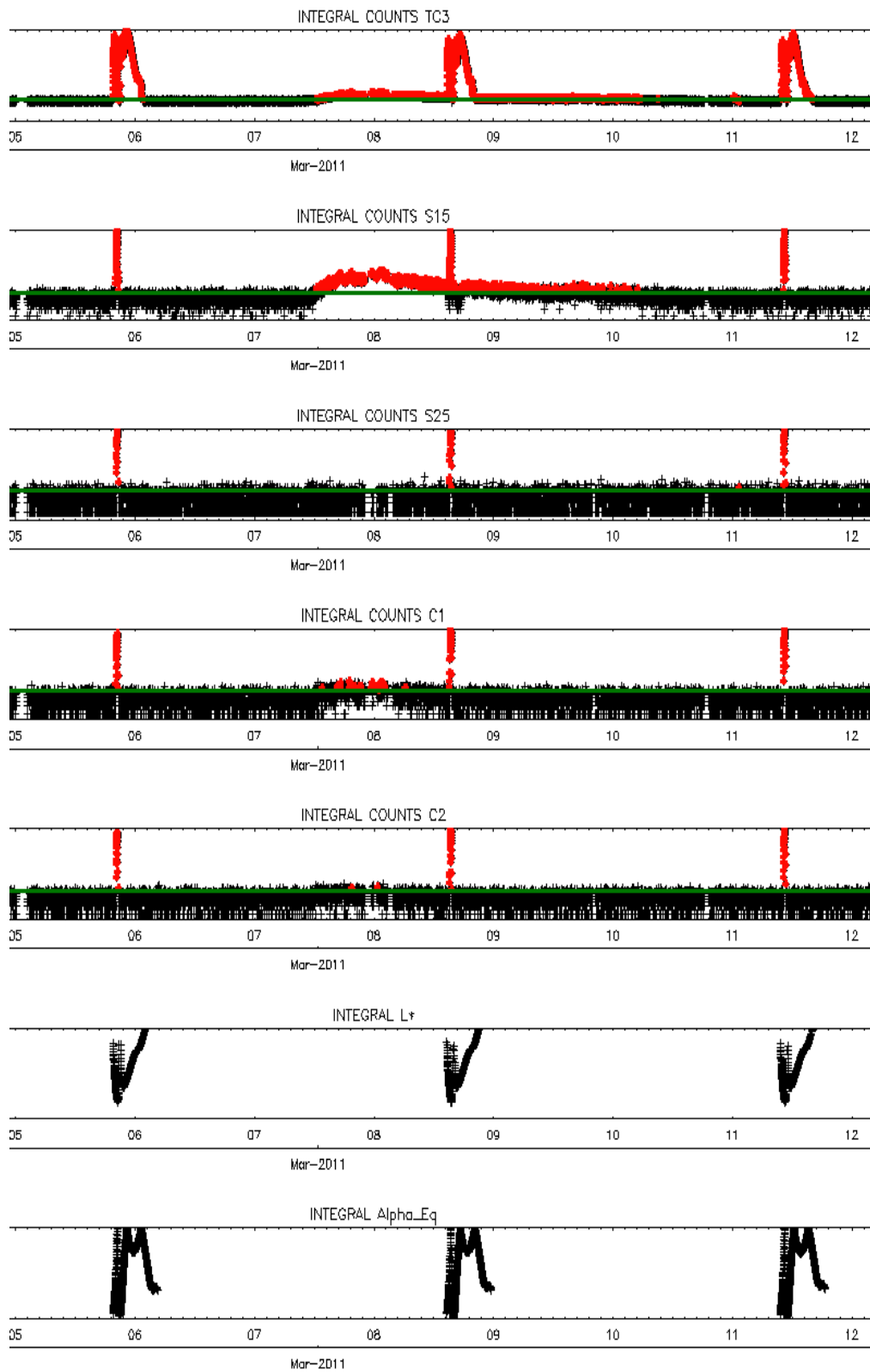


Figure A6: Extract of signal data from selected INTEGRAL/SREM counters

Appendix B: Characterization of SREM data

Characterisation of SREM measurements

We have developed a scheme for the characterisation of SREM data. The scheme is based on the successive application of two classification schemes.

Classification scheme A: Signal extraction from S15, S25, C1, C2 and TC3

We apply a signal extraction method (See APPENDIX A) to identify the time periods where the fluxes monitored by SREM provide:

- measurements above the limit of detection of TC3
- measurements above the limit of detection of one of the considered pure-proton counters S15, S25, C1, C2

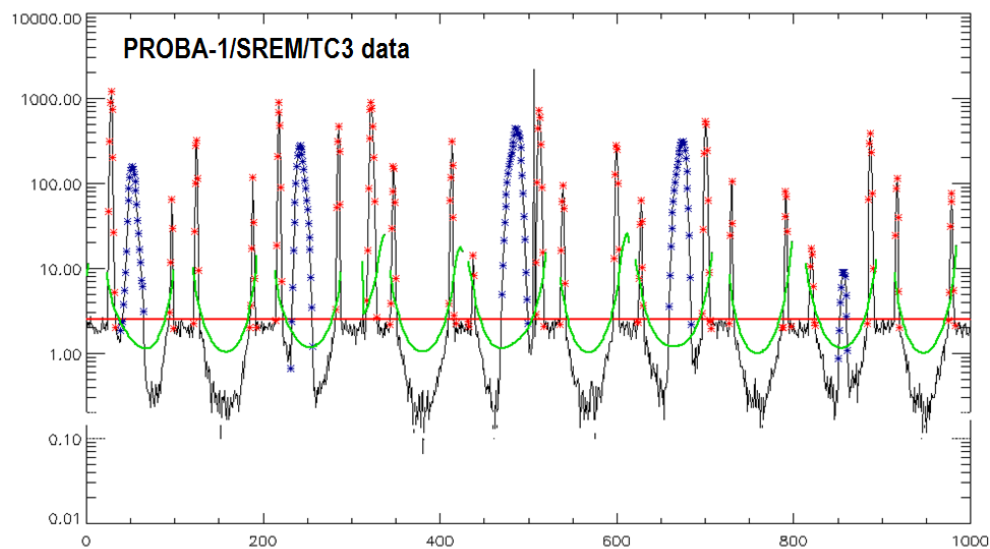


Figure B1: The blue points correspond to PROBA1/SREM data with proton signal, and the red one to the rest part of signal. The green curves correspond to L-values.

The signal extraction permits us to identify the SREM signal (defined here as the part of measurements above the background of the most sensitive SREM channel) and extract from that the part that contains proton signal signatures (defined here as the part of measurements above the background of pure proton counters).

- The proton signal part is likely attributed to protons: **FPDO_QUALITY=1**

The unknown (i.e. the non-proton part) signal may be attributed either to electron fluxes and/or to proton fluxes with energies below the thresholds of the S15, S25, C1, C2 channels. In this stage we consider that:

- The “unknown signal” is likely attributed to protons for regions where L cannot be defined: **FPDO_QUALITY=1**
- The “unknown signal” is likely attributed to electrons for regions where L is defined: **FEDO_QUALITY=1**

OBS: The latter selection is not valid in all cases (e.g. low energy proton fluxes measured in inner radiation belt will be classified as electrons) but it gets further refined by the proceeding classification scheme.

Classification scheme B: Relative response of S12 and S13 SREM channels

We make use of the relative proton & electron responses of S12 and S13 SREM channels in order to further refine the non-proton part of the signal.

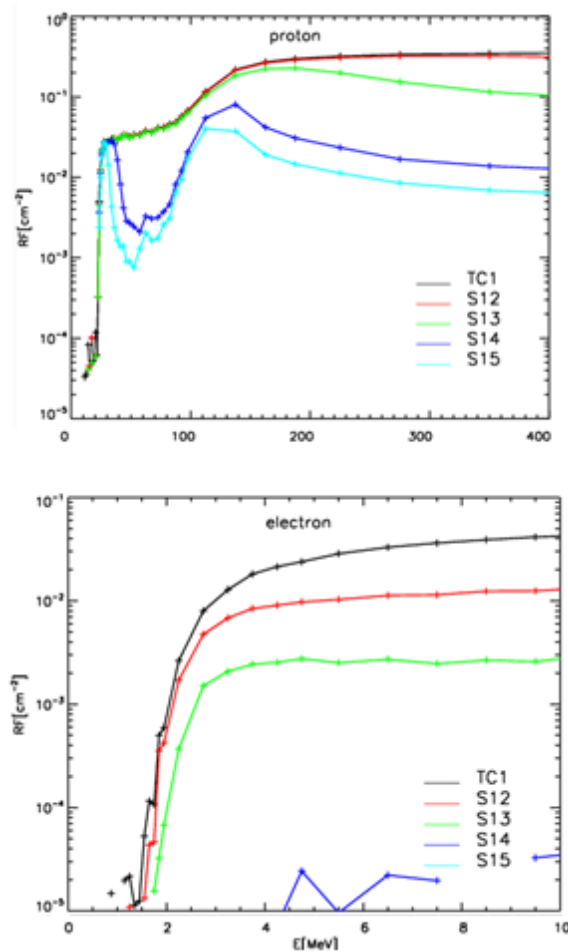


Figure B2: Proton and electron response functions of S12 & S13 channels.

In the following plot, we present cross-plots of the resulted virtual count-rates, derived by folding a large number of analytical proton and electron spectra with the corresponding proton and electron responses. Two well defined branches can be defined. Each is attributed to different particle species.

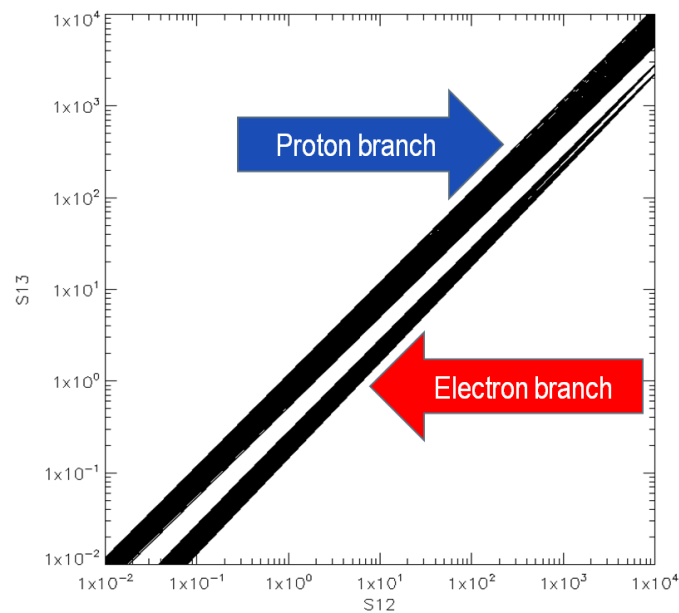


Figure B3: The black stripes represent simulated count rates when only protons (upper stripe) and only electrons (lower stripe) are considered.

In order to confirm the behavior of the actual measurements, we plot INTEGRAL/SREM and PROBA1/SREM measurements over the numerically defined proton and electron branches.

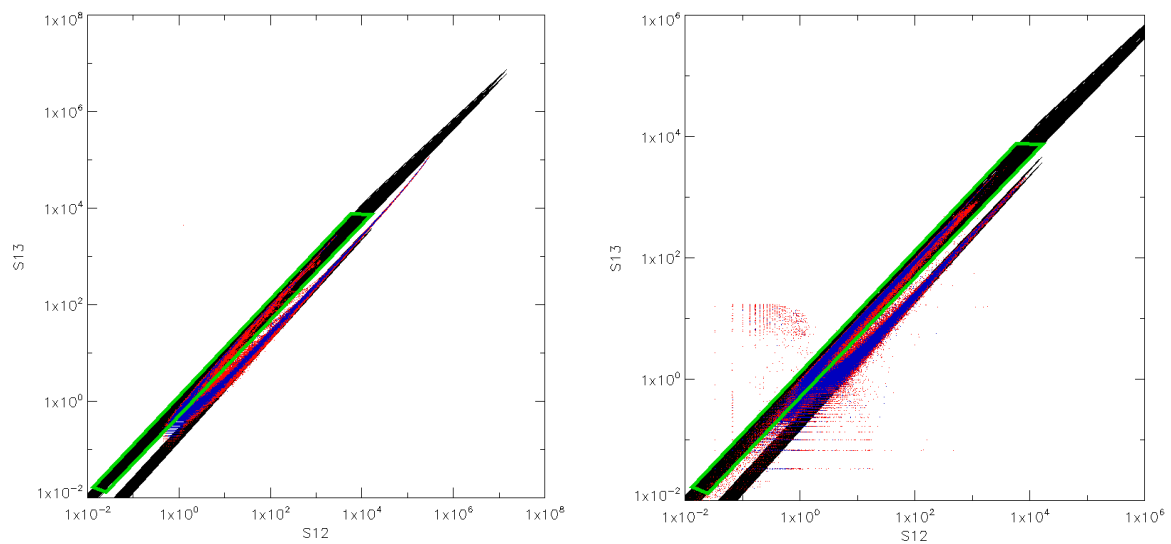


Figure B4: S13 versus S12 measurements for INTEGRAL (left plot) and PROBA1 (right plot). The red dots represent all the data, while the blue ones the data for the local maxima.

In addition, we provide more evidences on the relative behavior of S13 vs S12 measurements, by using different colors for the proton (blue) and the unknown (red) signal.

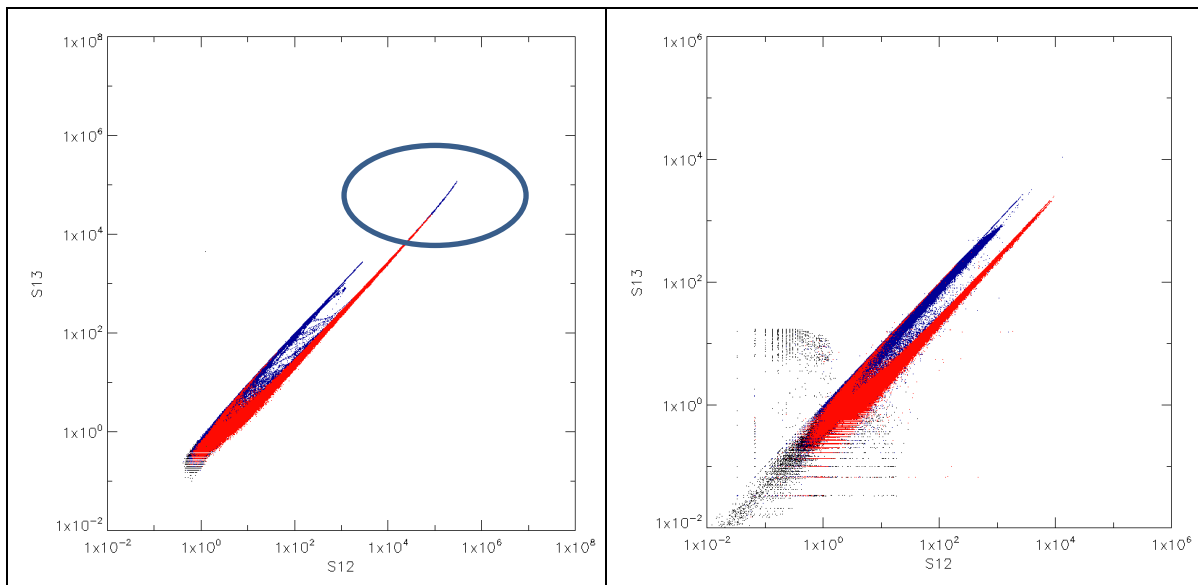


Figure B5: S13 versus S12 measurements for INTEGRAL (left plot) and PROBA1 (right plot): Protons signal (blue), electrons and low energy protons (red).

Based on these findings, we determine two rectangular regions that cover the proton and the electron branches and we proceed to the update of quality variables to characterize SREM data.

- Proton signal in proton branch is most likely attributed to protons: **FPDO_QUALITY=0**
- “Unknown signal” in proton branch in regions where L can be defined is likely attributed to protons: **FPDO_QUALITY=1**
- “Unknown signal” in electron branch in regions where L can be defined is most likely attributed to electrons: **FEDO_QUALITY=0**

This update applies only to the data that fall into the electron and proton branches. The classification of data that do not follow in the categories presented above is defined by the previous scheme.

Summary Results

In what follows, we present summary plots of the whole INTEGRAL and PROBA1 missions using results derived after the application of the classification scheme(s).

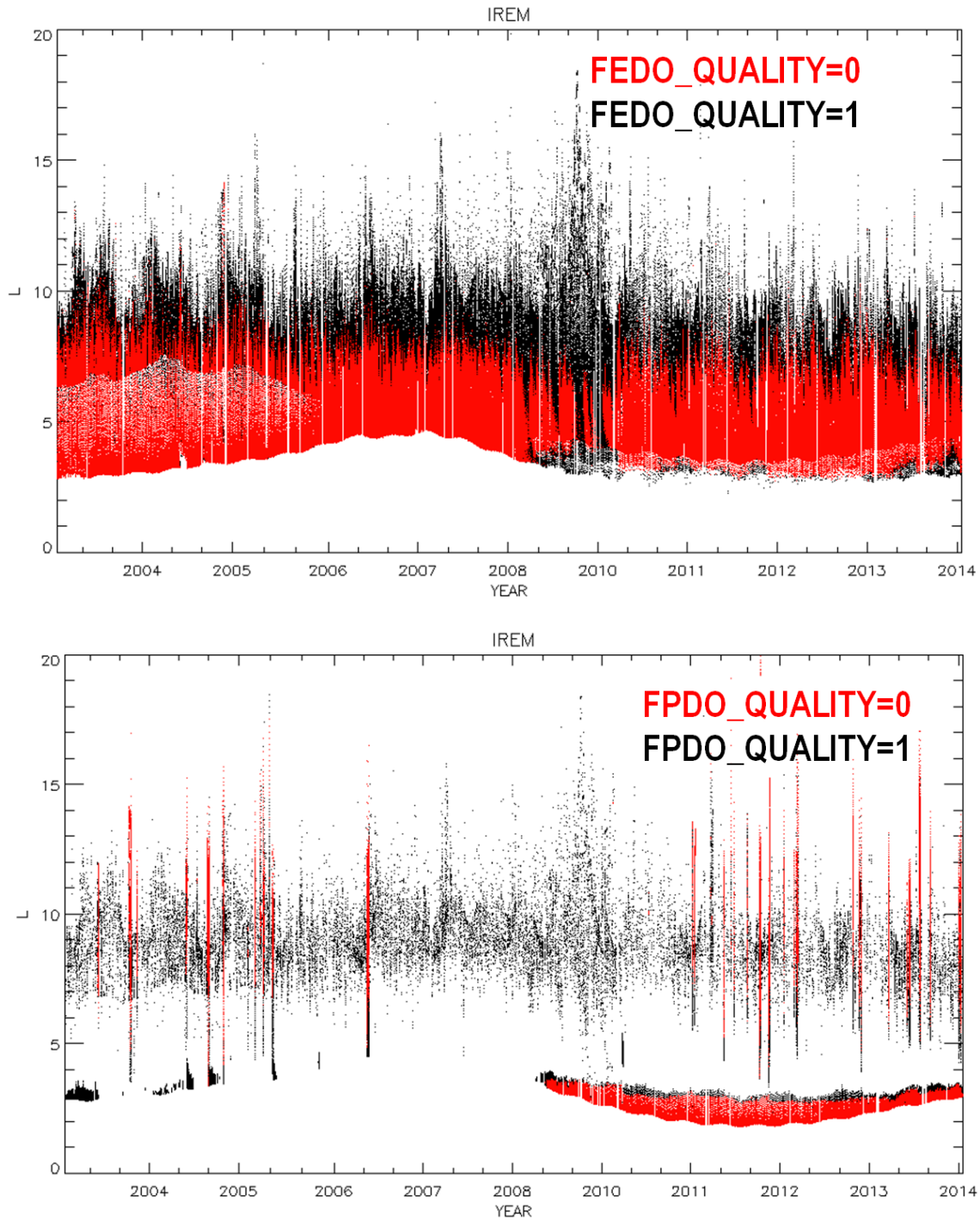


Figure B6: Summary plots of INTEGRAL/SREM measurements characterized by the FQDO_QUALITY variables (=0, most likely) and (= 1, likely).

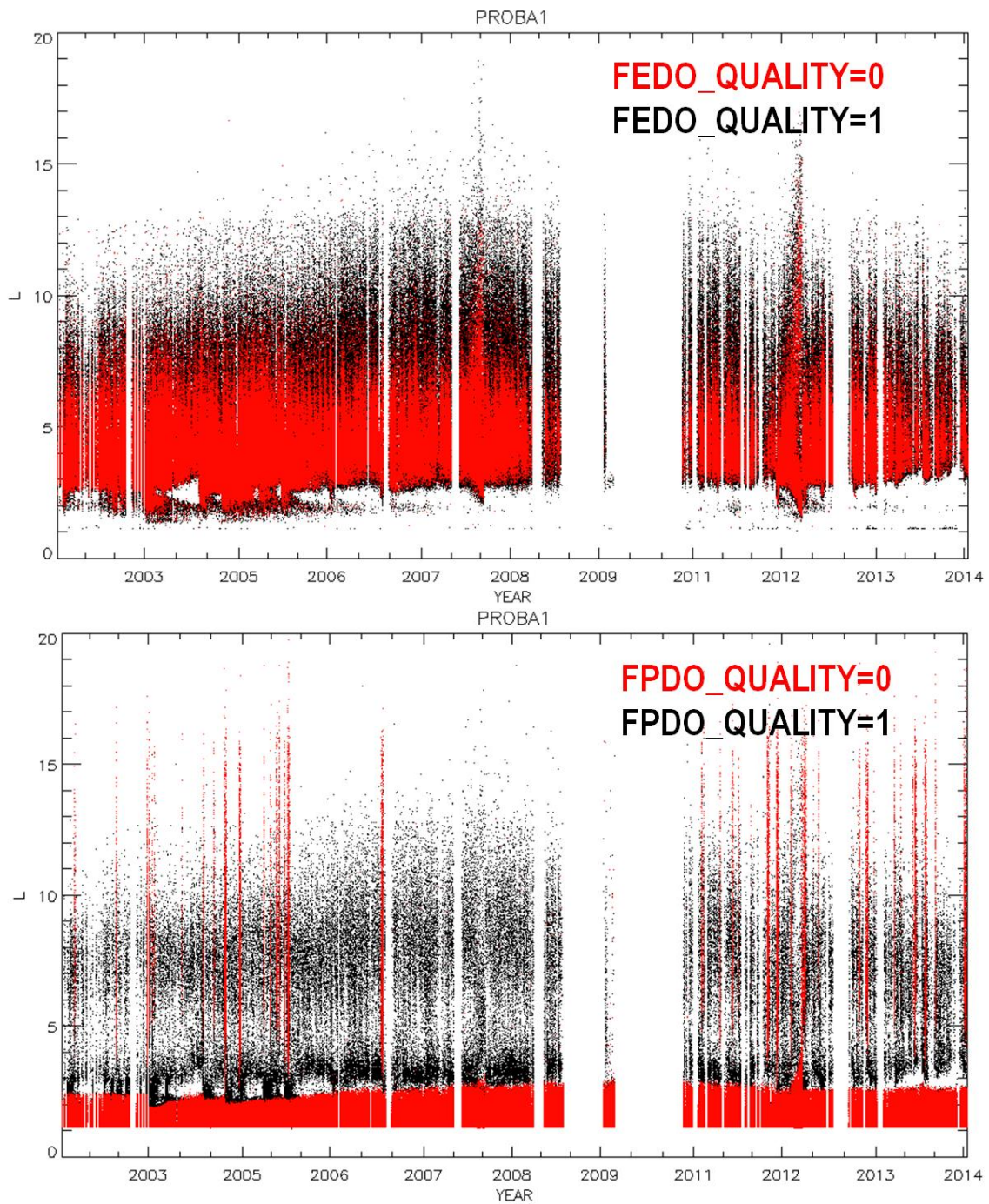


Figure B7: Summary plots of PROBA1/SREM measurements characterized by the FQDO_QUALITY variables (=0, most likely) and (= 1, likely)

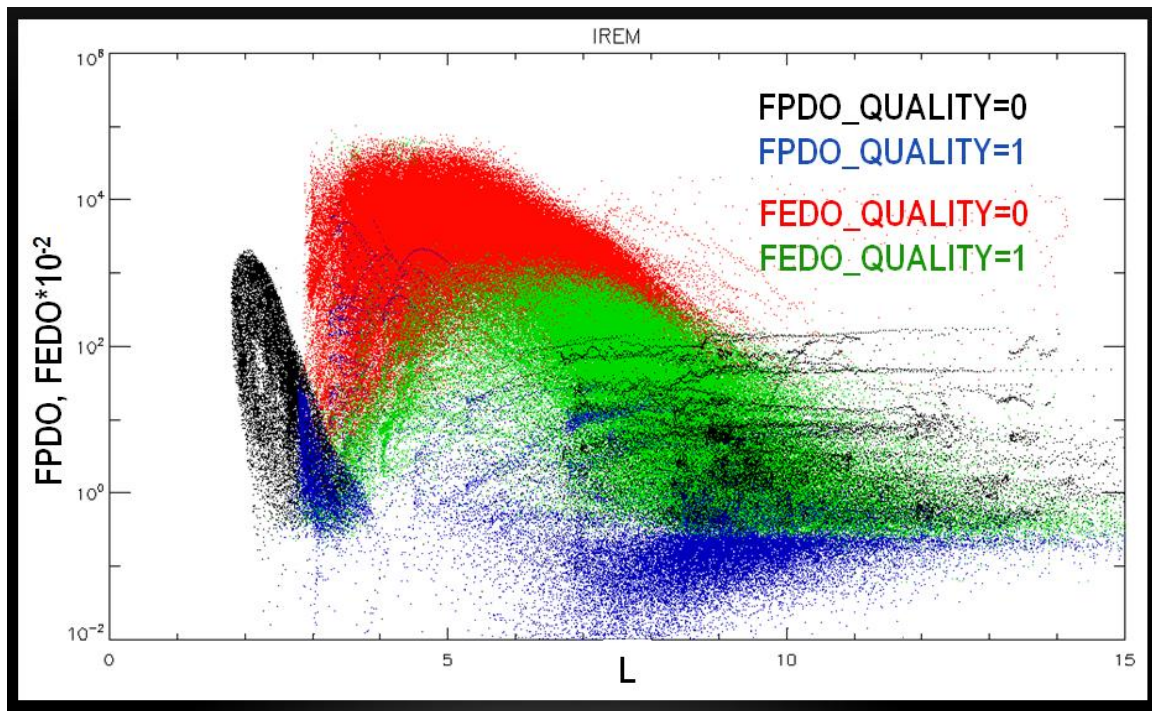


Figure B8: Summary plots of INTEGRAL/SREM fluxes versus L-shell value characterized by the FQDO_QUALITY variables (=0, most likely) and (= 1, likely)

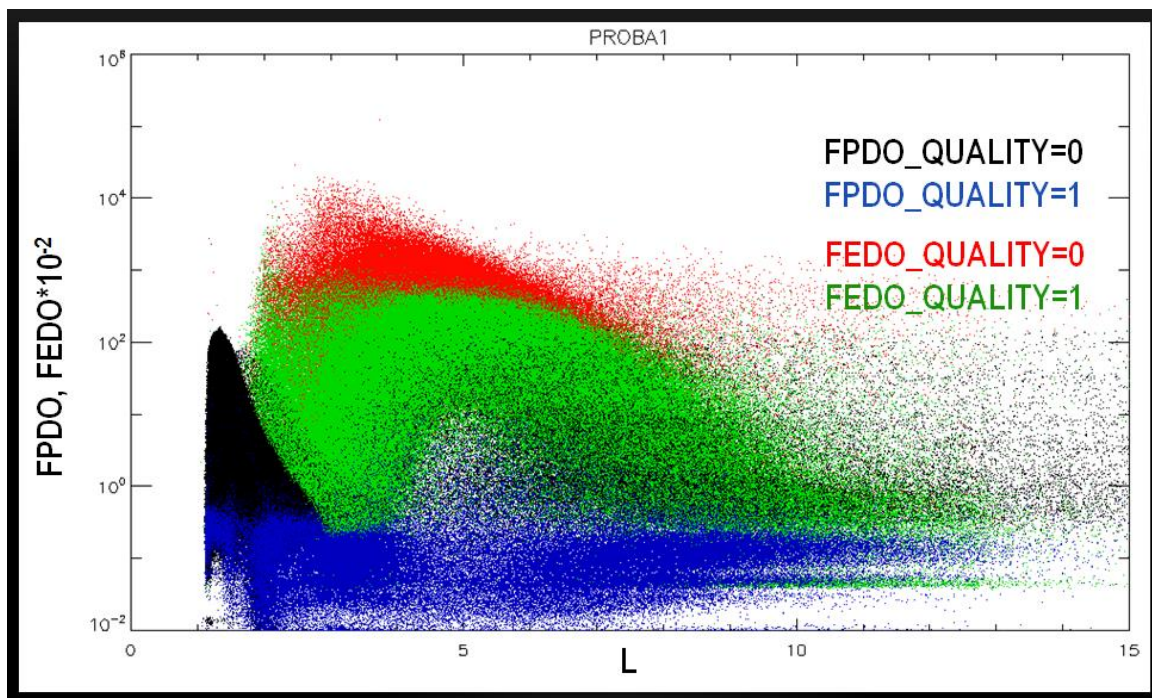


Figure B9: Summary plots of PROBA1/SREM fluxes versus L-shell value FQDO_QUALITY variables (=0, most likely) and (= 1, likely)

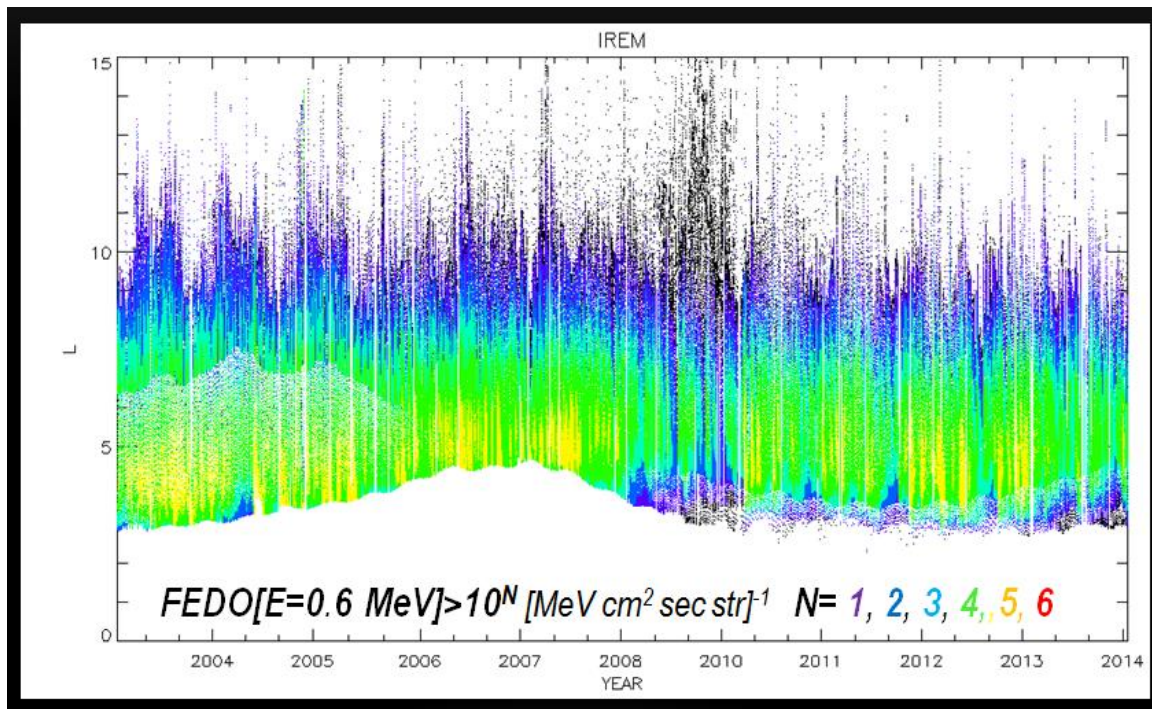


Figure B10: Summary plots of INTEGRAL/SREM SVD electron fluxes characterized by the FEDO_QUALITY variables (=0, most likely) and (= 1, likely).

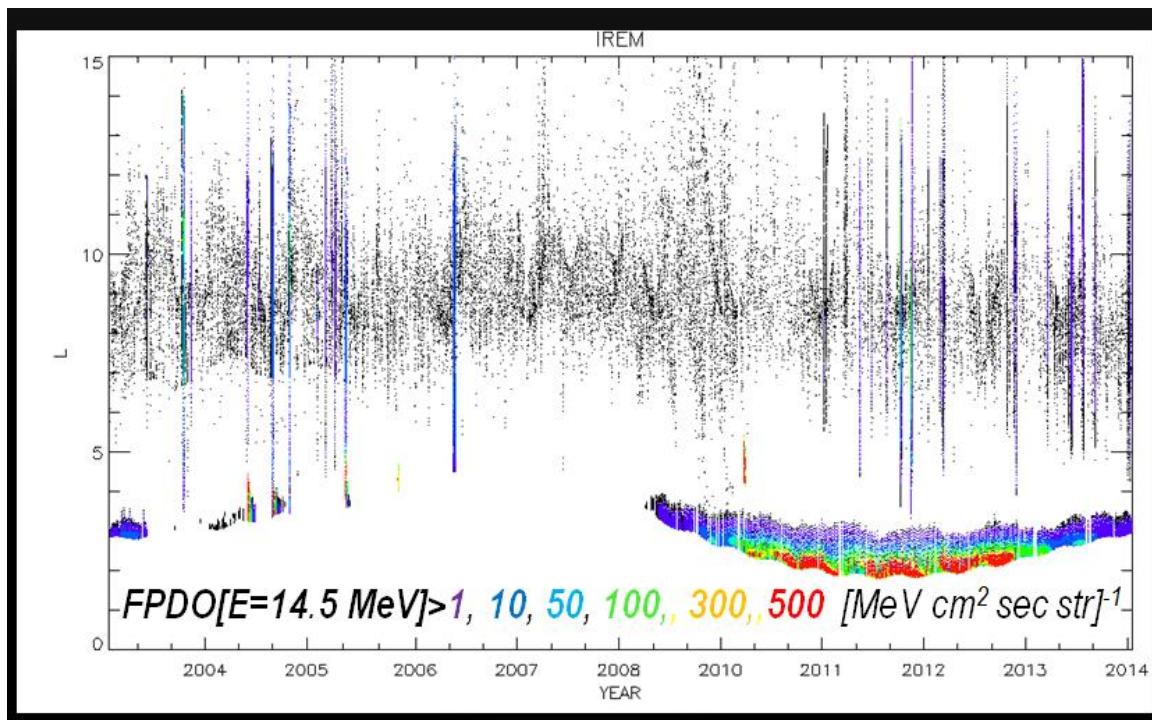


Figure B11: Summary plots of INTEGRAL/SREM SVD proton fluxes characterized by the FPDO_QUALITY variables (=0, most likely) and (= 1, likely).

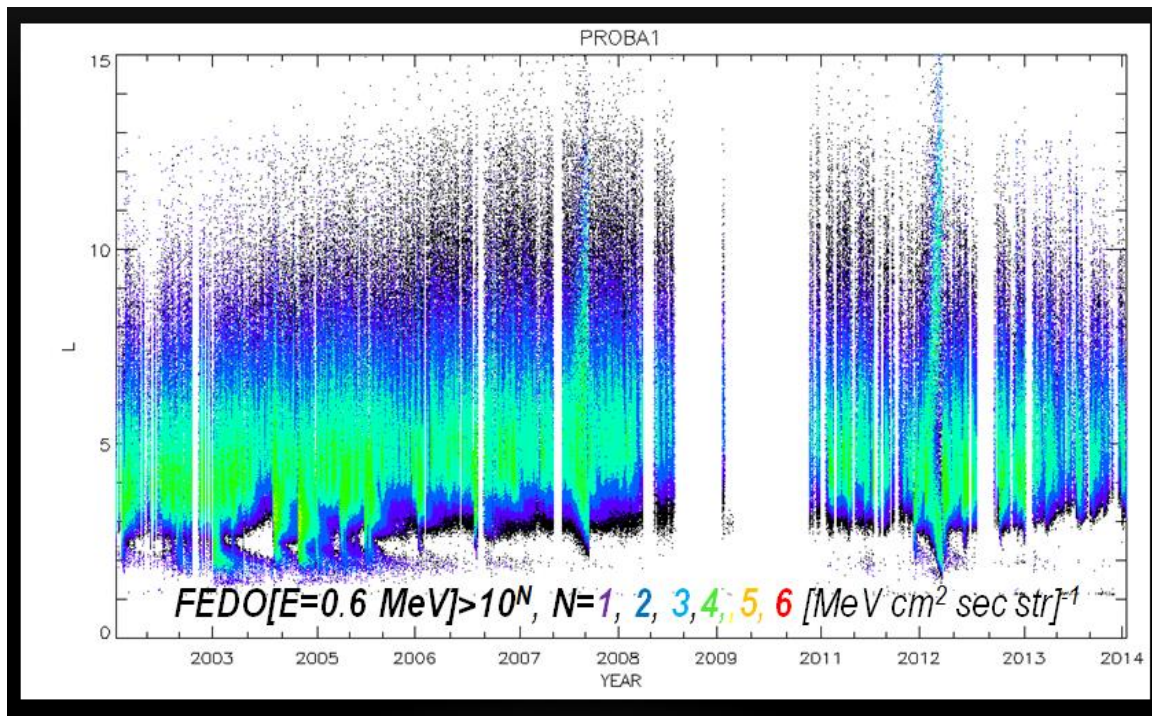


Figure B12: Summary plots of PROBA1/SREM SVD electron fluxes characterized by the FEDO_QUALITY variables (=0, most likely) and (= 1, likely).

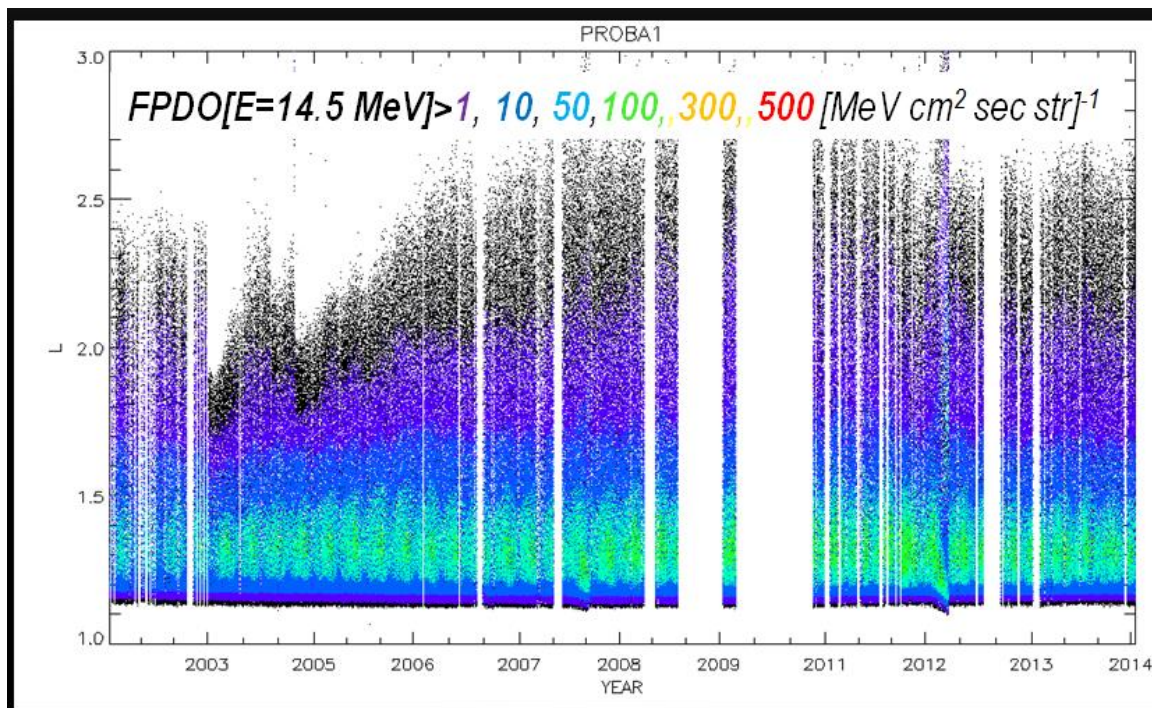


Figure B13: Summary plots of PROBA1/SREM SVD proton fluxes characterized by the FPDO_QUALITY variables (=0, most likely) and (= 1, likely).

Appendix C

Technical Note 1: Cross-Calibration of SREM data

Cross-calibration of ESA SREM SVD fluxes

For the case of proton flux datasets, we have selected SEPTEM RDS 2.0 as reference solar proton flux dataset. The SEPTEM RDS v2.0 contain processed data from the NOAA Energetic Particles Sensor (EPS), part of the Space Environment Monitor (SEM) package on-board GOES and earlier SMS satellites. The dataset time range is from 1974-07-01 until 2015-12-31 and is available for download at http://dev.sepem.oma.be/help/SEPTEM_RDS_v2-00.zip. These data have been cross-calibrated to find the effective (mean) energy of each energy bin using data from the Goddard Medium Energy (GME) instrument on-board the IMP-8 spacecraft. A description of the cross-calibration is available in *Sandberg et al [4]*. For the case of electron flux dataset, we have selected as reference the RBSP/MAGEIS scientific level measurements and seek for suitable magnetic conjunctions with INTEGRAL/IREM satellites.

Cross-calibration of ESA SREM proton fluxes

For the cross-calibration of the unfolded SREM proton fluxes based on the measurements of SREM units, we have used unfolded data from the unit on board INTEGRAL. The data were unfolded using the regularized Singular Deconvolution Method (SVD), described in [3]. As “gold” reference dataset, we have used ESA RDS 2.0. These data consist of GOES solar proton flux measurements cross-calibrated with corrected IMP8/GME data. The correction procedure for IMP8/GME data and the calibration procedure took place within SEPCALIB ESA project. Details can be found in SEPCALIB final report [5] and a brief description in [4].

The proton energies of SEPTEM differential proton flux reference dataset are:

FPDO_ENERGY_SEPEM= [6.0, 8.7, 12.6, 18.2, 26.3, 38.0, 55.0, 79.5, 115, 166, 244] MeV

while the nominal energies that are being used for the SVD unfolding of ESA INTEGRAL/SREM proton fluxes are:

FPDO_ENERGY_SREM= [12.4, 15.8, 20.0, 25.4, 32.3, 41.1, 52.2, 66.3, 84.3, 107, 136, 173, 220, 280, 354] MeV

In order to exclude the solar proton flux measurements affected by the magnetospheric shielding, we retain only the INTEGRAL/SREM measurements recorded at orbit segments where the L-shell values (calculated by IRBEM) were not defined. For the cross-calibration of SVD proton fluxes we first interpolated SEPTEM proton flux data at the measurement times of INTEGRAL/SREM and then applied the effective energy cross-calibration scheme which introduces new energy values to characterize the differential proton flux measurements [4].

This approach treats SEPTEM database as a virtual “tunable transmitter” while a scan over the whole energy range of interest is performed in order to determine the “a priori” unknown characteristic “energy lines of the absorbing” SREM differential proton fluxes. We re-binned SEPTEM data into 1500 energy bins and performed successive regression fits with the SREM SVD proton flux series.

The energy re-binned and time interpolated SEPTEM flux series are compared with SREM unfolded flux series through the evaluation of the behavior of the linear fit coefficients $Y_{SREM} = A_{fit}(E) + B_{fit}(E) \cdot X_{SEPEM}$ along the whole unfolding energy range. In what follows, the effective energy E_{eff} is defined by the value that minimizes the function $\delta B_{fit}(E) = |(B_{fit}(E) - 1)|$. In Figure 1, we present the “absorption lines” of the $\delta B_{fit}(E)$ function for SREM SVD proton channels versus the “tunable” SEPTEM energy. The minimum values of the curves are distinct, while the steepness of $\delta B_{fit}(E)$ defines the effective energy values. In other words, the energies of the re-binned SEPTEM flux data that provide the best fits, $B_{fit}=1$ with the SREM proton SVD flux series are defined as the “effective energies” of the SREM proton flux dataset.

Table C1: Effective energy values of the unfolded SREM SVD proton fluxes

SREM proton flux channel	Nominal unfolding energy	Effective Energy value
#1	12.4	14.50
#2	15.8	17.63
#3	20.0	20.69
#4	25.4	24.62
#5	32.3	29.31
#6	41.1	36.44
#7	52.2	44.33
#8	66.3	56.33
#9	84.3	73.16
#10	107.1	89.00
#11	136.1	116.4
#12	172.9	146.88
#13	219.7	194.9
#14	279.3	320
#15	354.8	361.3

NOTES:

- The effective energy values have been introduced in the processing chain of ESA SREM data and are included in Level 2 cdf data.
- We do not include the flux series of the highest two energy ranges.

Next, we present cross plots of the unfolded SVD INTEGRAL/SREM proton flux series versus SEPEM data re-binned at the derived effective energy values listed in Table 1.

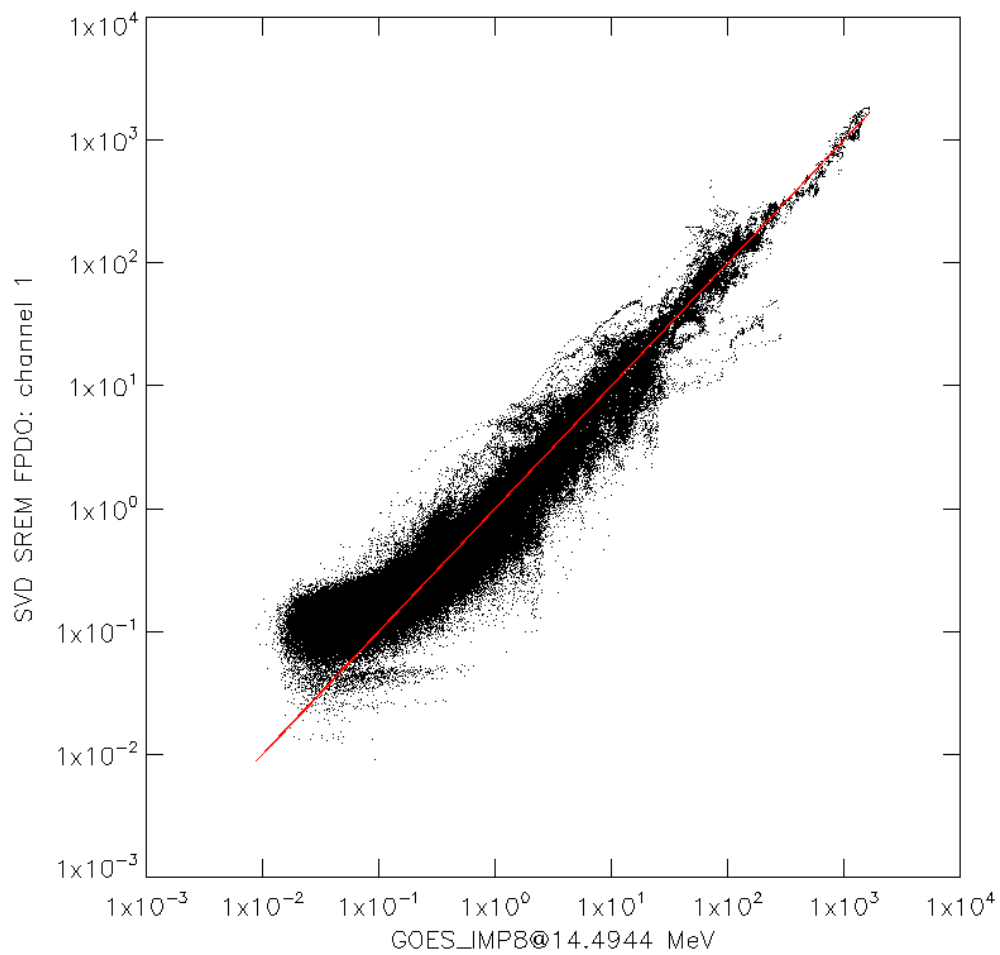


Figure C2: Scatter plot between the SREM SVD unfolded proton flux channel # 1 versus SEPEM proton flux data re-binned at 14.49 MeV.

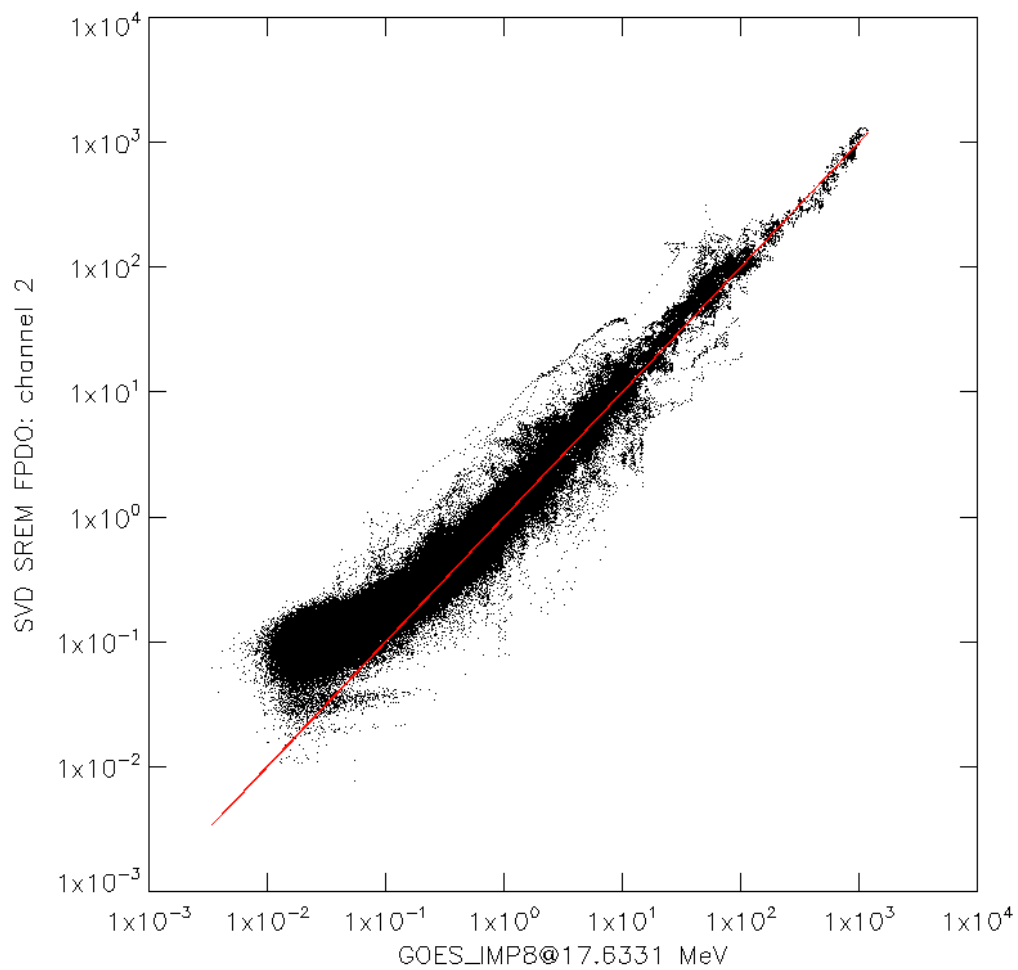


Figure C3: Scatter plot between the SREM SVD unfolded proton flux channel # 2 versus SEPEM proton flux data re-binned at 17.63 MeV.

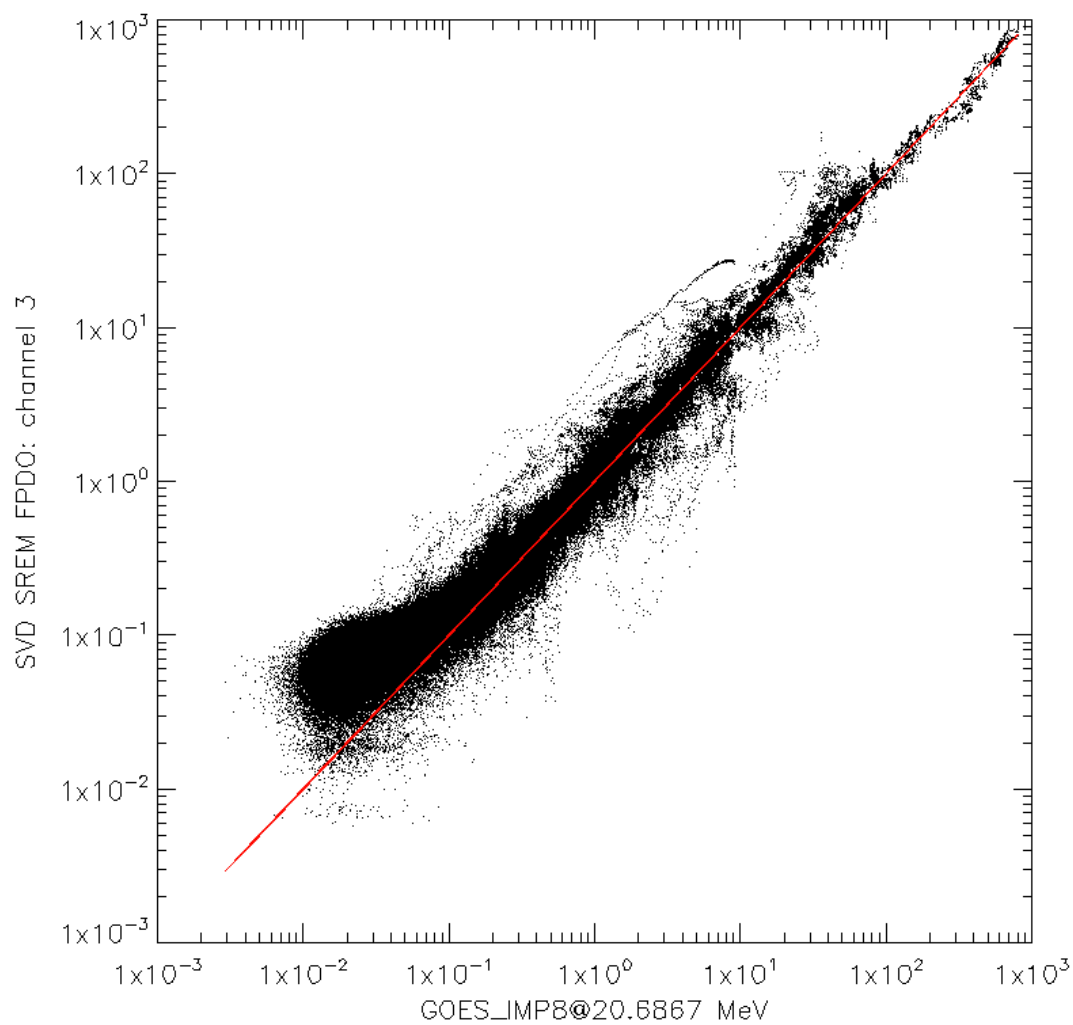


Figure C4: Scatter plot between the SREM SVD unfolded proton flux channel # 3 versus SEPEM proton flux data re-binned at 20.69 MeV.

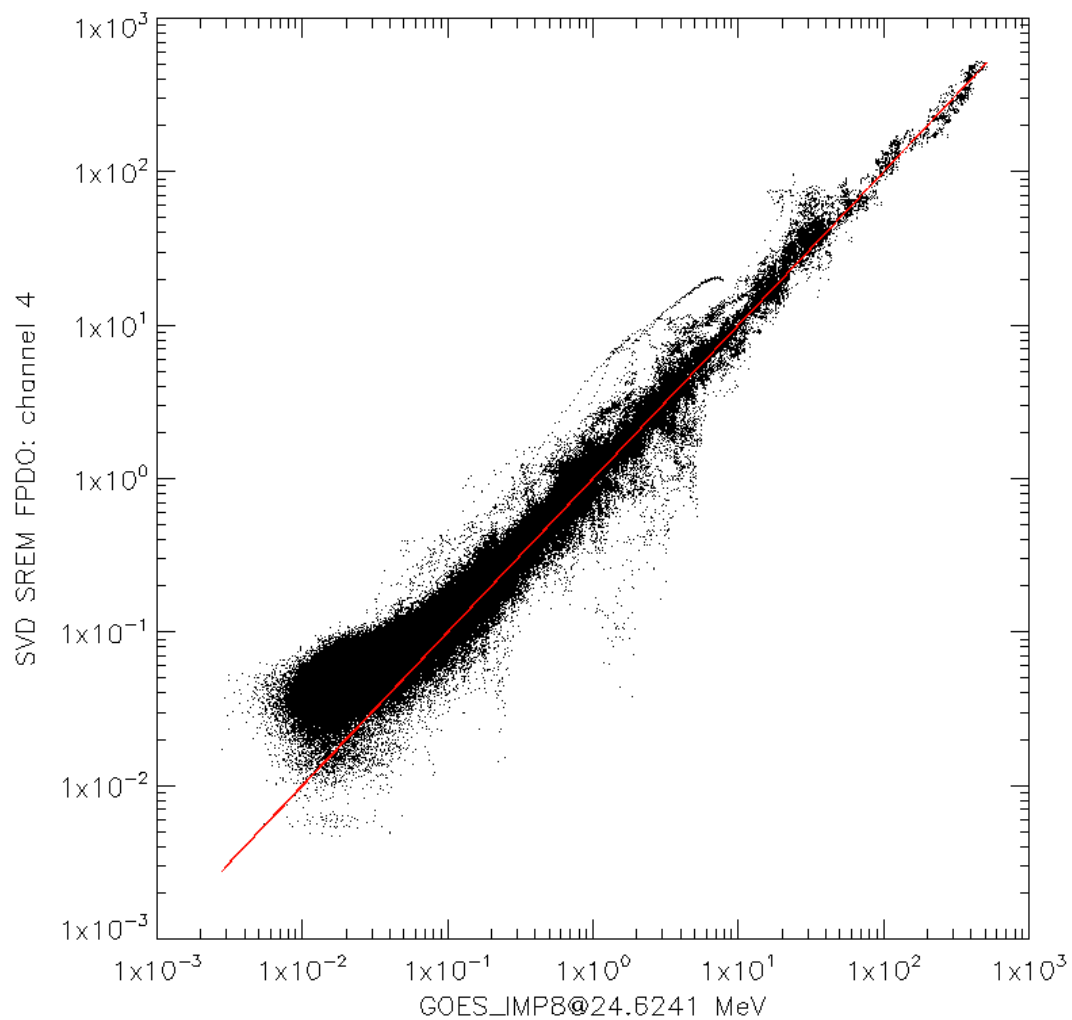


Figure C5: Scatter plot between the SREM SVD unfolded proton flux channel # 4 versus SEPEM proton flux data re-binned at 24.62 MeV.

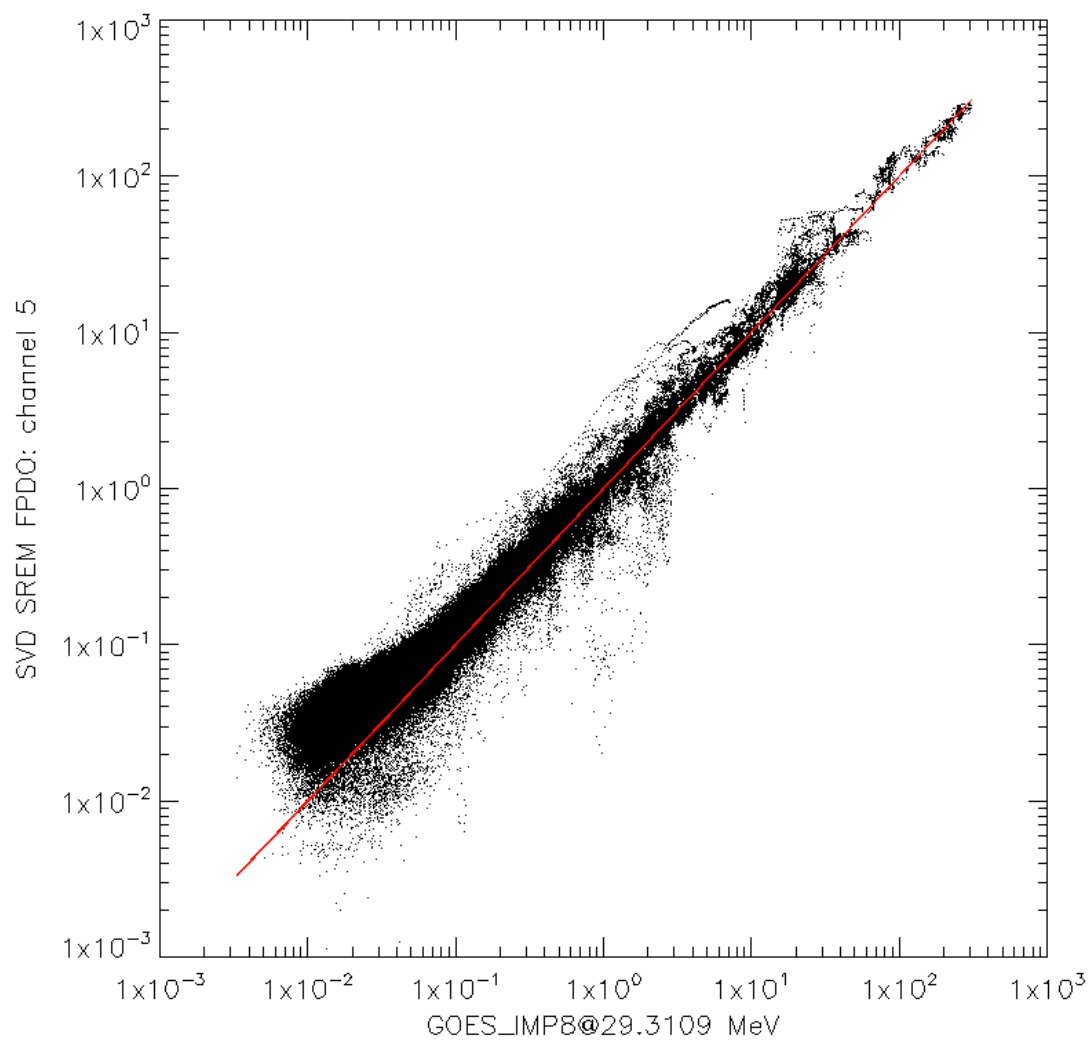


Figure C6: Scatter plot between the SREM SVD unfolded proton flux channel # 5 versus SEPEM proton flux data re-binned at 29.31 MeV.

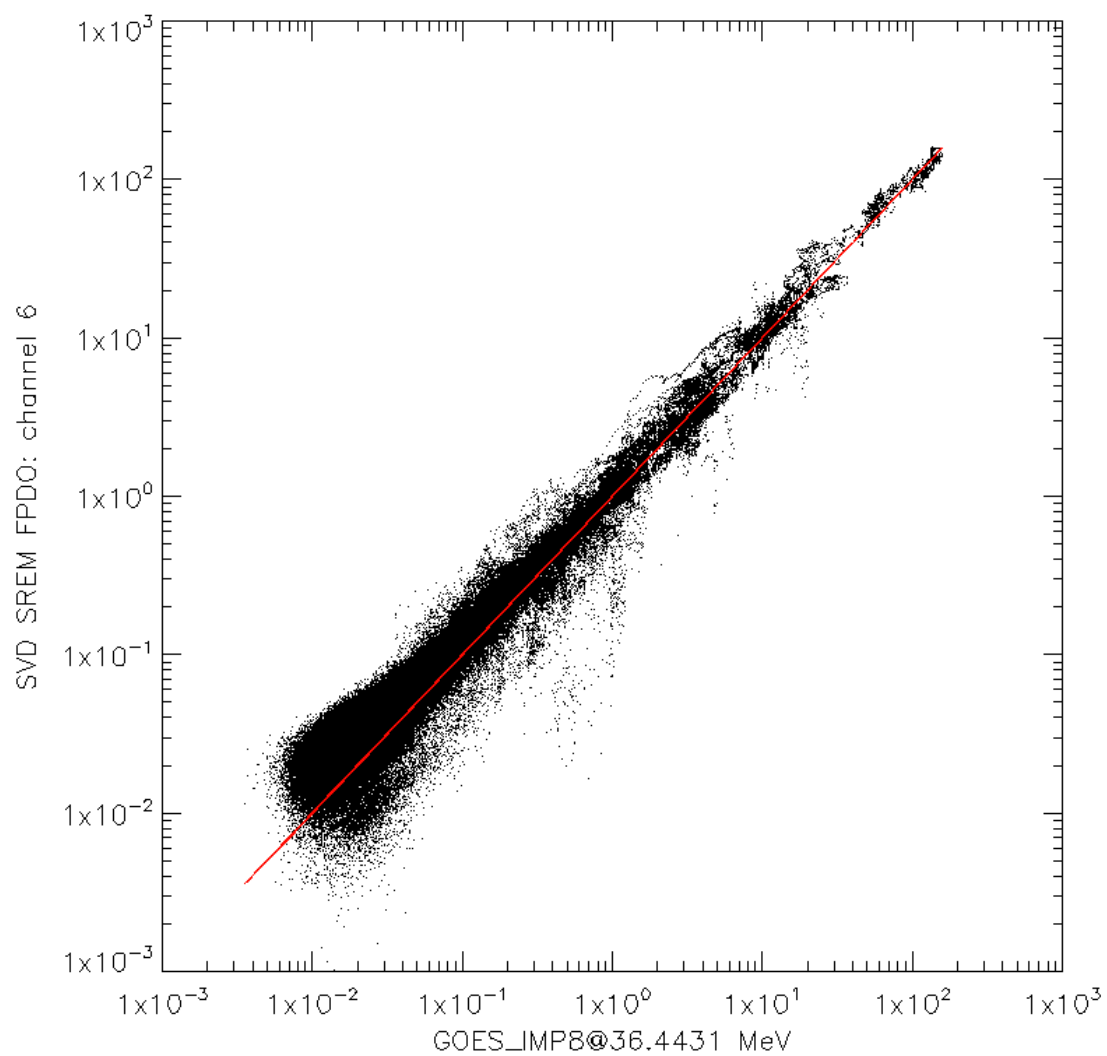


Figure C7: Scatter plot between the SREM SVD unfolded proton flux channel # 6 versus SEPEM proton flux data re-binned at 36.44 MeV.

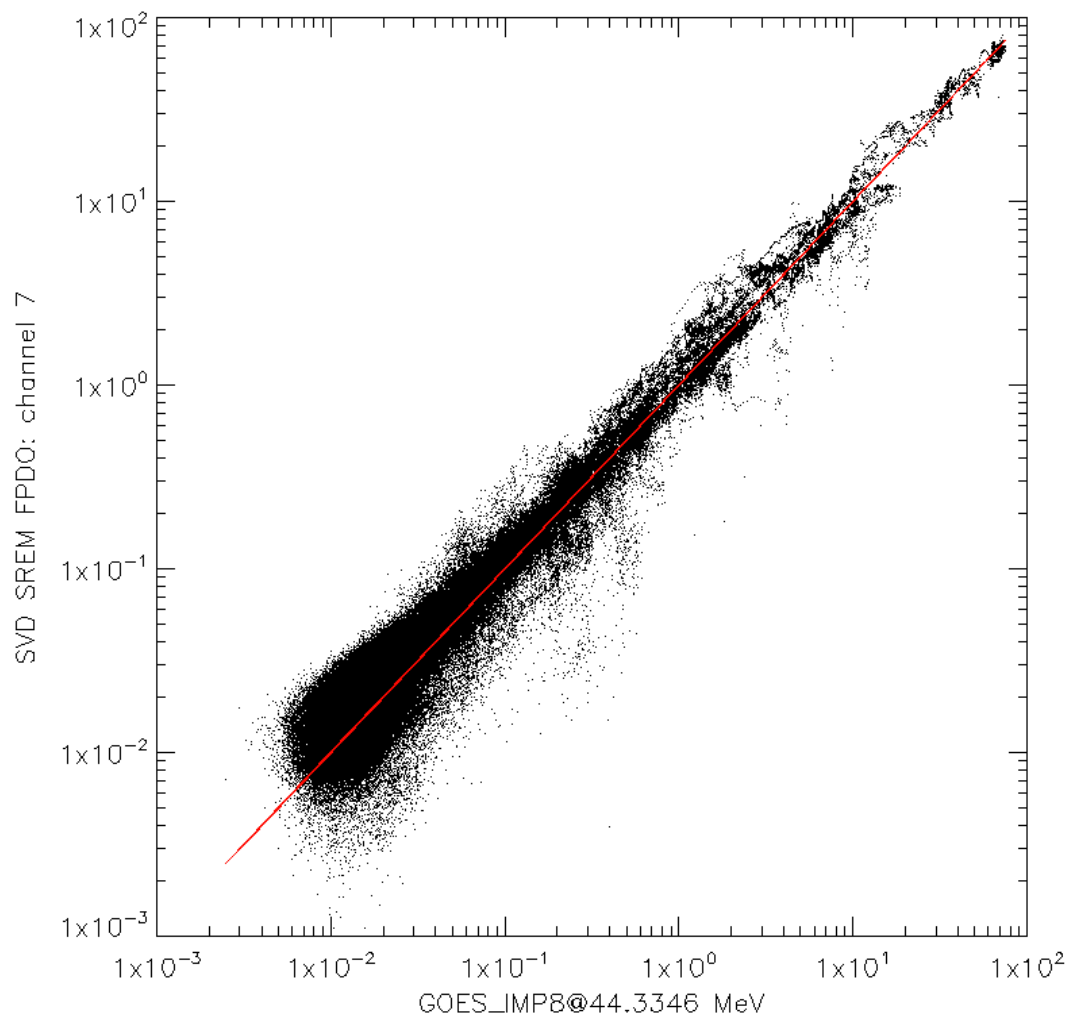


Figure C8: Scatter plot between the SREM SVD unfolded proton flux channel # 7 versus SEPEM proton flux data re-binned at 44.33 MeV.

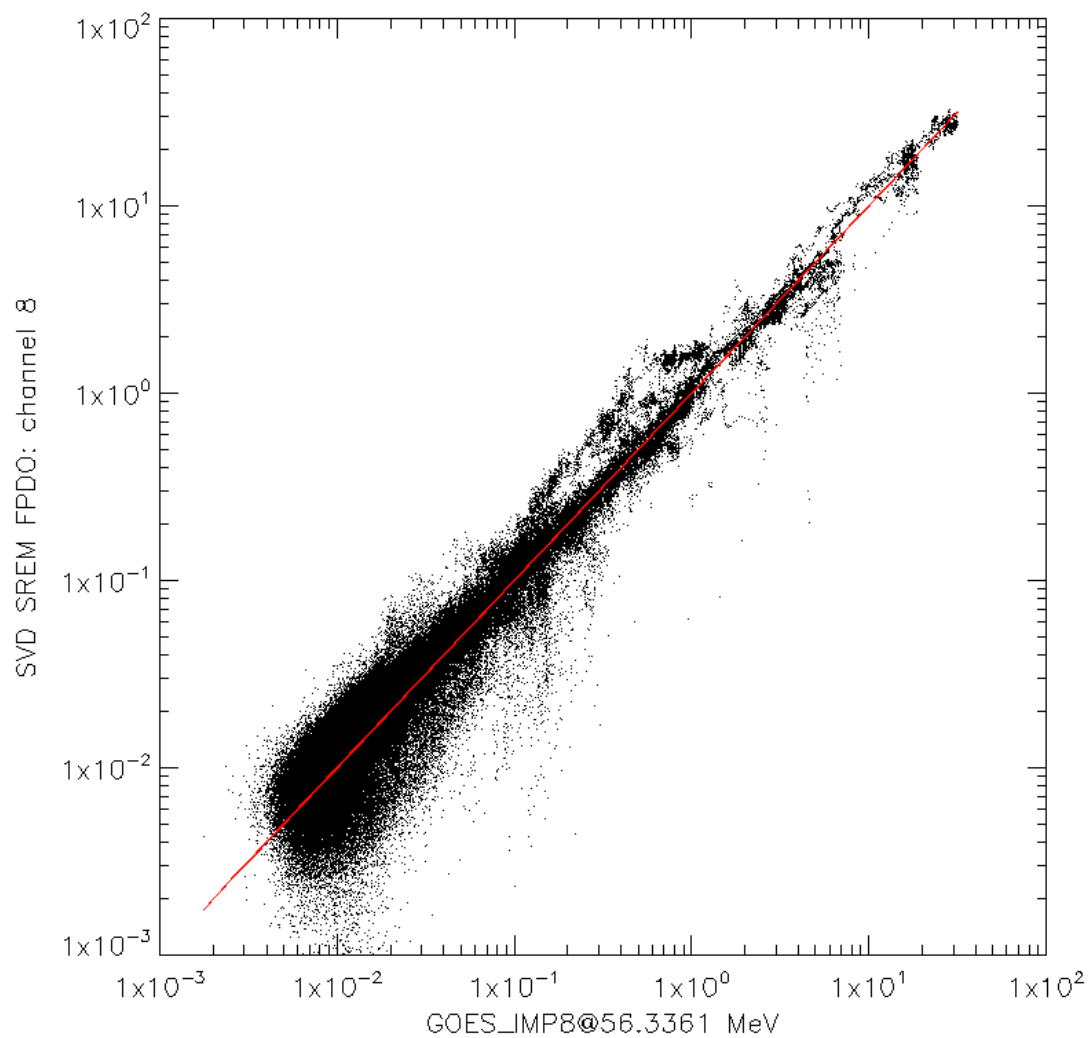


Figure C9: Scatter plot between the SREM SVD unfolded proton flux channel # 8 versus SEPEM proton flux data re-binned at 56.33 MeV.

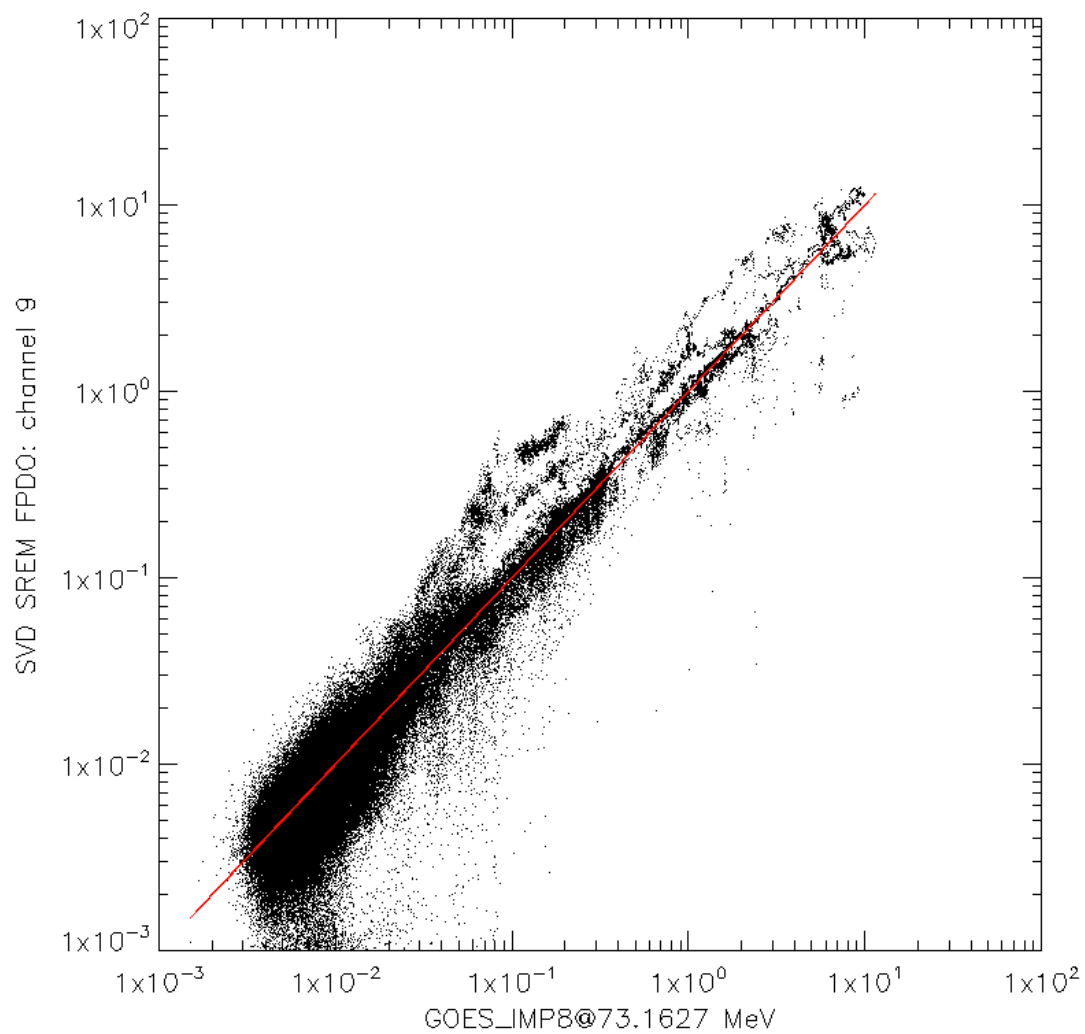


Figure C10: Scatter plot between the SREM SVD unfolded proton flux channel # 9 versus SEPEM proton flux data re-binned at 73.17 MeV.

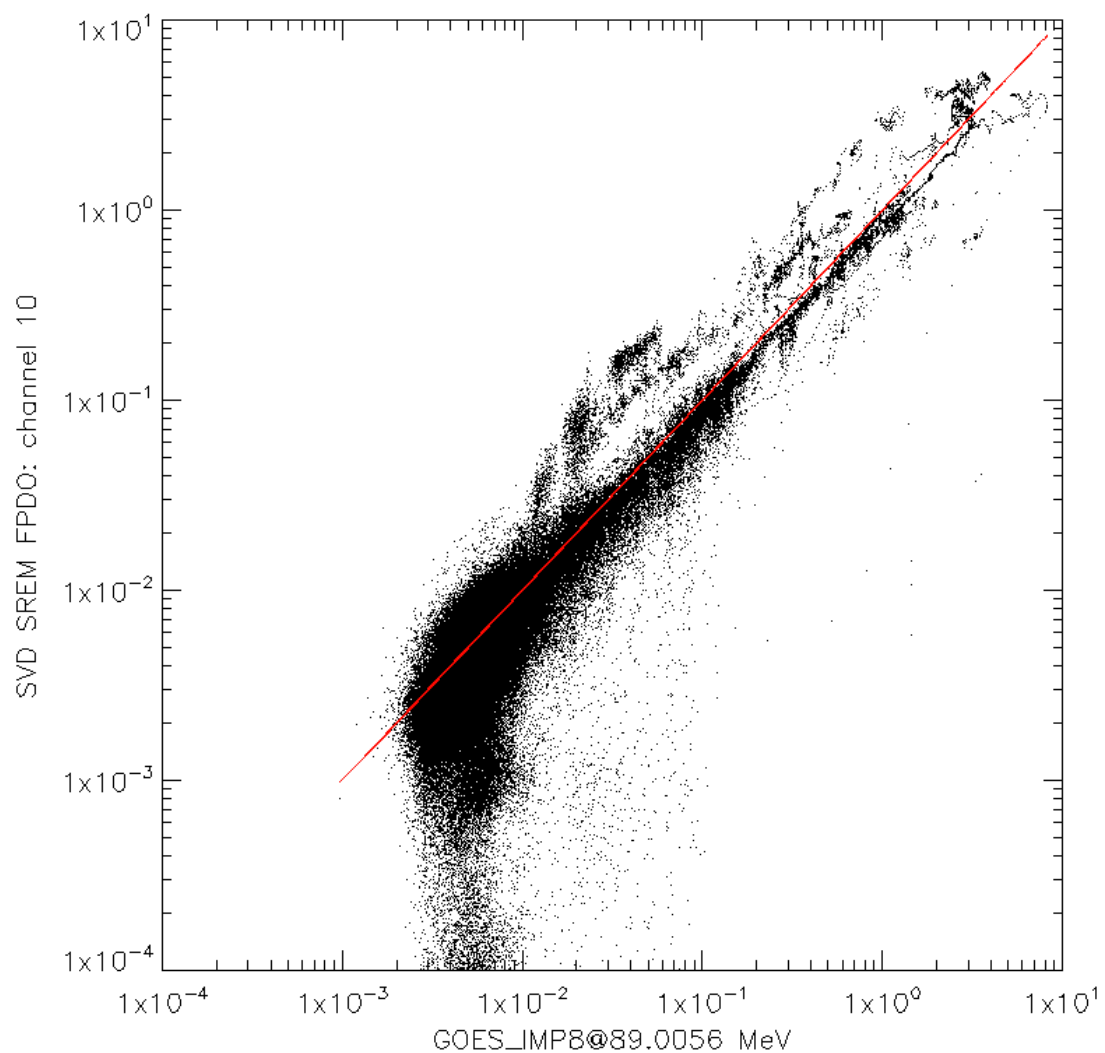


Figure C11: Scatter plot between the SREM SVD unfolded proton flux channel # 10 versus SEPEM proton flux data re-binned at 89.00 MeV.

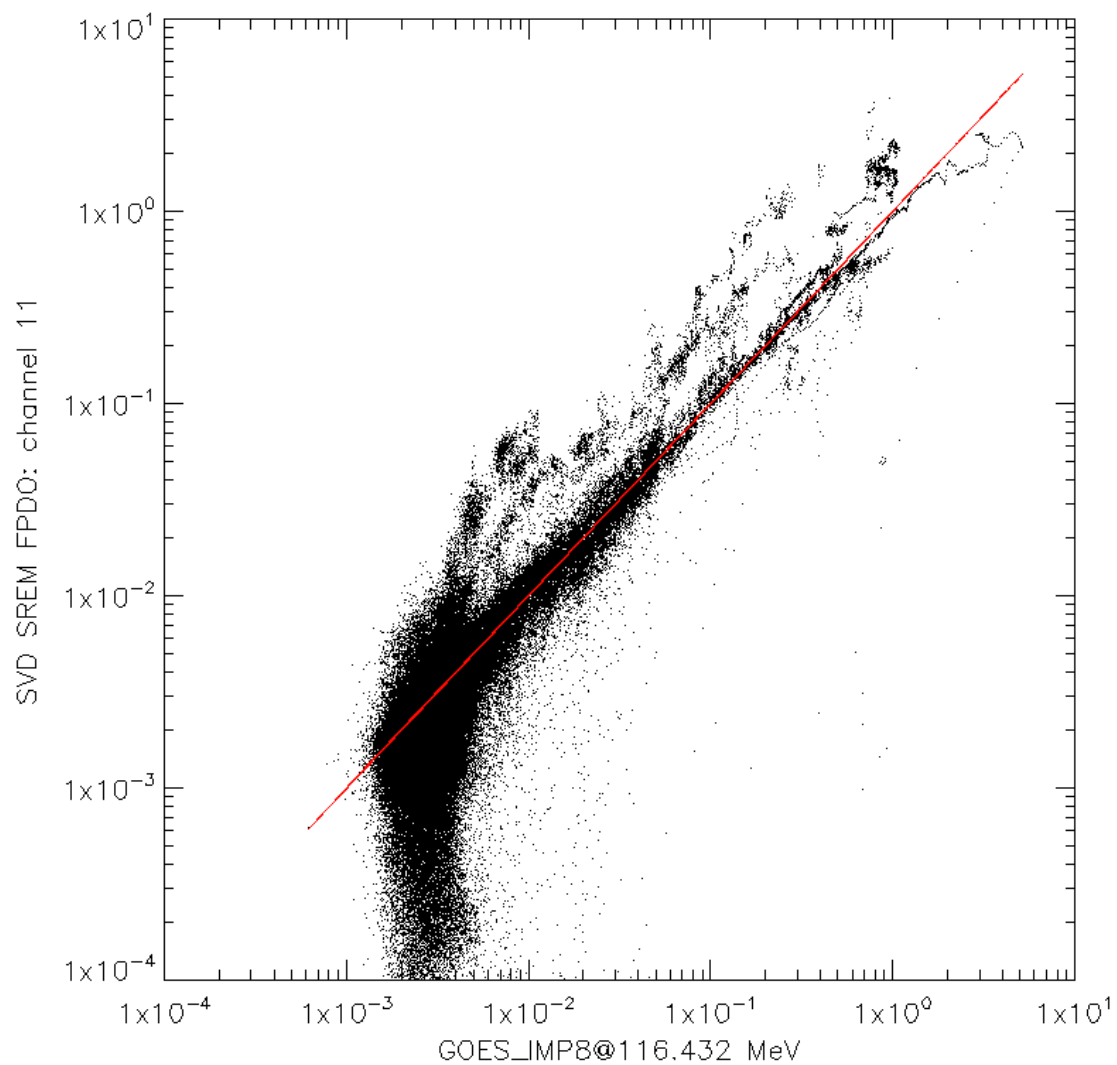


Figure C12: Scatter plot between the SREM SVD unfolded proton flux channel # 10 versus SEPEM proton flux data re-binned at 116.43 MeV.

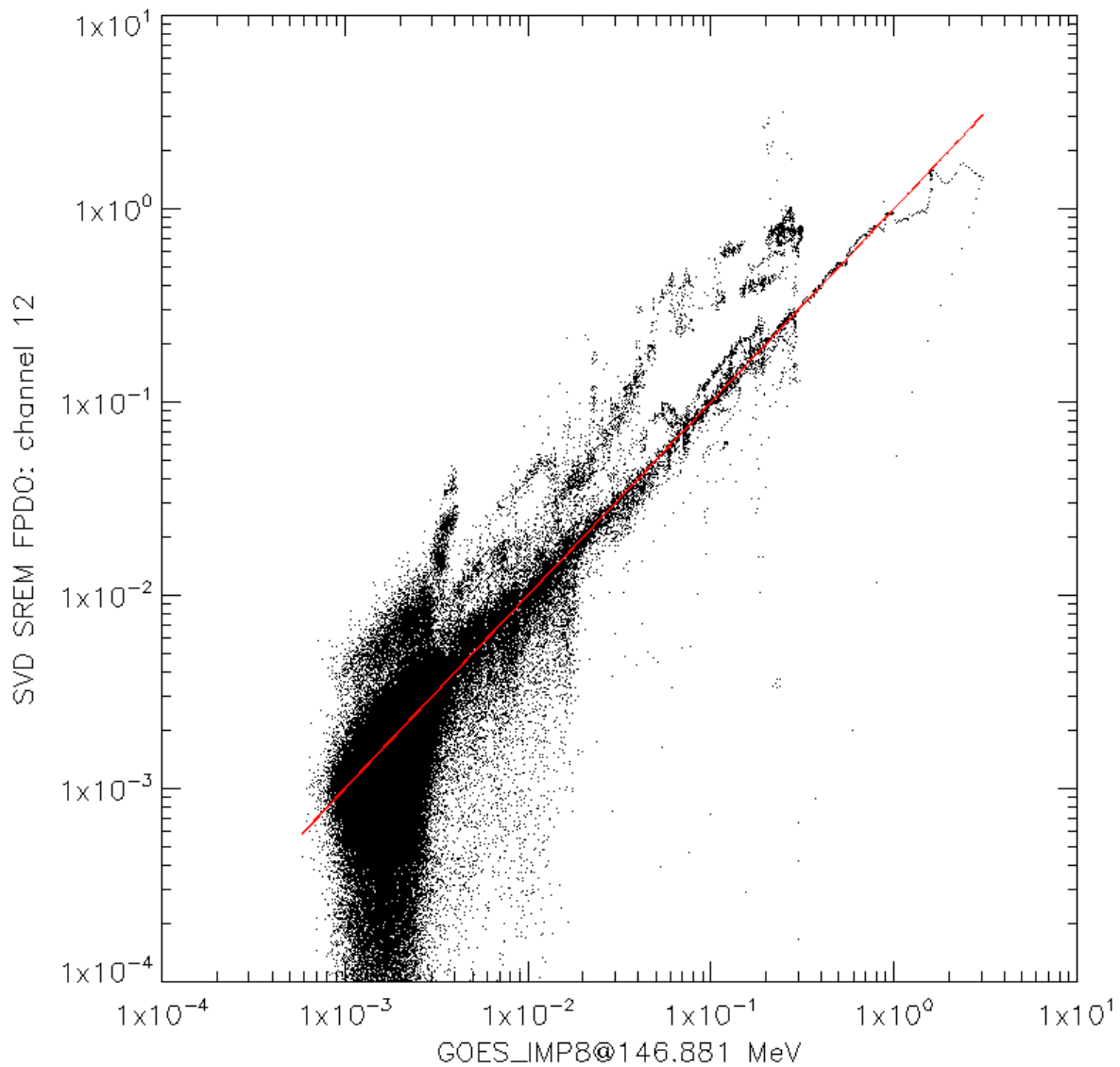


Figure C13: Scatter plot between the SREM SVD unfolded proton flux channel # 11 versus SEPEM proton flux data re-binned at 146.88 MeV.

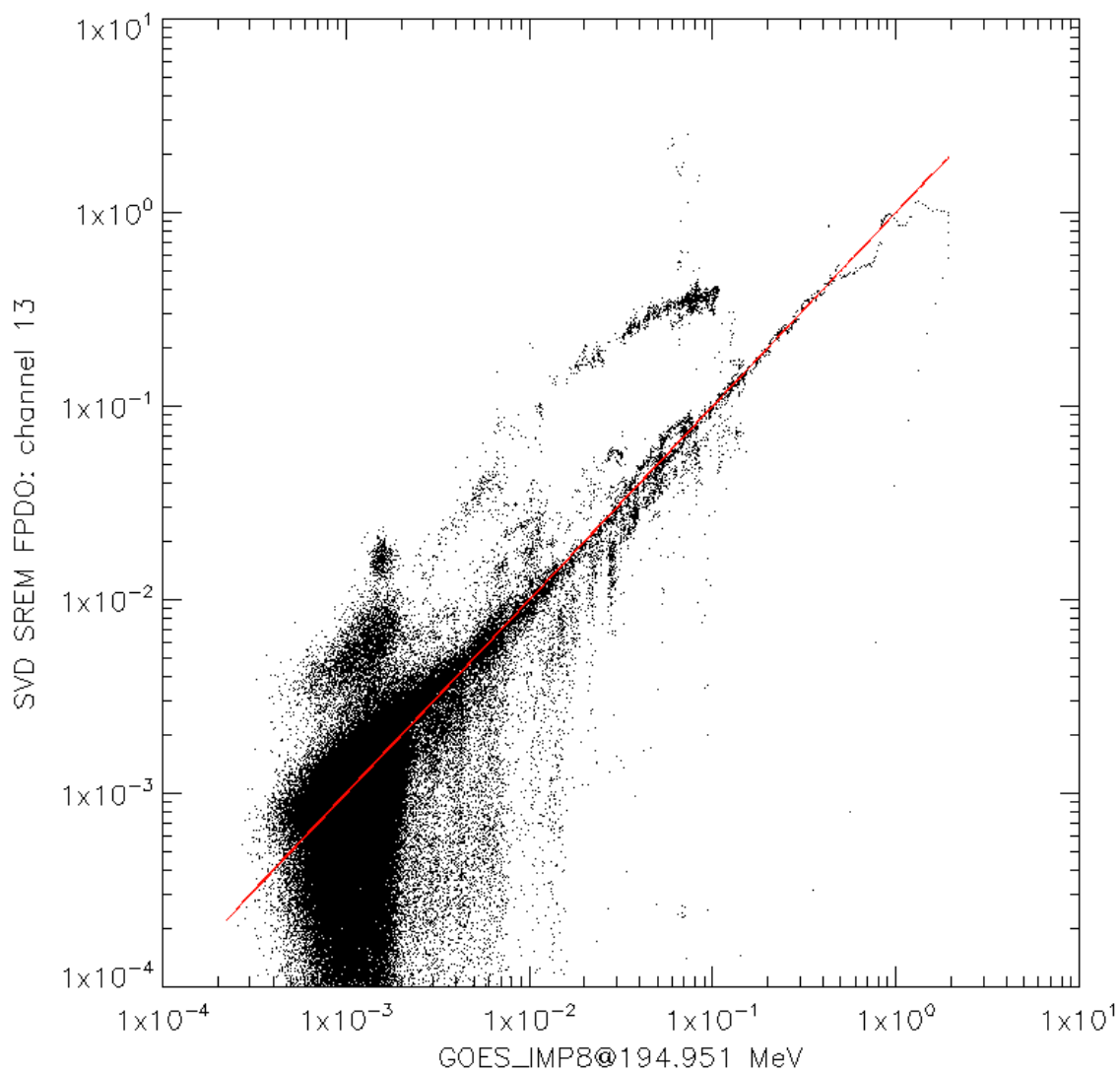


Figure C14: Scatter plot between the SREM SVD unfolded proton flux channel # 13 versus SEPEM proton flux data re-binned at 194.95 MeV.

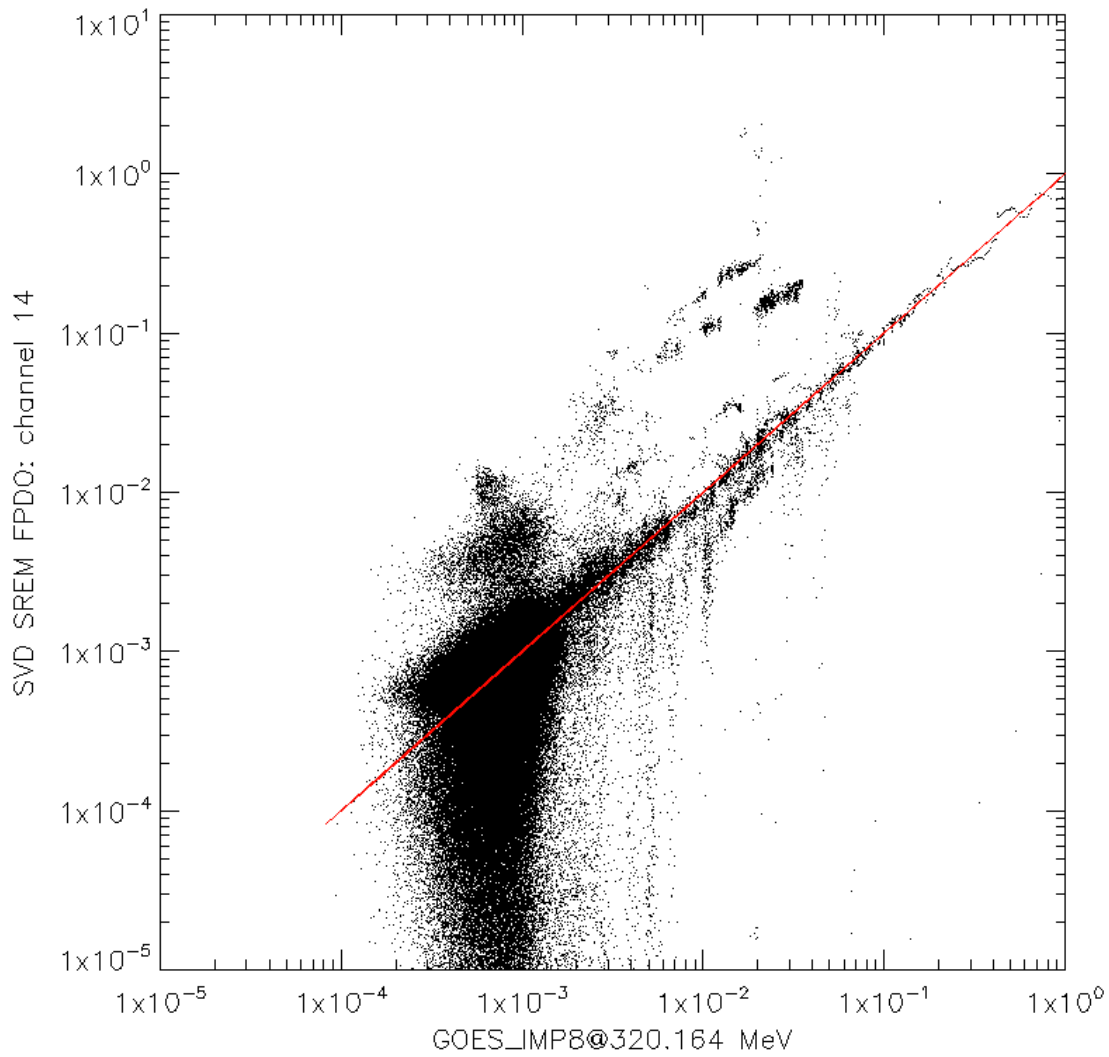


Figure C15: Scatter plot between the SREM SVD unfolded proton flux channel # 14 versus SEPEM proton flux data re-binned at 320.16 MeV.

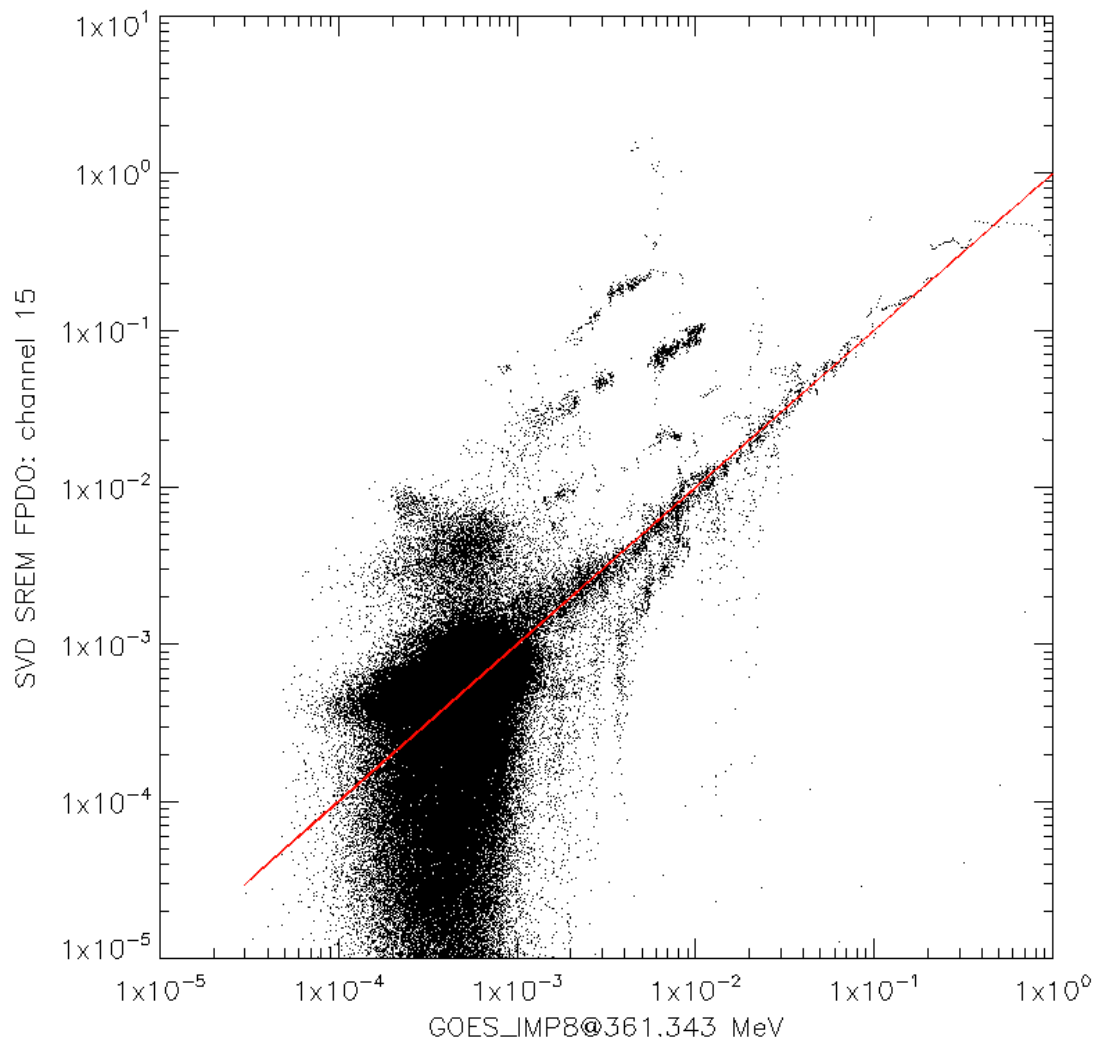


Figure C16: Scatter plot between the SREM SVD unfolded proton flux channel # 15 versus SEPEM proton flux data re-binned at 361.34 MeV.

Cross-calibration of SREM SVD electron fluxes

For the calibration of SREM electron fluxes, we have selected RBSP-A-B/MageIS. The corresponding flux measurements are unidirectional differential fluxes binned in 11 (8.18, 24.54, 40.91, 57.27, 73.64, 90, 106.36, 122.73, 139.09, 155.45 and 171.82 degrees) pitch angle bins. We have performed a numerical integration over the pitch angles and calculated the omni-directional differential electron fluxes. The resulted datasets have the following energies:

FEDO_ENERGY_RBSP-A_MAGEIS=

[0.0315, 0.0538, 0.0798, 0.1083, 0.1435, 0.1834, 0.2261, 0.2318, 0.3421, 0.4644, 0.5930, 0.7416, 0.9018, 0.9990, 1.0777, 1.5470, 1.7010, 2.2750, 2.6510, 3.6810, 4.2160] MeV

FEDO_ENERGY_RBSP-B_MAGEIS=

[0.0319, 0.0544, 0.0752, 0.1016, 0.1324, 0.1693, 0.2096, 0.2422, 0.3498, 0.4668, 0.5996, 0.7425, 0.8919, 1.0130, 1.0498, 1.5410, 1.704, 2.2490, 2.5960, 3.5190, 4.0090] MeV

Suitable conjunctions between the target and the reference satellites, are defined as the spatiotemporal locations - according to the physics of particles trajectories inside the magnetosphere - where the respective instruments should measure the same environment. The criteria for these positions, concerning trapped particle measurements (radiation belts data) are defined on the basis of adiabatic invariants. We have followed the concept of the recommendations of the Panel on Radiation Belt Environment Modeling (PRBEM/COSPAR) and adopted more strict conditions for the cross-calibration of SREM SVD electron fluxes:

$$\begin{aligned} 3 < L^* < 6 \text{ and } dL^* < 0.1 \\ d(B / \text{Beq}) < 0.1 \text{ and } B / \text{Beq} \sim 1 \\ 4 < \text{MLT} < 8 \text{ and } 16 < \text{MLT} < 20 \\ dt < 1 \text{ h} \end{aligned}$$

The first constraint requires measurements to be on closed magneto-shells. The magnetic field limitations ensure that both instruments may count the same distribution of particles bouncing along a magnetic line close to the geomagnetic equator. Reducing the local time excludes the abrupt changes of field due to the magnetosphere compressions or sub-storm-related dynamics around noon and midnight, respectively. It should be noted that we did not apply any restriction associated with the geomagnetic activity described by Kp value. After few tests we made, it was evident that the presence of these conjunctions improves the statistics without biasing the derived scaling factors.

NOTE: The magnetic coordinate variables were calculated using UNILIB library (<http://trend.aeronomie.be/NEEDLE/unilib.html>).

Using the conjunction conditions described above, we found 430 multiple magnetic conjunctions between RBSP_MAGEIS_B and INTEGRAL. With the term multiple, we refer to the case where for given position of INTEGRAL s/c a series of orbital segments of RBSP satisfy the conjunction criteria.

For each multiple conjunction, we:

- Averaged MAGEIS data
- Re-binned averaged MAGEIS data to SREM SVD FEDO_ENERGY
- Reject the low energy part of MAGEIS spectra who present local maximum
- Calculate the ratios FEDO_RBSPB_MAGEIS/FEDO_INTEGRAL_SREM

We adopt the mean values $\langle SF(E) \rangle$ as scaling factors for the electron SVD fluxes.

SREM SVD electron flux channel	Nominal unfolding energy	Scaling Factor
#1	0.65	2.85
#2	0.73	2.05
#3	0.83	1.77
#4	0.93	1.64
#5	1.06	1.47
#6	1.19	1.19
#7	1.35	0.96
#8	1.52	0.79
#9	1.71	0.63
#10	1.93	0.58
#11	2.18	0.57
#12	2.46	0.55
#13	2.78	0.36
#14	3.14	0.156
#15	3.54	0.078

In what follows, we present plots of the mean and the quartile values of SF series.

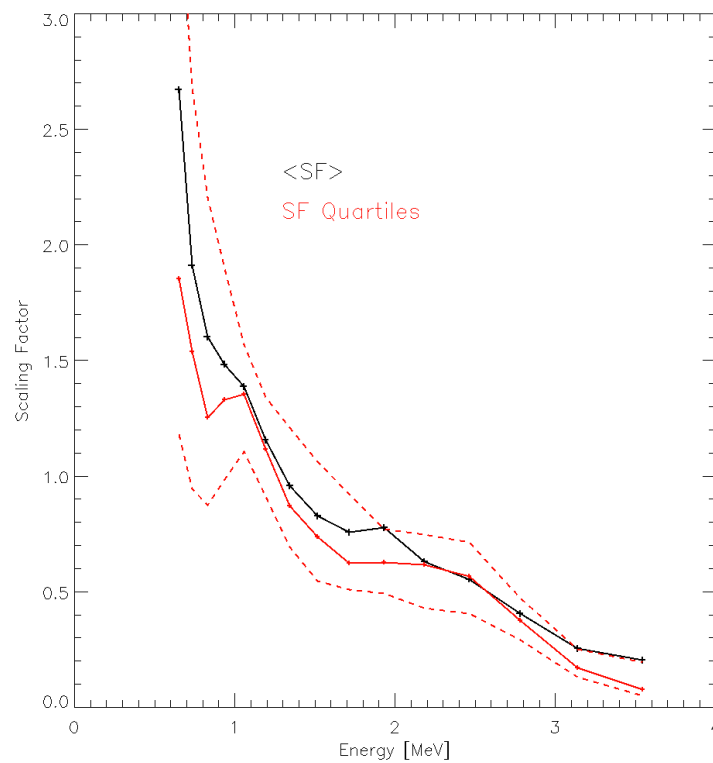


Figure C17: Mean and quartiles of the ratios SF=FEDO_RBSPB_MAGEIS/FEDO_INTEGRAL_SREM.

In what follows, we present the averaged spectra of the SREM SVD electron fluxes (in black) rescaled with the scaling factors (in red) for two different cases. As it can be seen the derived scaling factors preserve the smoothness of the electron spectra.

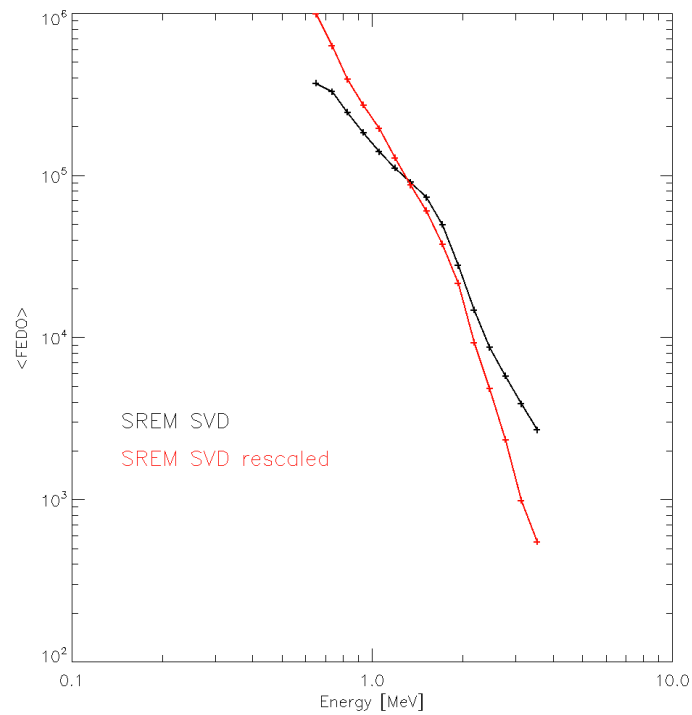


Figure C18: Mean and rescaled mean electron SVD SREM spectra using the measurements during the selected conjunctions.

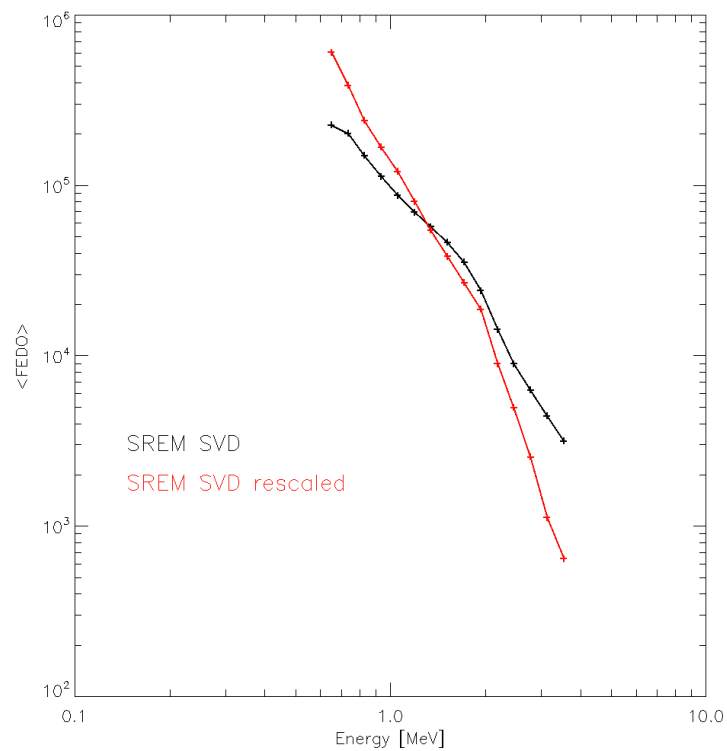


Figure C19: Mean and rescaled mean electron SVD SREM spectra using the whole INTEGRAL/SREM dataset under the condition FEDO_QUALITY=0.

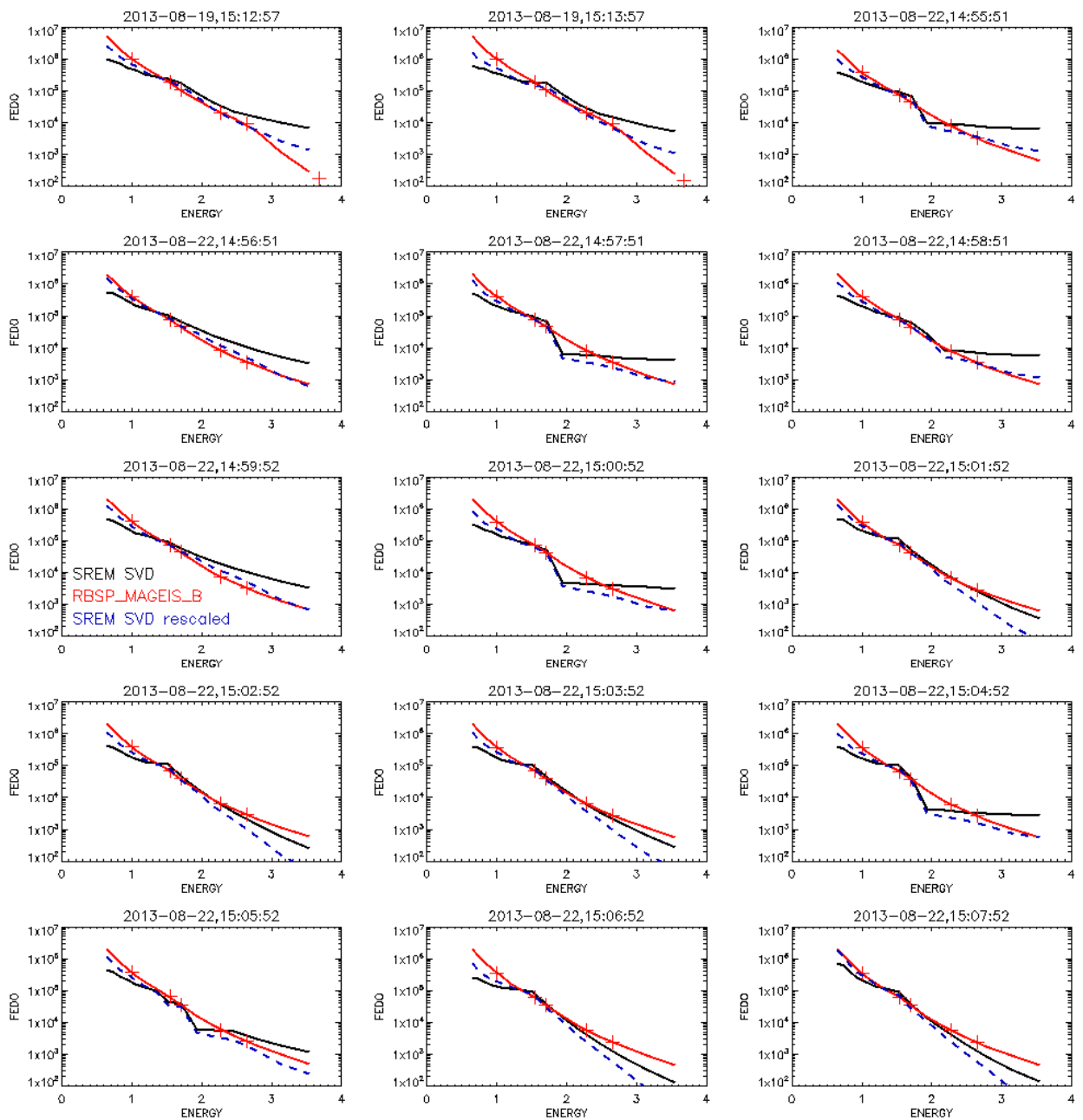


Figure C20: MAGEIS (in red) and SREM SVD (in black) differential electron flux spectra during the considered conjunctions. The red crosses denote MAGEIS data and the red line the MAGEIS data - re-binned at nominal SREM SVD electron energies – that were used for the derivation of the Scaling Factor. The blue dashed line corresponds to the re-scaled (cross-calibrated) SREM SVD spectra.

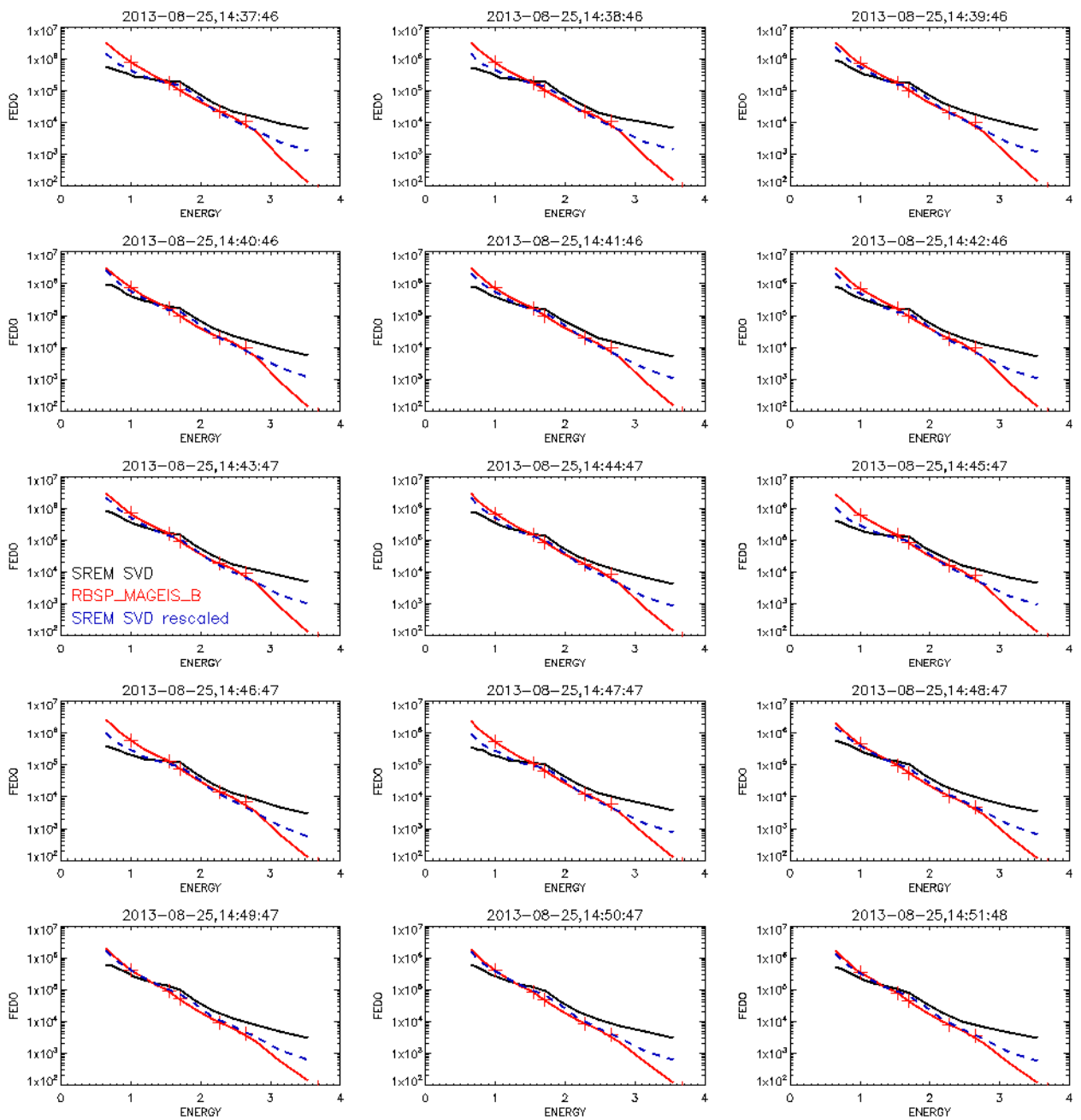


Figure C21: MAGEIS (in red) and SREM SVD (in black) differential electron flux spectra during the considered conjunctions. The red crosses denote MAGEIS data and the red line the MAGEIS data - re-binned at nominal SREM SVD electron energies – that were used for the derivation of the Scaling Factor. The blue dashed line corresponds to the re-scaled (cross-calibrated) SREM SVD spectra.

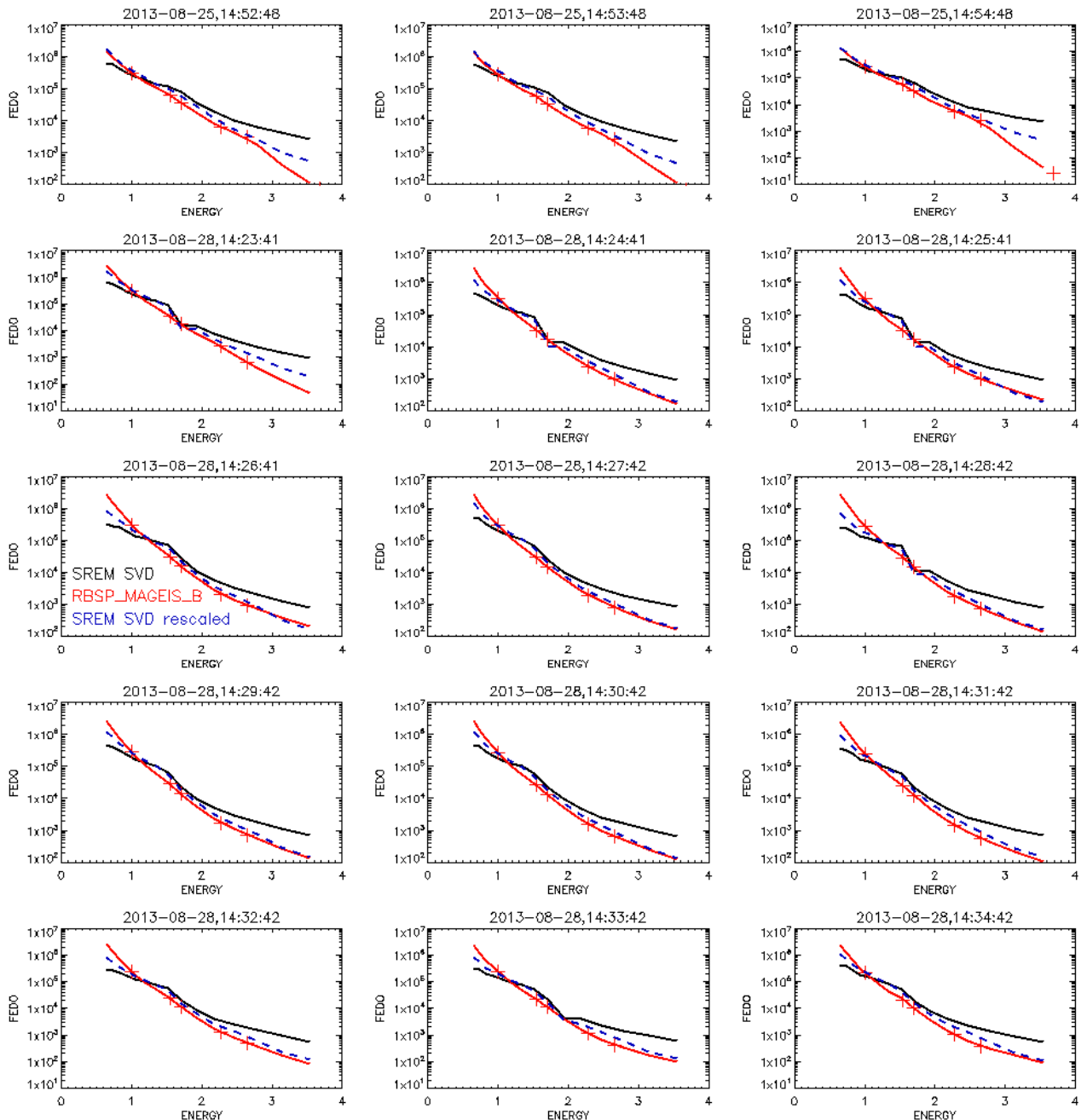


Figure C22: MAGEIS (in red) and SREM SVD (in black) differential electron flux spectra during the considered conjunctions. The red crosses denote MAGEIS data and the red line the MAGEIS data - re-binned at nominal SREM SVD electron energies – that were used for the derivation of the Scaling Factor. The blue dashed line corresponds to the re-scaled (cross-calibrated) SREM SVD spectra.

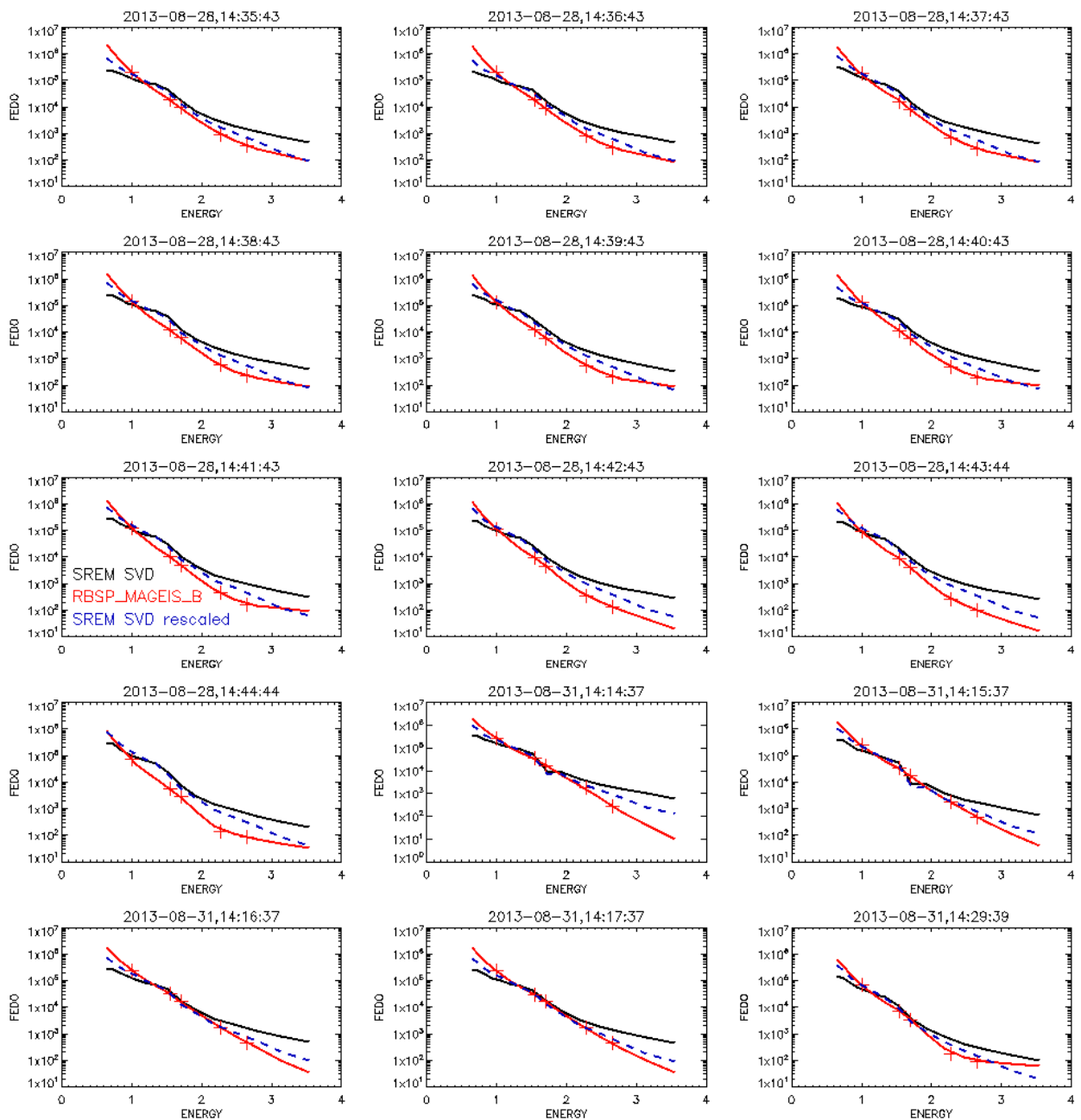


Figure C23: MAGEIS (in red) and SREM SVD (in black) differential electron flux spectra during the considered conjunctions. The red crosses denote MAGEIS data and the red line the MAGEIS data - re-binned at nominal SREM SVD electron energies – that were used for the derivation of the Scaling Factor. The blue dashed line corresponds to the re-scaled (cross-calibrated) SREM SVD spectra.

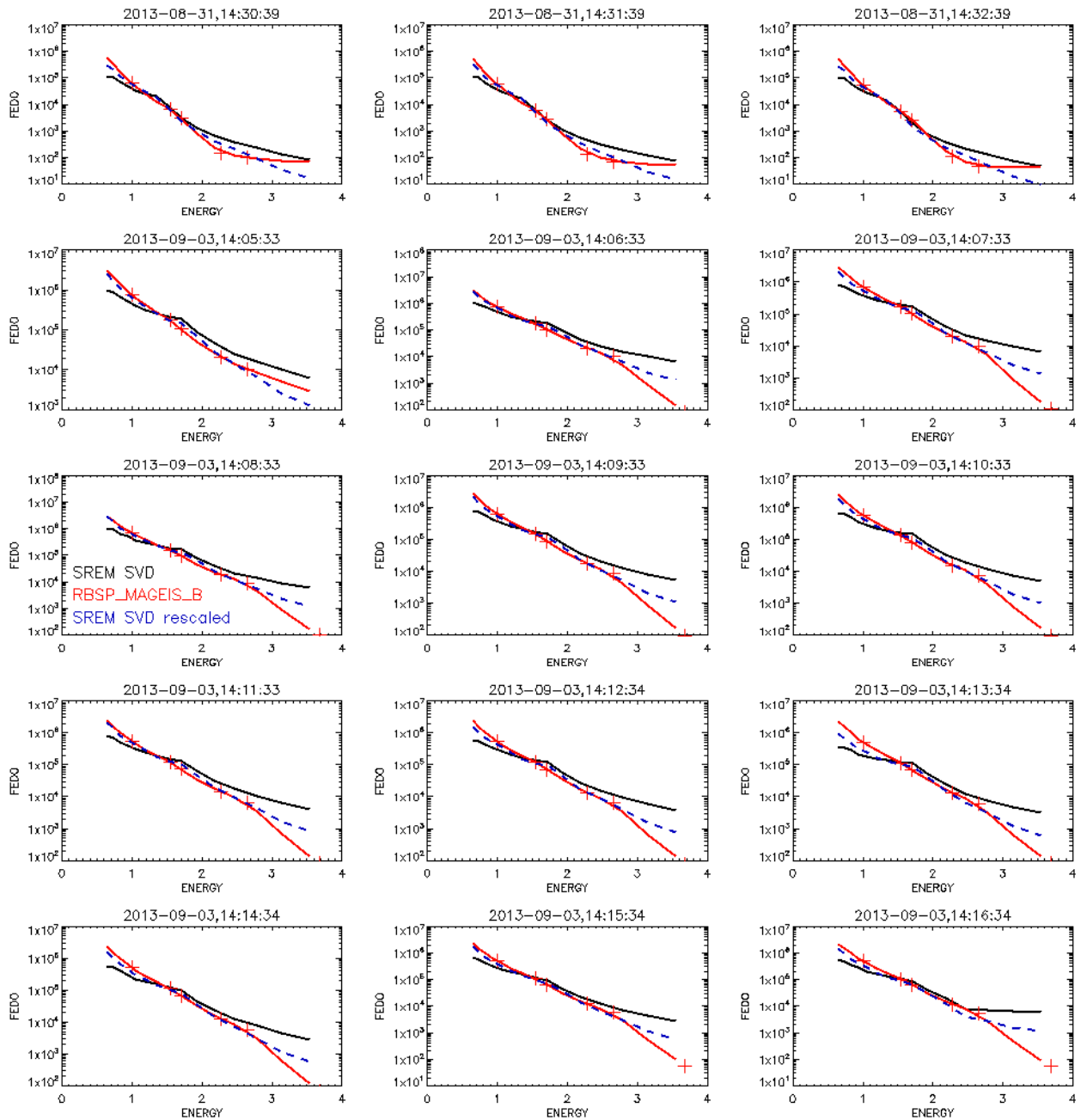


Figure C24: MAGEIS (in red) and SREM SVD (in black) differential electron flux spectra during the considered conjunctions. The red crosses denote MAGEIS data and the red line the MAGEIS data - re-binned at nominal SREM SVD electron energies – that were used for the derivation of the Scaling Factor. The blue dashed line corresponds to the re-scaled (cross-calibrated) SREM SVD spectra.

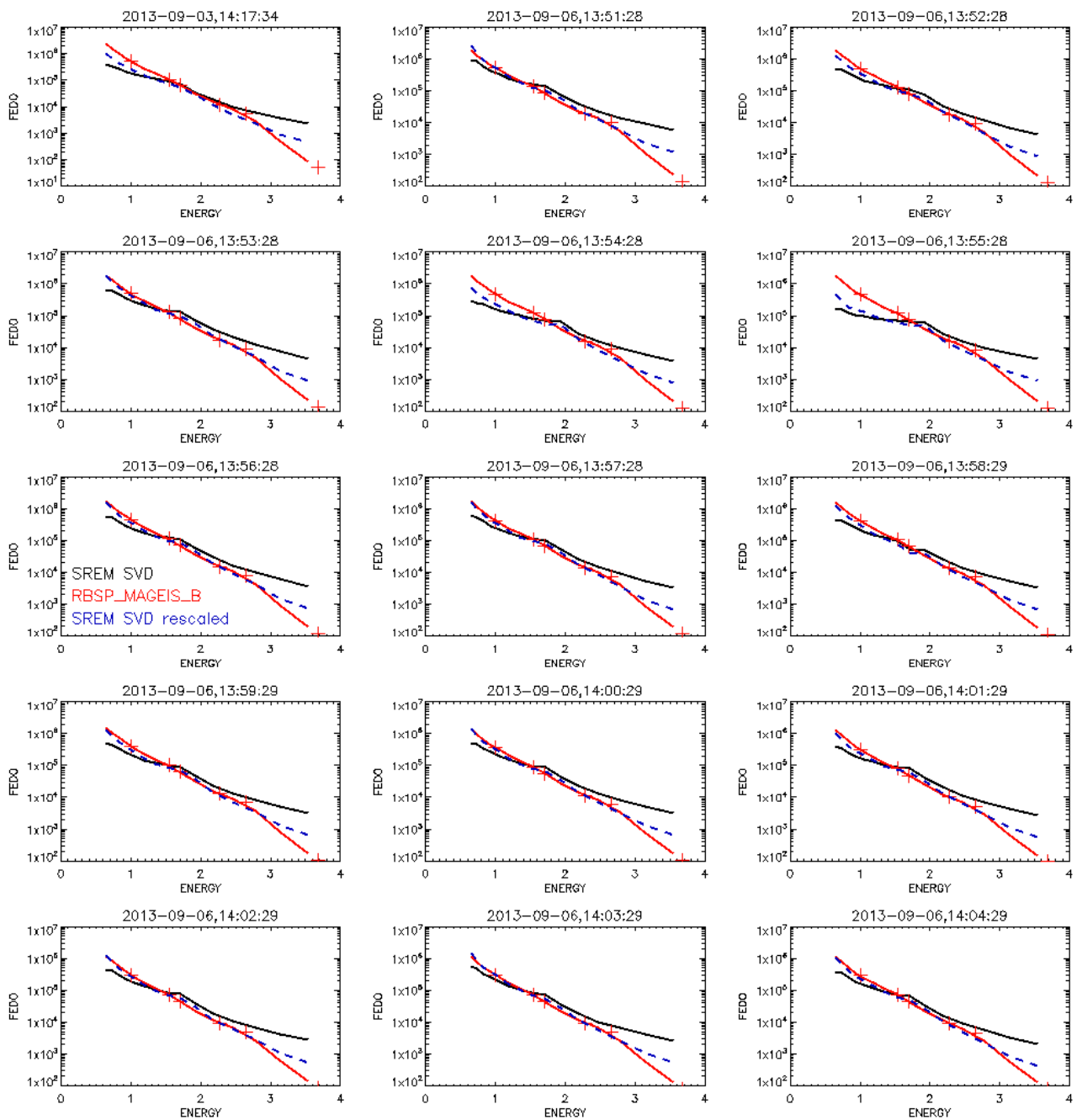


Figure C25: MAGEIS (in red) and SREM SVD (in black) differential electron flux spectra during the considered conjunctions. The red crosses denote MAGEIS data and the red line the MAGEIS data - re-binned at nominal SREM SVD electron energies – that were used for the derivation of the Scaling Factor. The blue dashed line corresponds to the re-scaled (cross-calibrated) SREM SVD spectra.

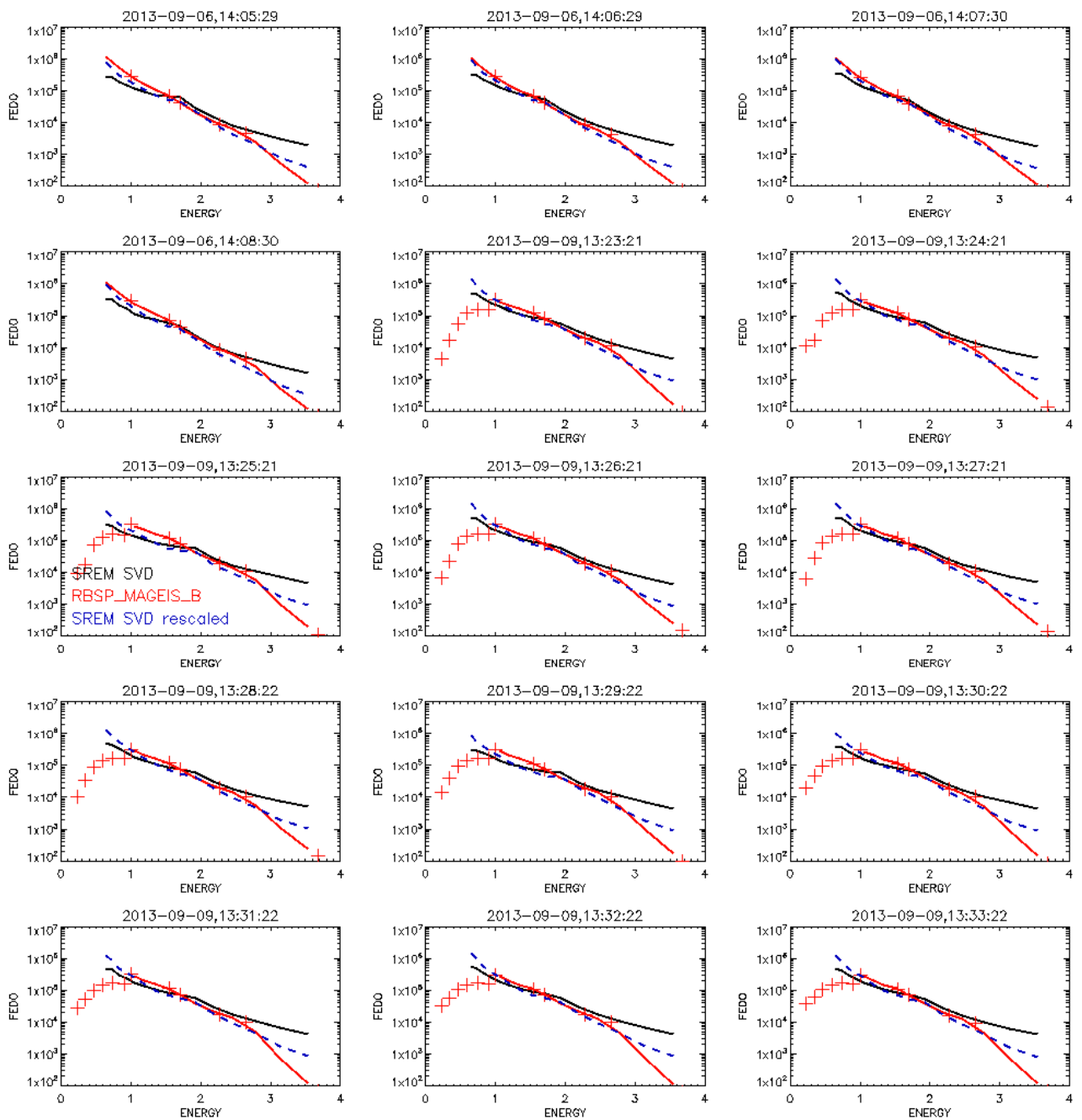


Figure C26: MAGEIS (in red) and SREM SVD (in black) differential electron flux spectra during the considered conjunctions. The red crosses denote MAGEIS data and the red line the MAGEIS data - re-binned at nominal SREM SVD electron energies – that were used for the derivation of the Scaling Factor. The blue dashed line corresponds to the re-scaled (cross-calibrated) SREM SVD spectra.

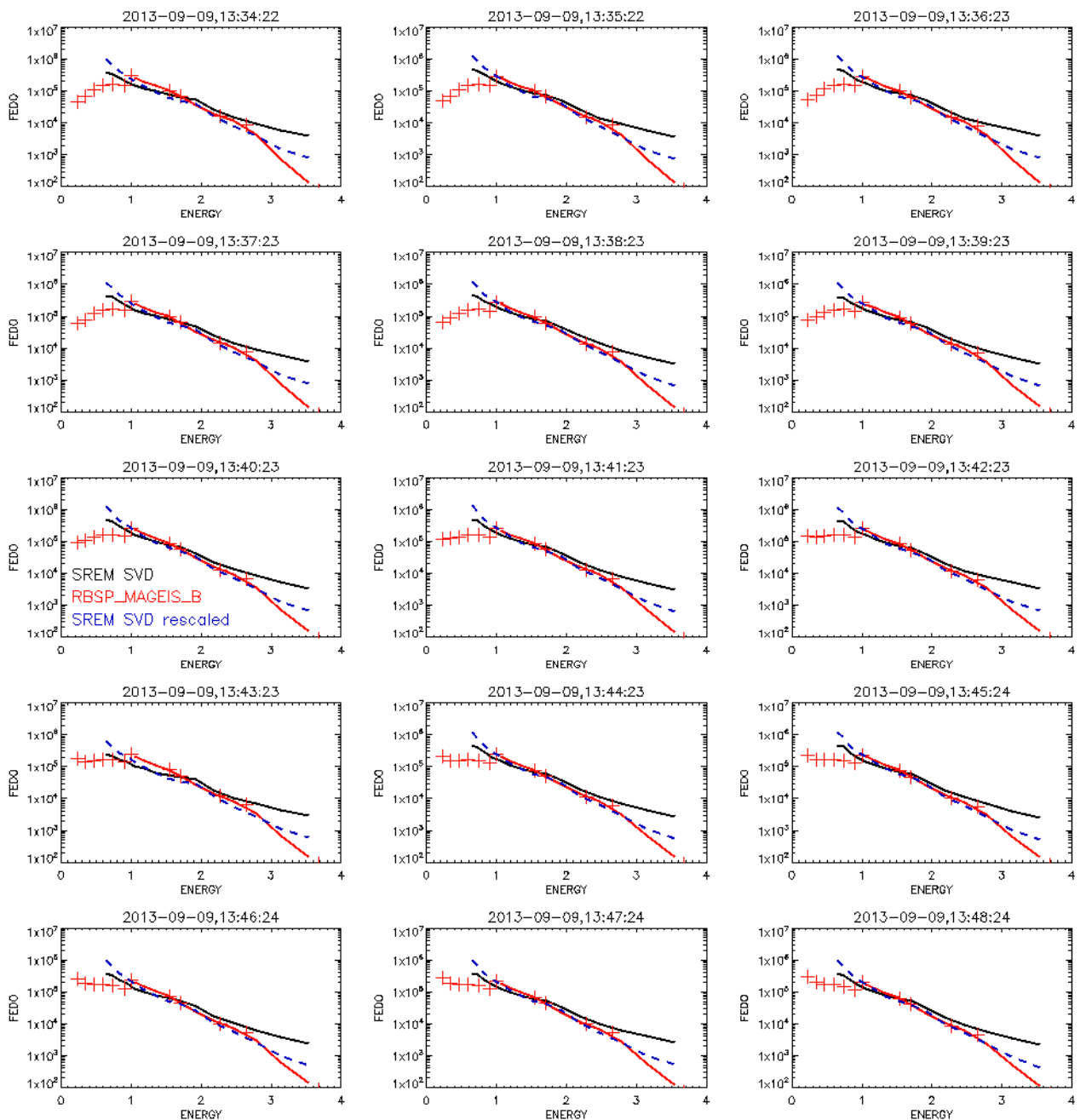


Figure C27: MAGEIS (in red) and SREM SVD (in black) differential electron flux spectra during the considered conjunctions. The red crosses denote MAGEIS data and the red line the MAGEIS data - re-binned at nominal SREM SVD electron energies – that were used for the derivation of the Scaling Factor. The blue dashed line corresponds to the re-scaled (cross-calibrated) SREM SVD spectra.

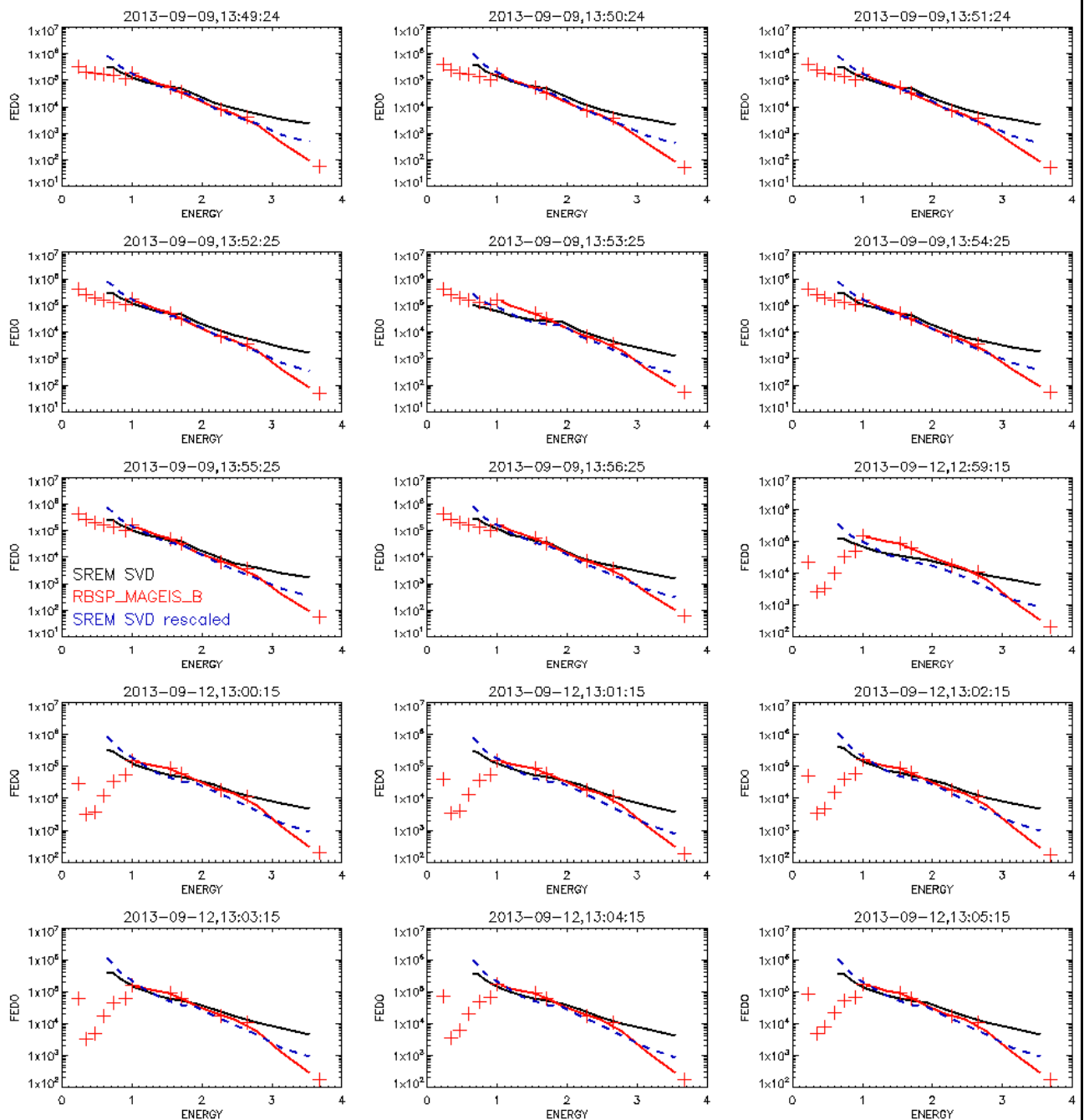


Figure C28: MAGEIS (in red) and SREM SVD (in black) differential electron flux spectra during the considered conjunctions. The red crosses denote MAGEIS data and the red line the MAGEIS data - re-binned at nominal SREM SVD electron energies – that were used for the derivation of the Scaling Factor. The blue dashed line corresponds to the re-scaled (cross-calibrated) SREM SVD spectra.

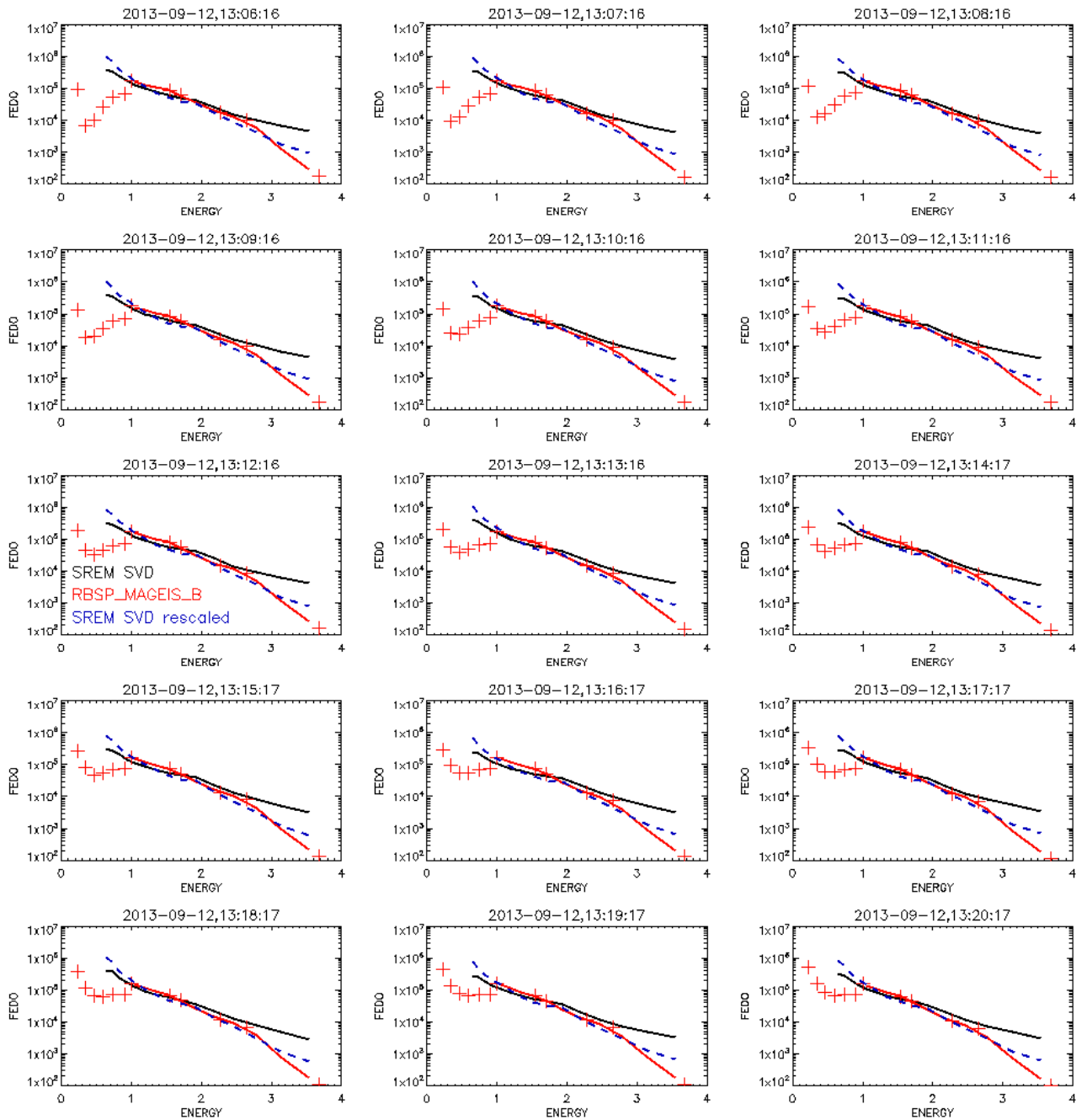


Figure C29: MAGEIS (in red) and SREM SVD (in black) differential electron flux spectra during the considered conjunctions. The red crosses denote MAGEIS data and the red line the MAGEIS data - re-binned at nominal SREM SVD electron energies – that were used for the derivation of the Scaling Factor. The blue dashed line corresponds to the re-scaled (cross-calibrated) SREM SVD spectra.

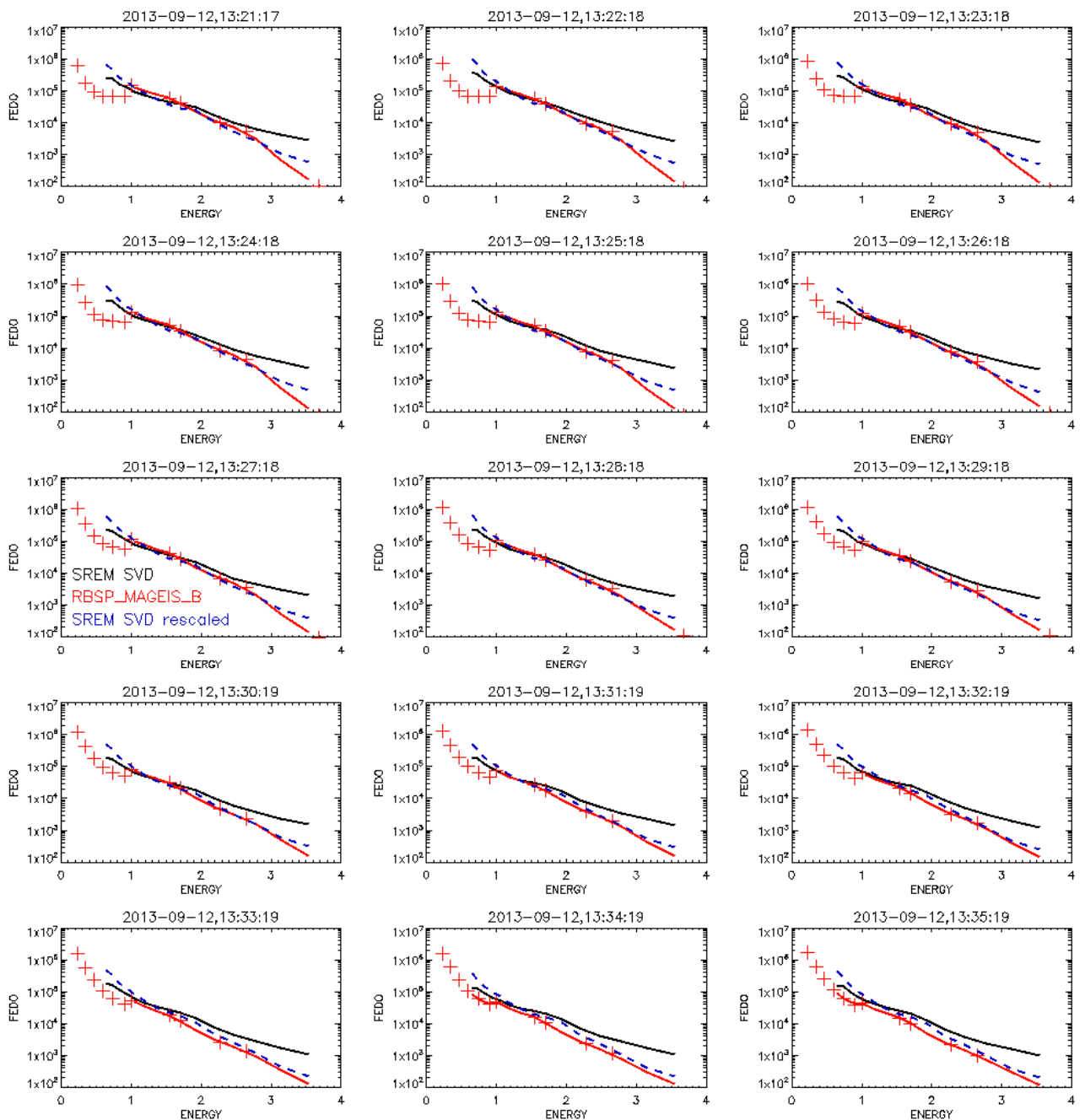


Figure C30: MAGEIS (in red) and SREM SVD (in black) differential electron flux spectra during the considered conjunctions. The red crosses denote MAGEIS data and the red line the MAGEIS data - re-binned at nominal SREM SVD electron energies – that were used for the derivation of the Scaling Factor. The blue dashed line corresponds to the re-scaled (cross-calibrated) SREM SVD spectra.

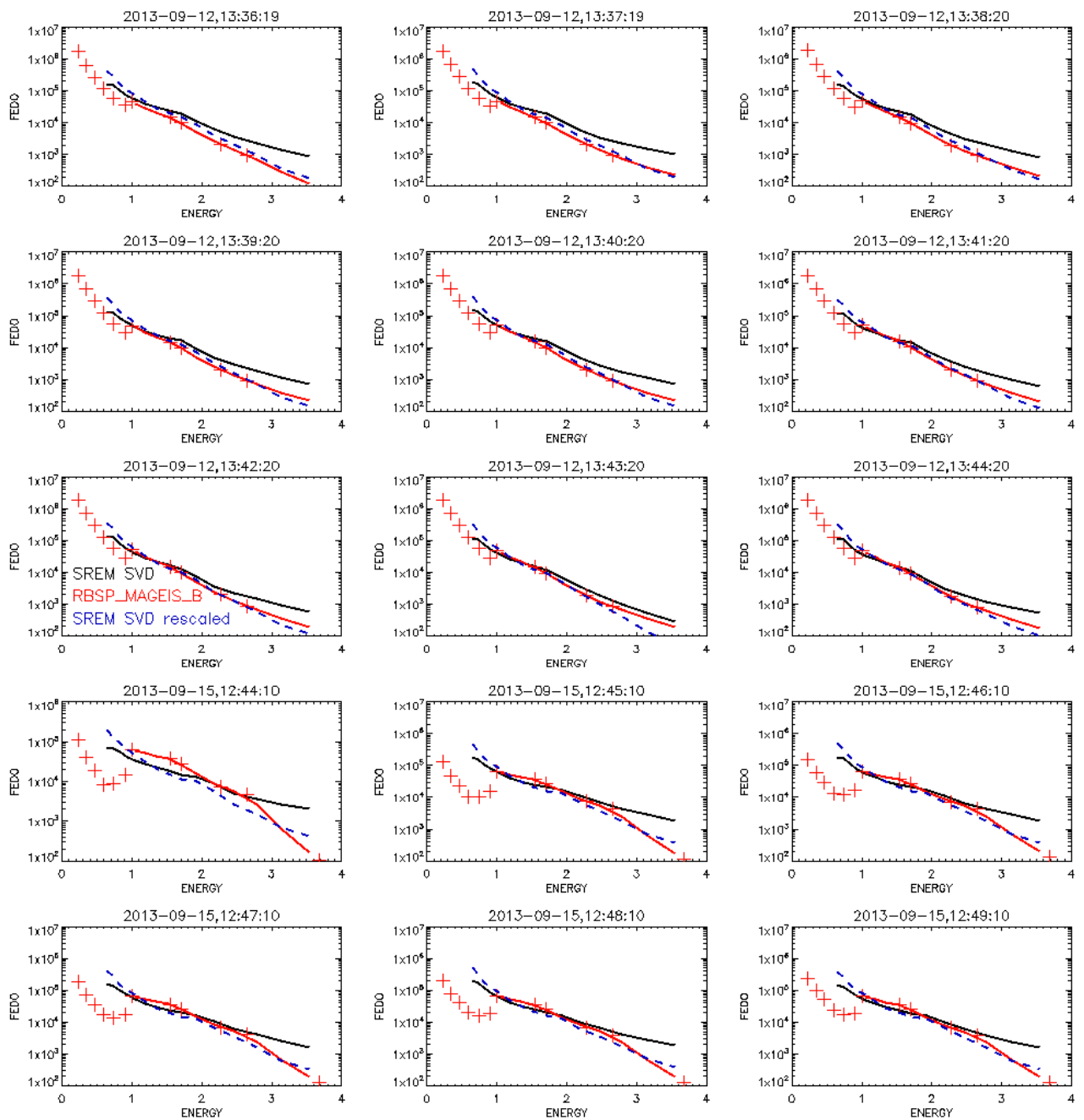


Figure C31: MAGEIS (in red) and SREM SVD (in black) differential electron flux spectra during the considered conjunctions. The red crosses denote MAGEIS data and the red line the MAGEIS data - re-binned at nominal SREM SVD electron energies – that were used for the derivation of the Scaling Factor. The blue dashed line corresponds to the re-scaled (cross-calibrated) SREM SVD spectra.

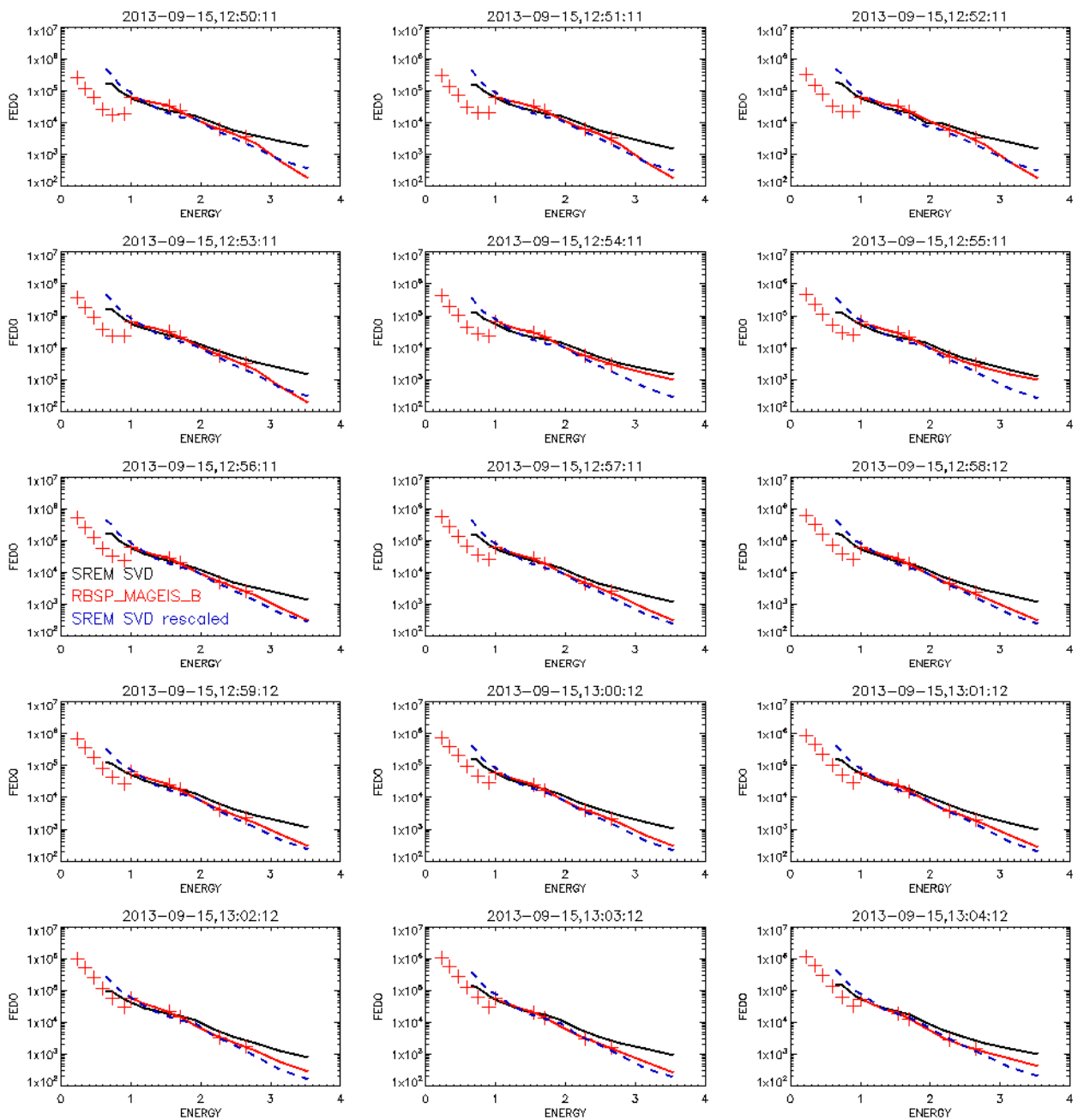


Figure C32: MAGEIS (in red) and SREM SVD (in black) differential electron flux spectra during the considered conjunctions. The red crosses denote MAGEIS data and the red line the MAGEIS data - re-binned at nominal SREM SVD electron energies – that were used for the derivation of the Scaling Factor. The blue dashed line corresponds to the re-scaled (cross-calibrated) SREM SVD spectra.

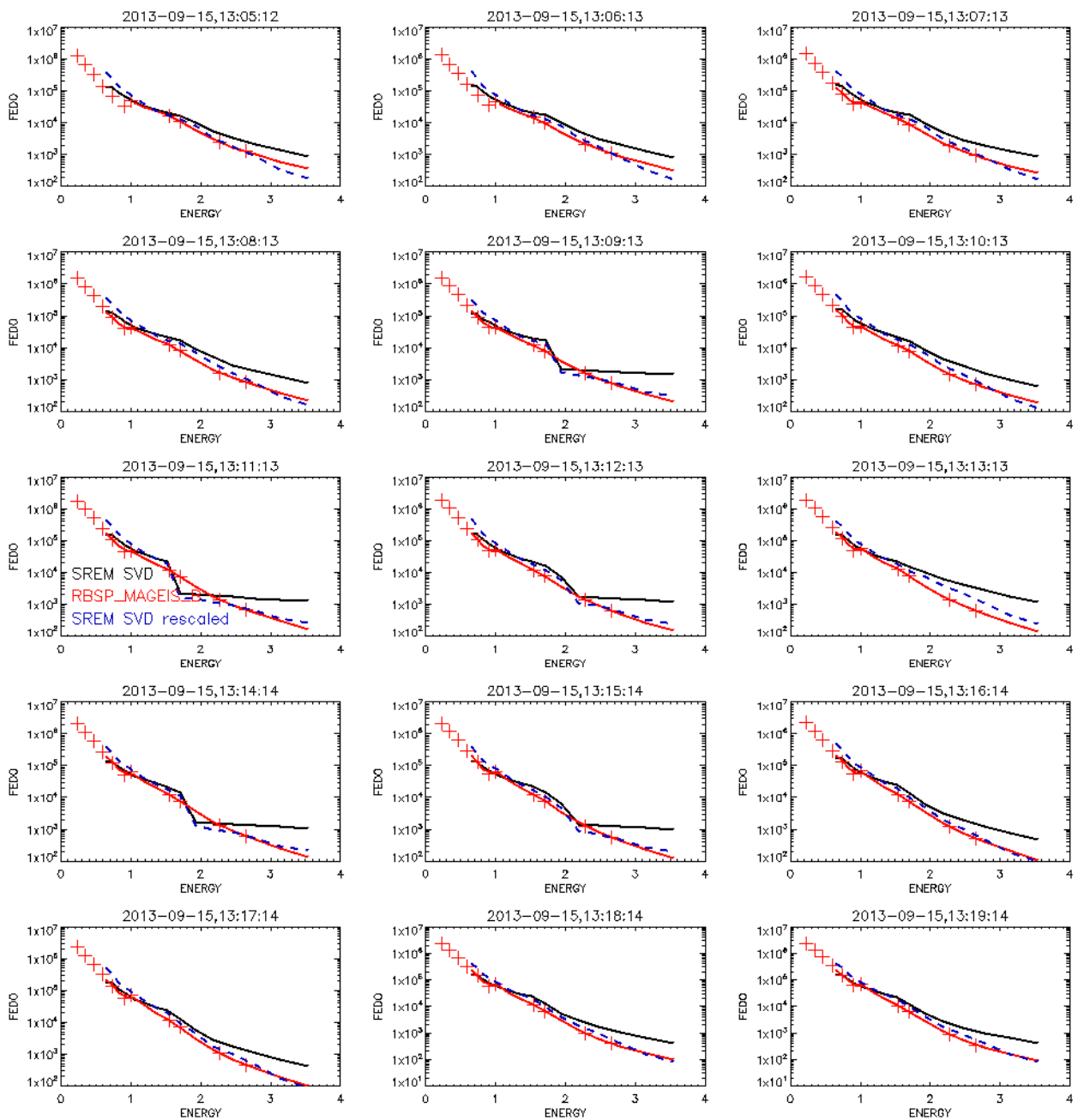


Figure C33: MAGEIS (in red) and SREM SVD (in black) differential electron flux spectra during the considered conjunctions. The red crosses denote MAGEIS data and the red line the MAGEIS data - re-binned at nominal SREM SVD electron energies – that were used for the derivation of the Scaling Factor. The blue dashed line corresponds to the re-scaled (cross-calibrated) SREM SVD spectra.

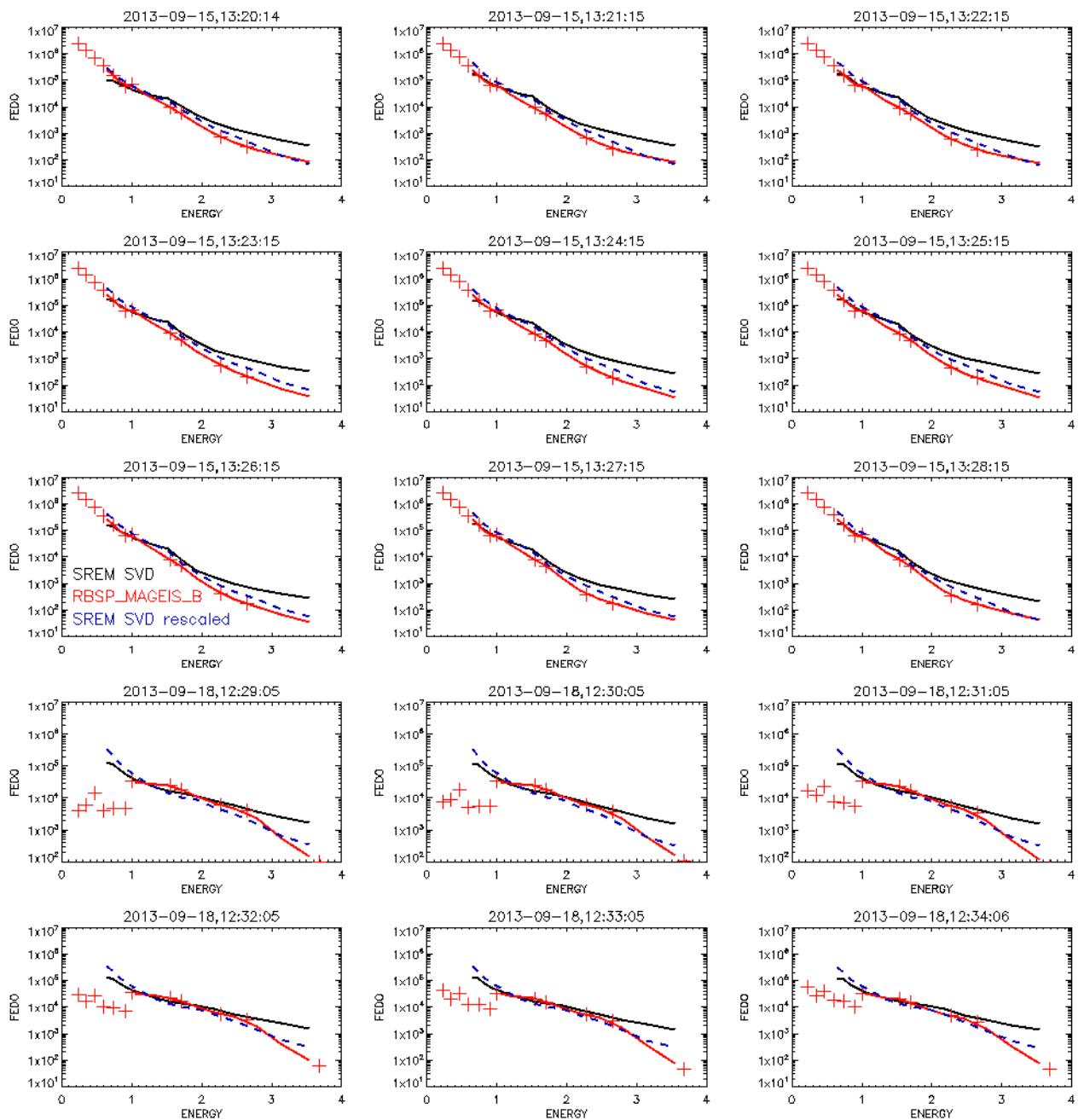


Figure C34: MAGEIS (in red) and SREM SVD (in black) differential electron flux spectra during the considered conjunctions. The red crosses denote MAGEIS data and the red line the MAGEIS data - re-binned at nominal SREM SVD electron energies – that were used for the derivation of the Scaling Factor. The blue dashed line corresponds to the re-scaled (cross-calibrated) SREM SVD spectra.

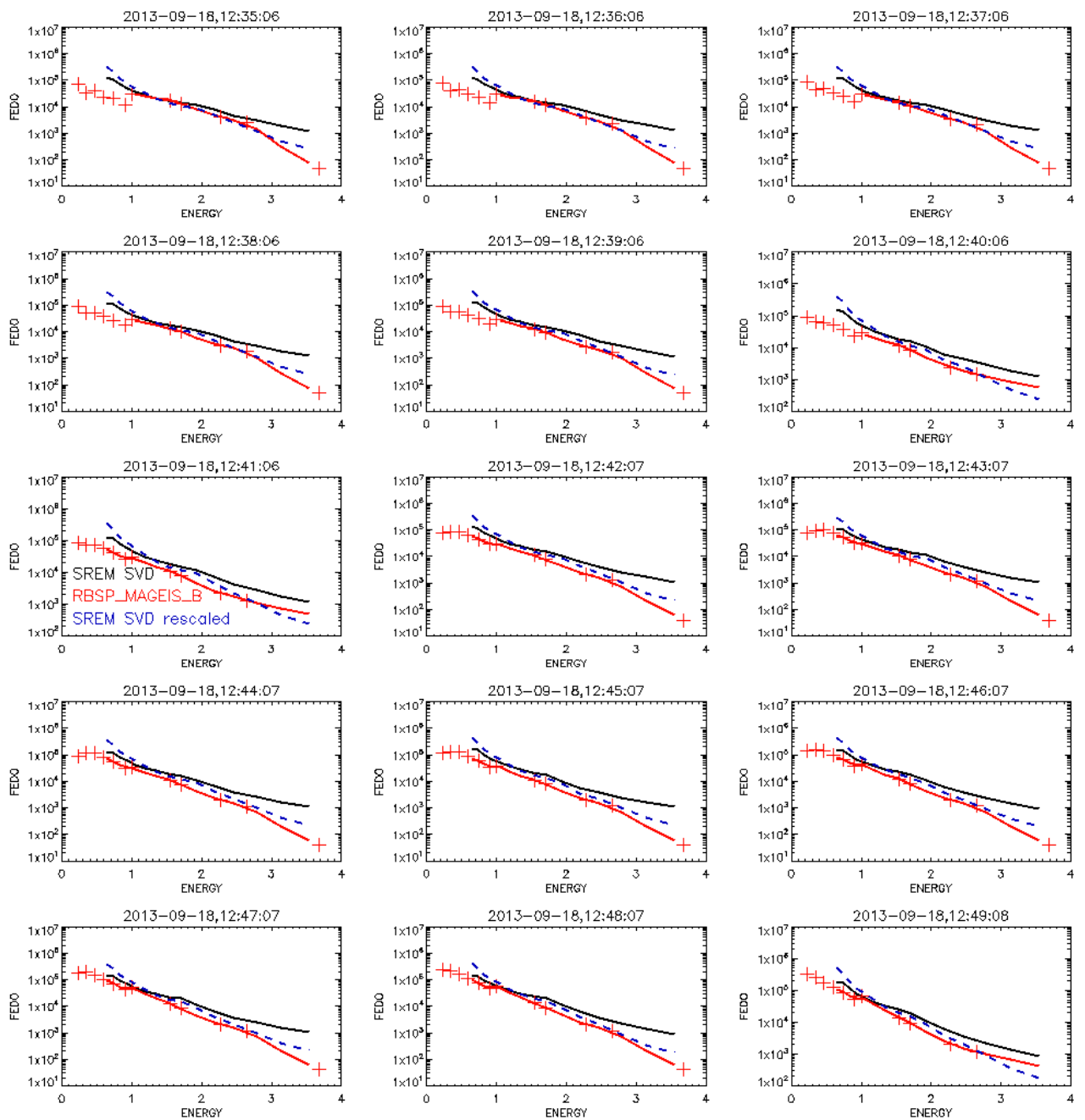


Figure C35: MAGEIS (in red) and SREM SVD (in black) differential electron flux spectra during the considered conjunctions. The red crosses denote MAGEIS data and the red line the MAGEIS data - re-binned at nominal SREM SVD electron energies – that were used for the derivation of the Scaling Factor. The blue dashed line corresponds to the re-scaled (cross-calibrated) SREM SVD spectra.

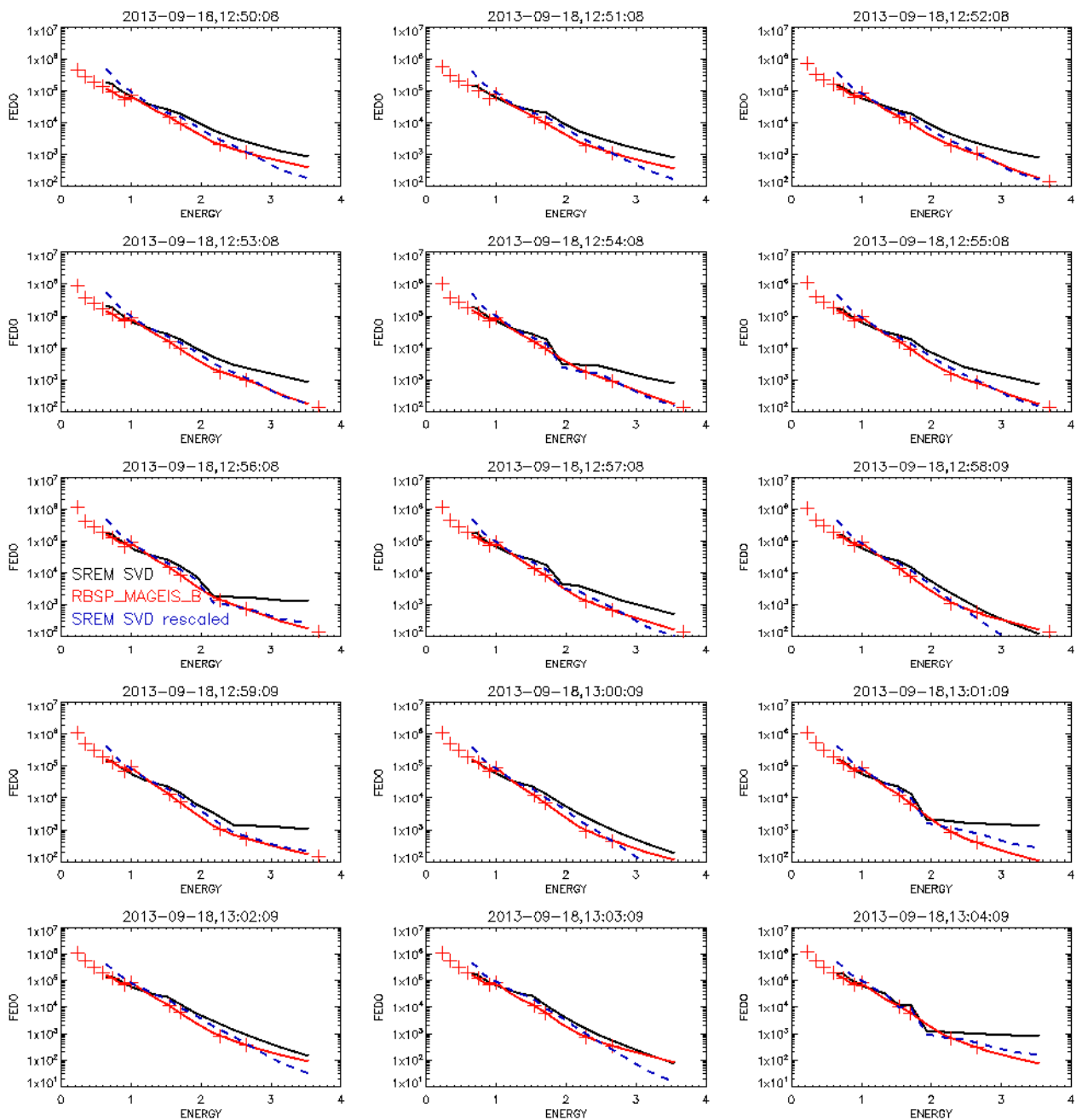


Figure C36: MAGEIS (in red) and SREM SVD (in black) differential electron flux spectra during the considered conjunctions. The red crosses denote MAGEIS data and the red line the MAGEIS data - re-binned at nominal SREM SVD electron energies – that were used for the derivation of the Scaling Factor. The blue dashed line corresponds to the re-scaled (cross-calibrated) SREM SVD spectra.

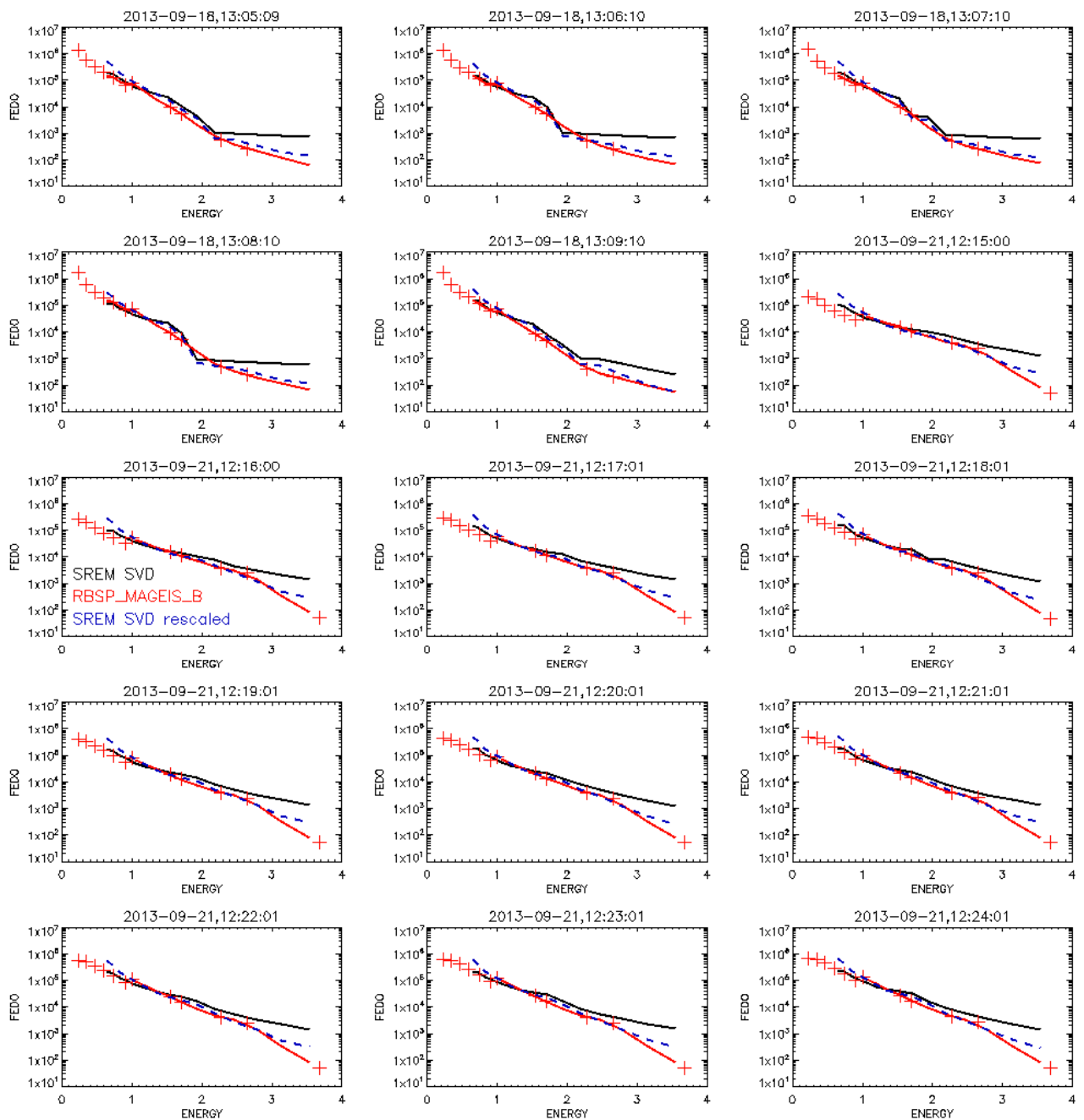


Figure C37: MAGEIS (in red) and SREM SVD (in black) differential electron flux spectra during the considered conjunctions. The red crosses denote MAGEIS data and the red line the MAGEIS data - re-binned at nominal SREM SVD electron energies – that were used for the derivation of the Scaling Factor. The blue dashed line corresponds to the re-scaled (cross-calibrated) SREM SVD spectra.

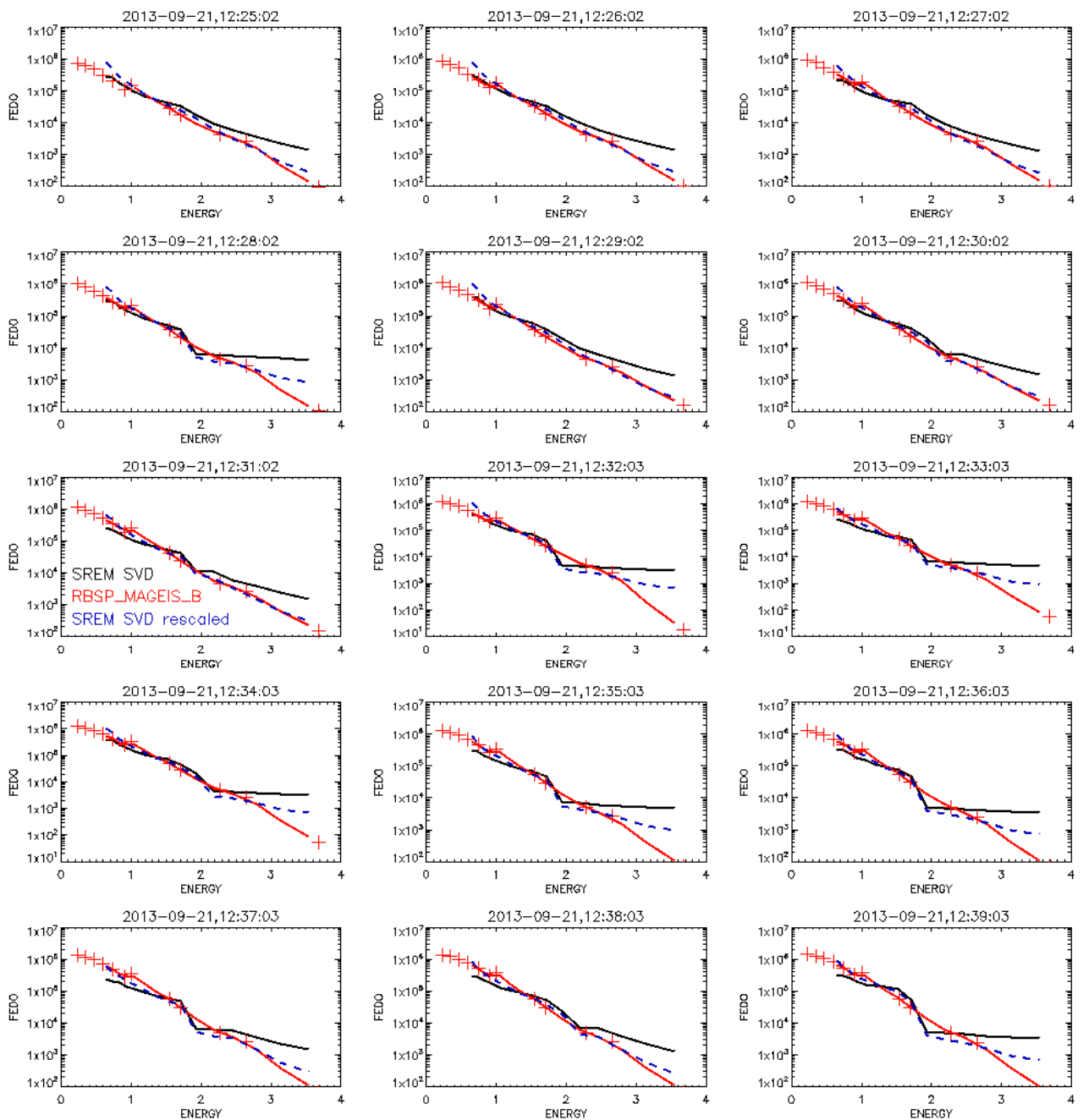


Figure C38: MAGEIS (in red) and SREM SVD (in black) differential electron flux spectra during the considered conjunctions. The red crosses denote MAGEIS data and the red line the MAGEIS data - re-binned at nominal SREM SVD electron energies – that were used for the derivation of the Scaling Factor. The blue dashed line corresponds to the re-scaled (cross-calibrated) SREM SVD spectra.

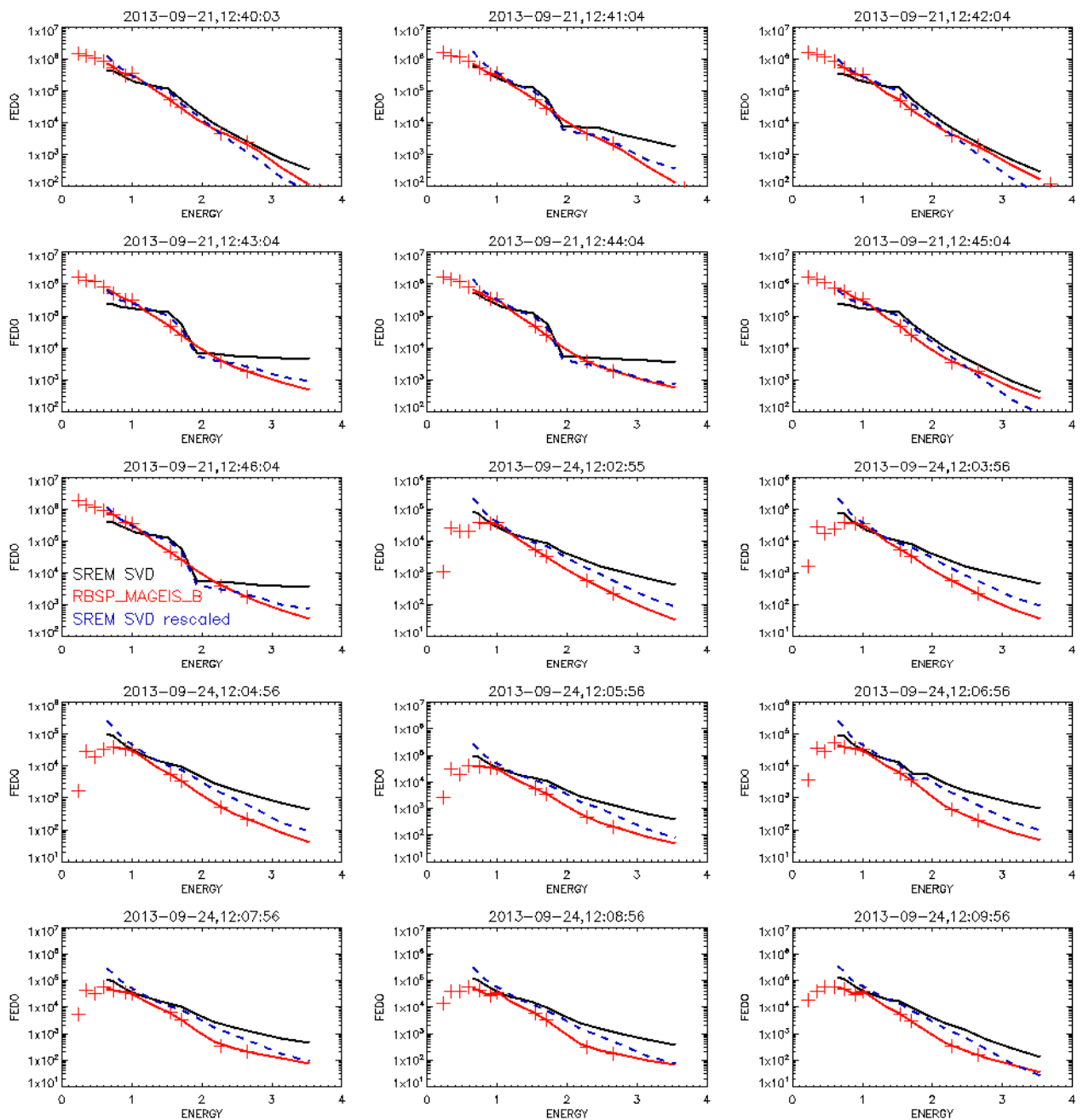


Figure C39: MAGEIS (in red) and SREM SVD (in black) differential electron flux spectra during the considered conjunctions. The red crosses denote MAGEIS data and the red line the MAGEIS data - re-binned at nominal SREM SVD electron energies – that were used for the derivation of the Scaling Factor. The blue dashed line corresponds to the re-scaled (cross-calibrated) SREM SVD spectra.

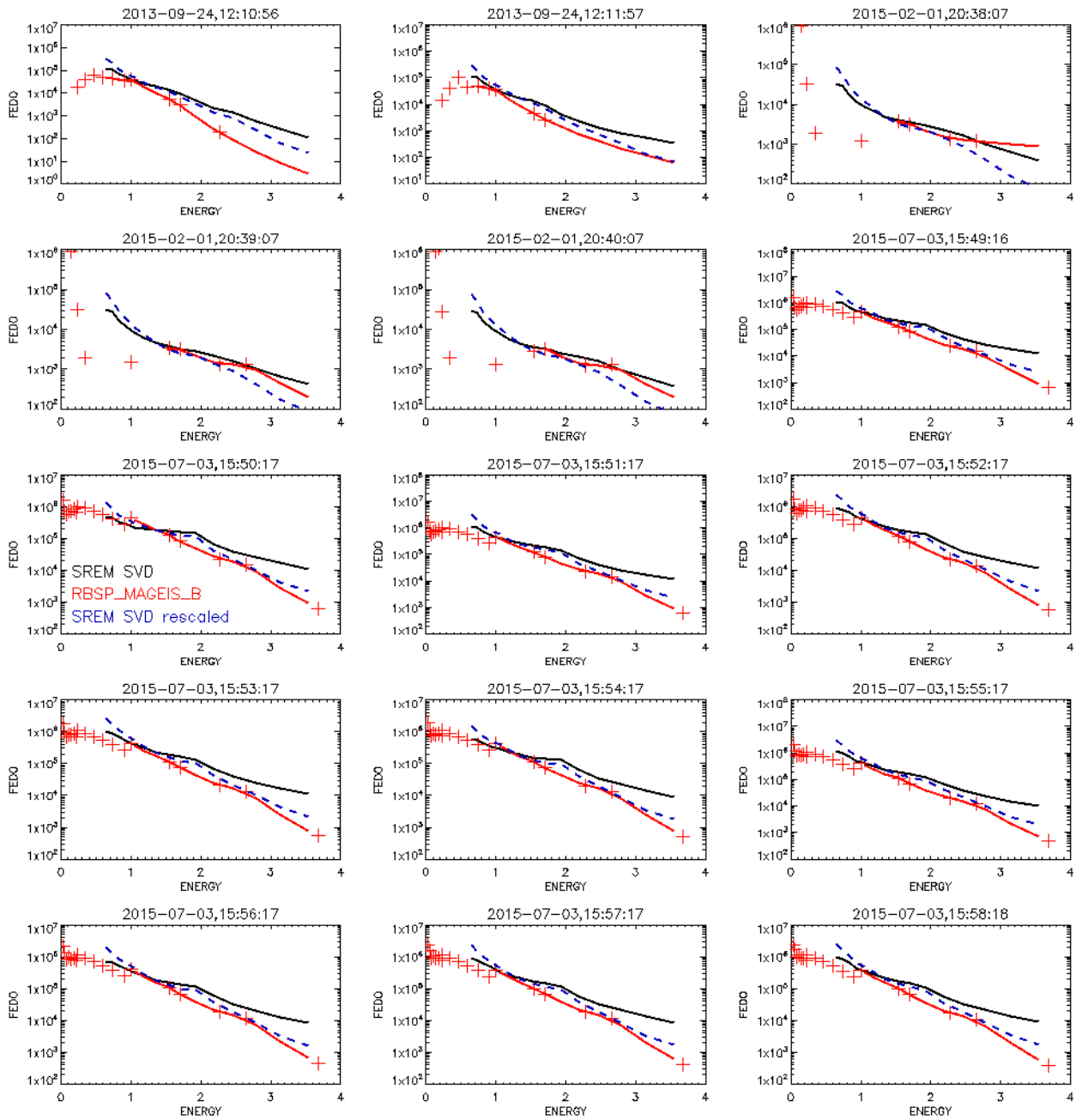


Figure C40: MAGEIS (in red) and SREM SVD (in black) differential electron flux spectra during the considered conjunctions. The red crosses denote MAGEIS data and the red line the MAGEIS data - re-binned at nominal SREM SVD electron energies – that were used for the derivation of the Scaling Factor. The blue dashed line corresponds to the re-scaled (cross-calibrated) SREM SVD spectra.

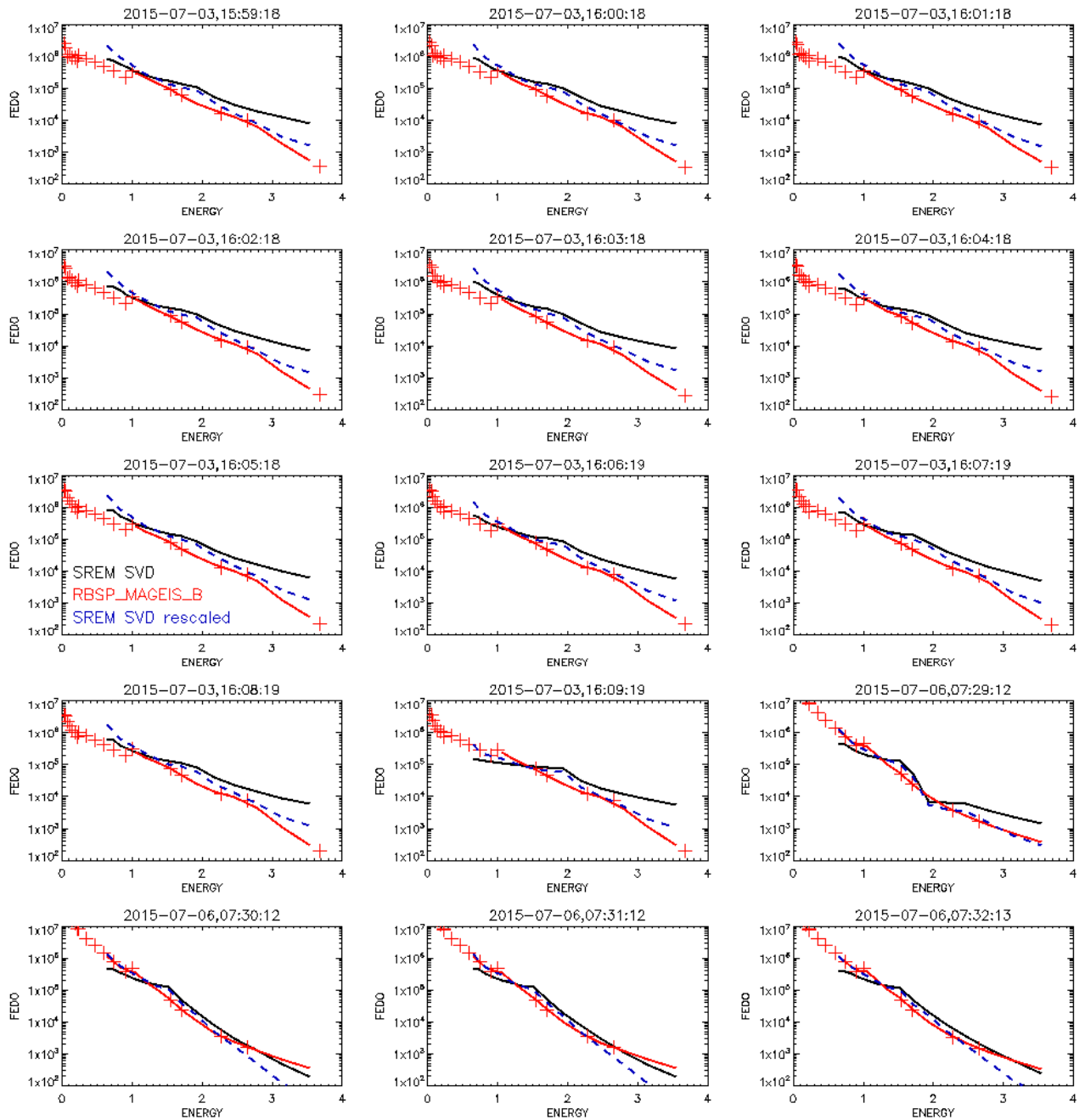


Figure C41: MAGEIS (in red) and SREM SVD (in black) differential electron flux spectra during the considered conjunctions. The red crosses denote MAGEIS data and the red line the MAGEIS data - re-binned at nominal SREM SVD electron energies – that were used for the derivation of the Scaling Factor. The blue dashed line corresponds to the re-scaled (cross-calibrated) SREM SVD spectra.

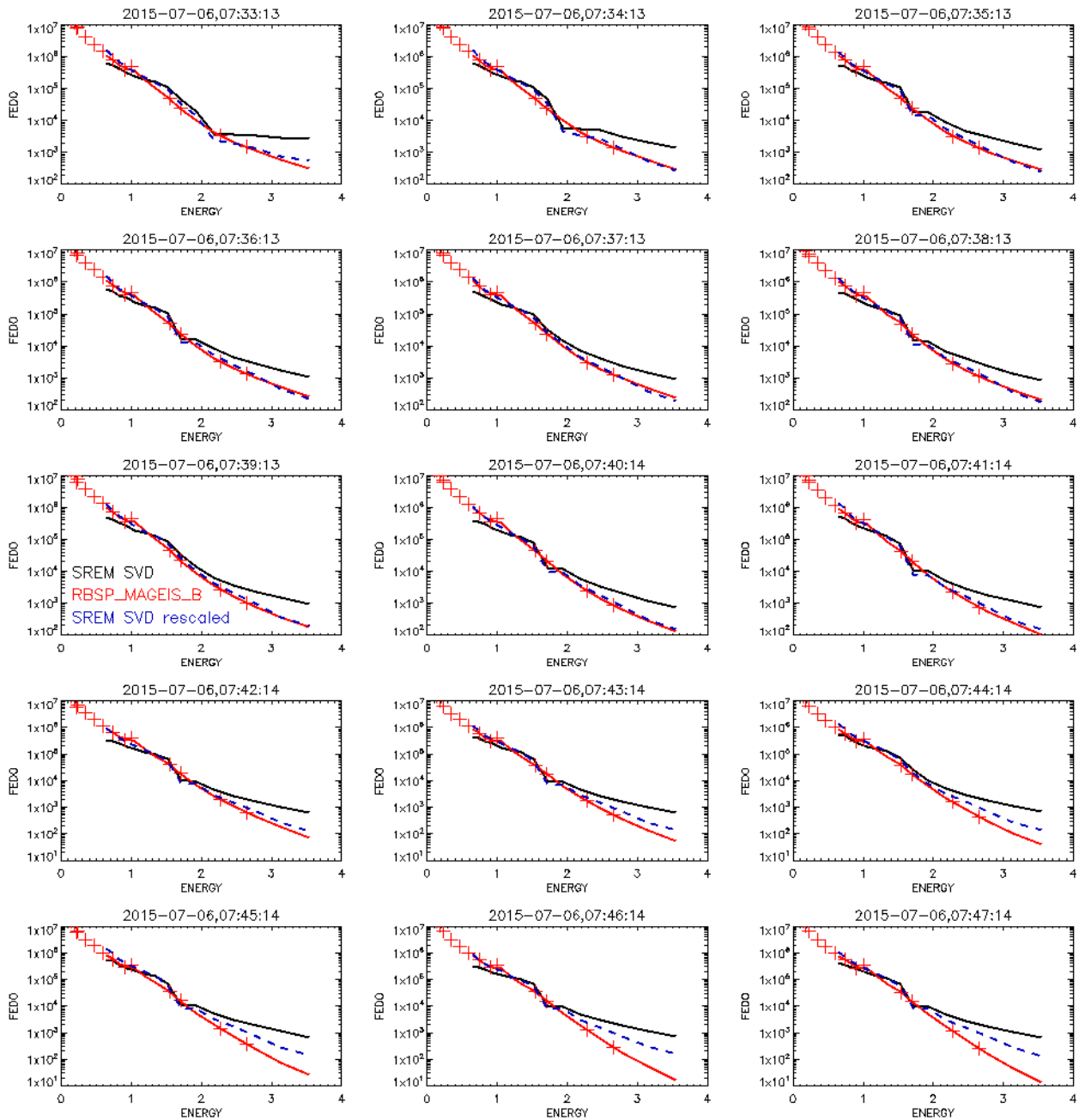


Figure C42: MAGEIS (in red) and SREM SVD (in black) differential electron flux spectra during the considered conjunctions. The red crosses denote MAGEIS data and the red line the MAGEIS data - re-binned at nominal SREM SVD electron energies – that were used for the derivation of the Scaling Factor. The blue dashed line corresponds to the re-scaled (cross-calibrated) SREM SVD spectra.

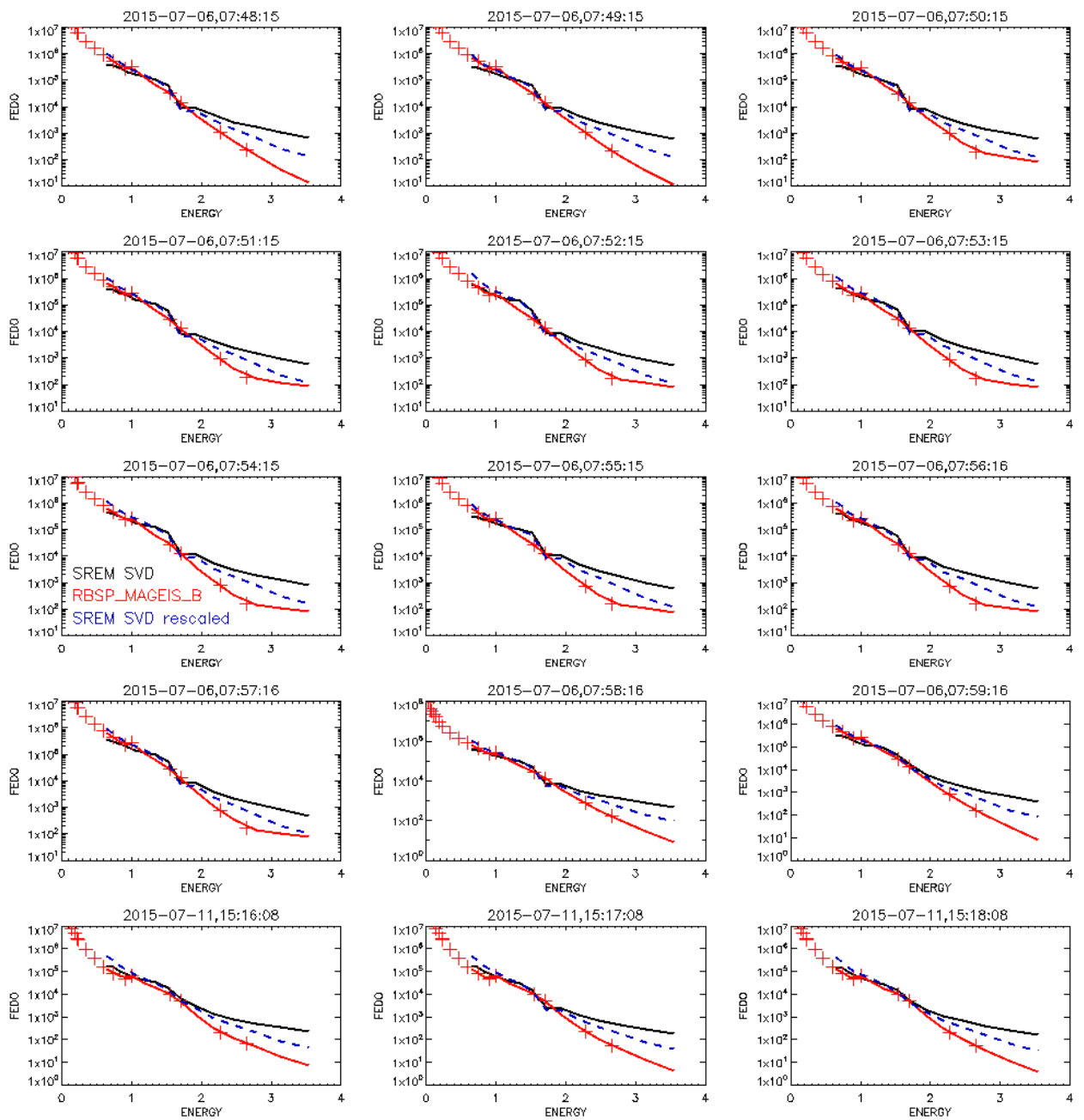


Figure C43: MAGEIS (in red) and SREM SVD (in black) differential electron flux spectra during the considered conjunctions. The red crosses denote MAGEIS data and the red line the MAGEIS data - re-binned at nominal SREM SVD electron energies – that were used for the derivation of the Scaling Factor. The blue dashed line corresponds to the re-scaled (cross-calibrated) SREM SVD spectra.

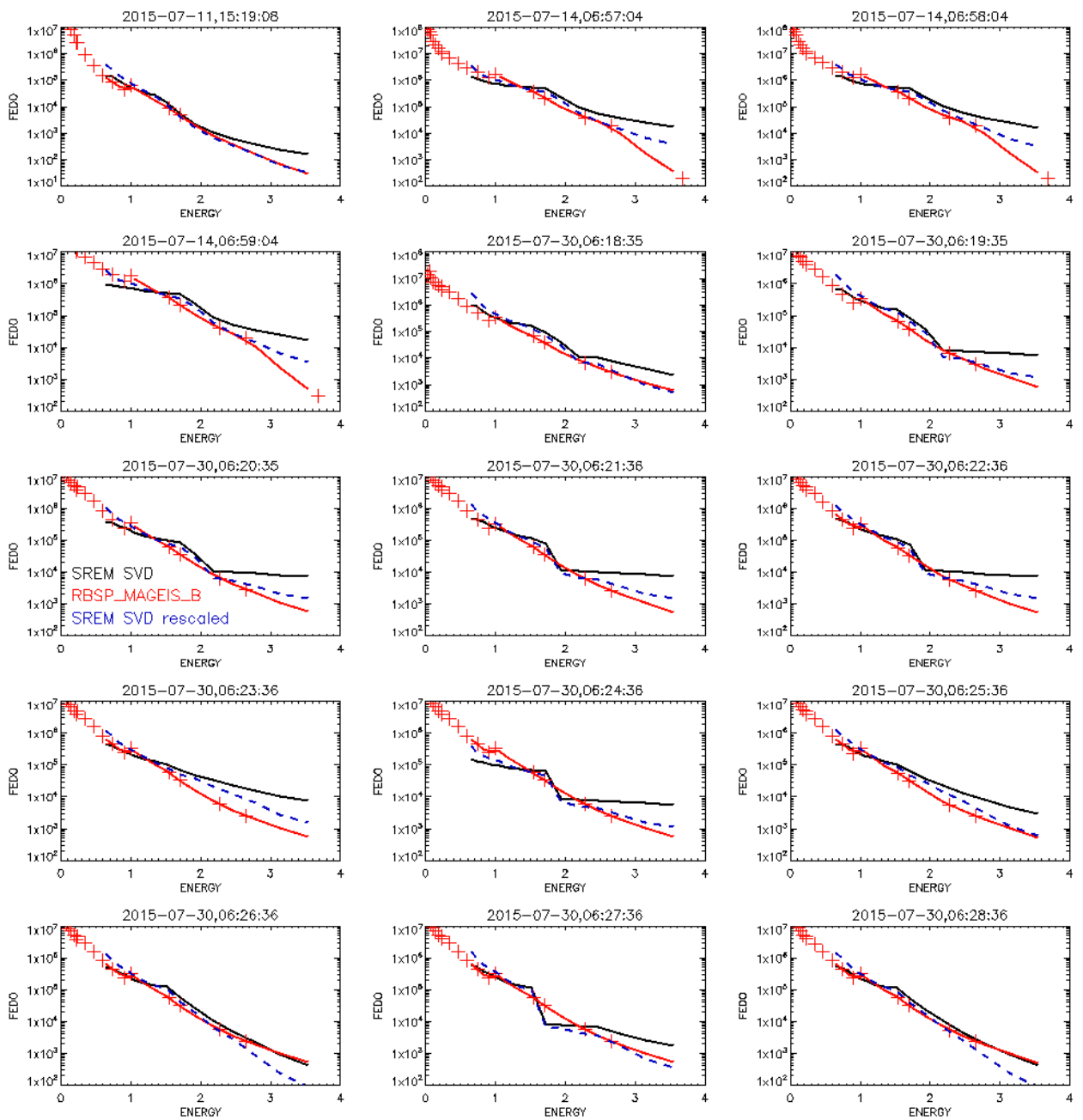


Figure C44: MAGEIS (in red) and SREM SVD (in black) differential electron flux spectra during the considered conjunctions. The red crosses denote MAGEIS data and the red line the MAGEIS data - re-binned at nominal SREM SVD electron energies – that were used for the derivation of the Scaling Factor. The blue dashed line corresponds to the re-scaled (cross-calibrated) SREM SVD spectra.

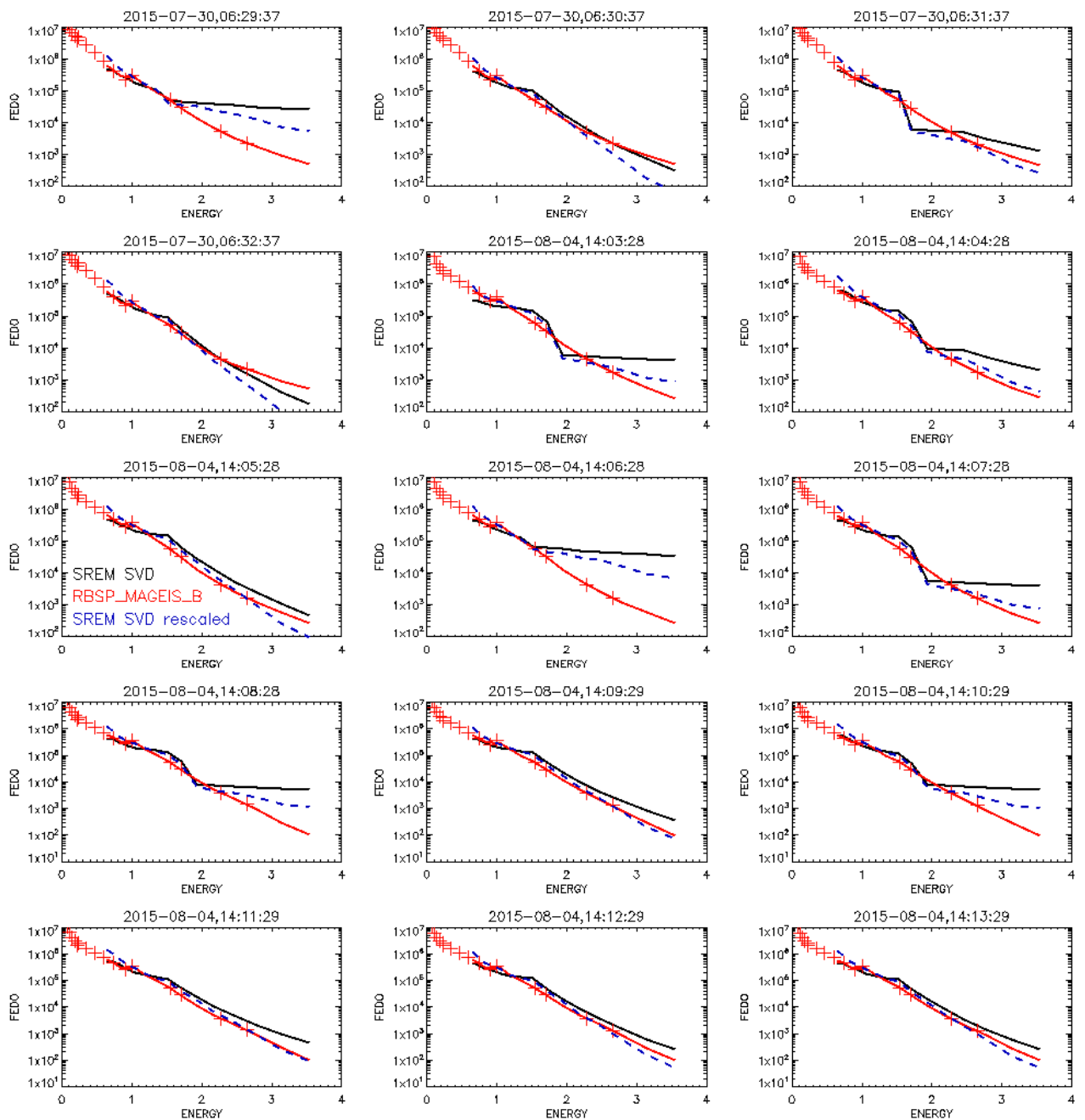


Figure C45: MAGEIS (in red) and SREM SVD (in black) differential electron flux spectra during the considered conjunctions. The red crosses denote MAGEIS data and the red line the MAGEIS data - re-binned at nominal SREM SVD electron energies – that were used for the derivation of the Scaling Factor. The blue dashed line corresponds to the re-scaled (cross-calibrated) SREM SVD spectra.

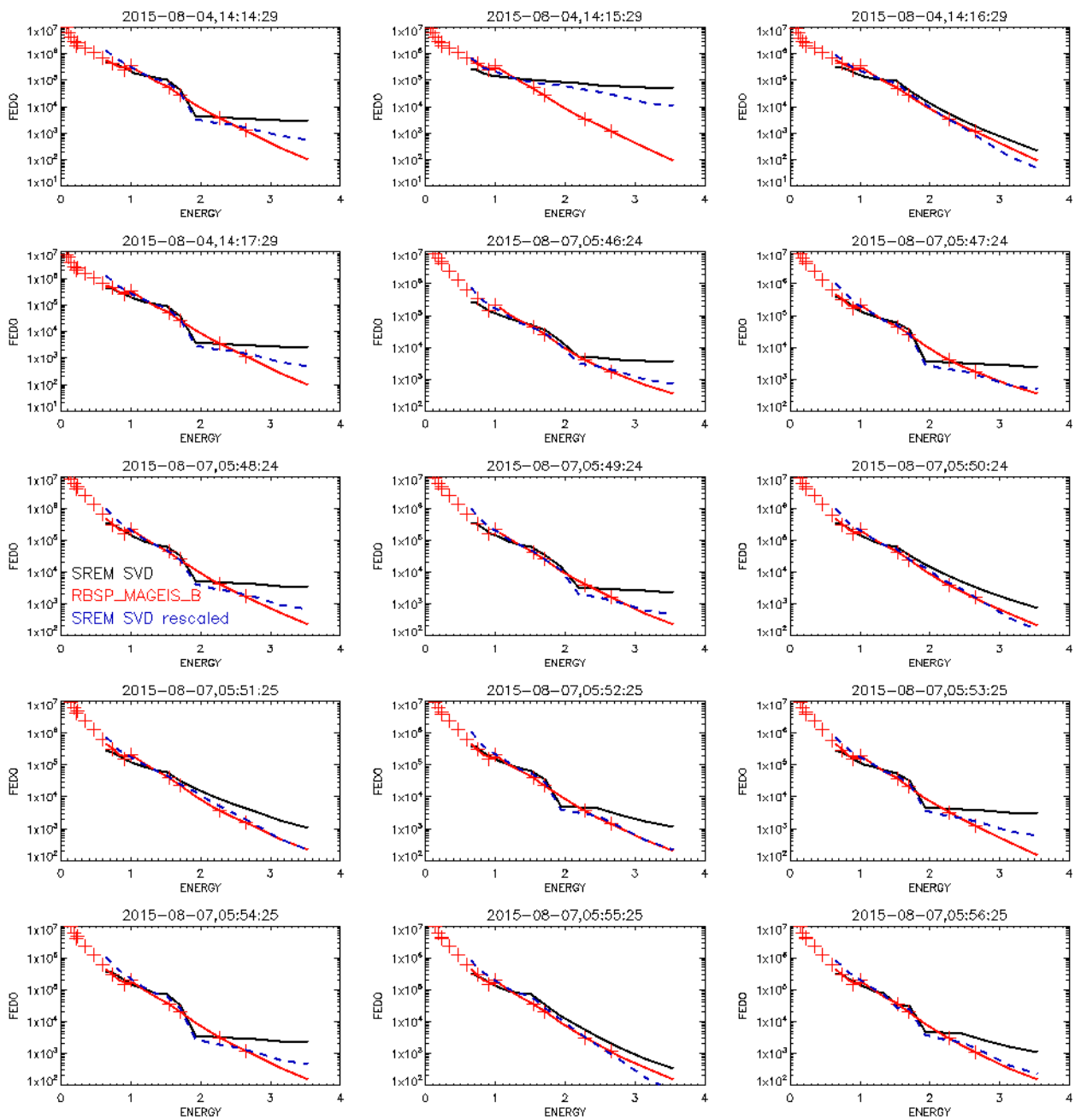


Figure C46: MAGEIS (in red) and SREM SVD (in black) differential electron flux spectra during the considered conjunctions. The red crosses denote MAGEIS data and the red line the MAGEIS data - re-binned at nominal SREM SVD electron energies – that were used for the derivation of the Scaling Factor. The blue dashed line corresponds to the re-scaled (cross-calibrated) SREM SVD spectra.

Appendix D

Technical Note 2: Lessons learned in the processing and calibration of the SREM

Strengths/weakness of the SREM design with respect to the final production of particle flux data for various species

As its name states, SREM is in the first instance a radiation monitor and not a perfect spectrometer. It was built with the goal to be light in weight, low in power consumption and nevertheless provide spectral information of the incident proton and electron fluxes. It is a successor of the REM instrument and its design must be understood as a continuous development of that device [6], [5].

Compared with REM, all parameters of the instrument which use resources of a host spacecraft could be reduced with SREM. The weight was reduced from 2.8 to 2.5 kg, the power consumption from 5 to 2 W and the size of the box containing the full detector with readout electronics was cut by half.

In both instruments, silicon detectors are used for the measurement of ionizing particles. Particles penetrating the sensitive volumes, deposit energy in the volume, which is converted into a detector signal. Silicon detectors are sensitive to electrons and ions. With a single silicon detector differentiation between electrons and ions is hence difficult, since the same signal can be produced by particles of different species and energy. To solve this problem, three silicon detectors with different shieldings are used in SREM. Electrons and protons differ in their ability to traverse material. In the energy range one is mainly concerned about for space radiation applications - of $E_e > 0.1$ MeV and $E_p > 10$ MeV – the electrons can be more easily stopped than protons. In a heavily shielded detector the detection of electrons is therefore suppressed with respect to the protons and lower energetic particles are suppressed with respect to higher energies. In SREM it is thus by combining the information of all three detectors that the resolving power for particle species and particle energy is obtained.

There are 15 SREM detector channels, which are defined according to the energy deposited in the three silicon sensors. Most of the SREM counters are mixed channels in the sense, that they are sensitive to more than one particle species. The response functions of the 15 counters as function of energy E – the probability that an incident particle of energy E is counted into a specific counter – are very broad. In an ideal detector, the response function is a delta function, such that a detection in a given counter is unambiguously related to the species and energy of the initial particle. In SREM the accumulated number of counts in a counter is not proportional to a particle flux at a fixed energy, but rather represents a weighted integral of the incident particle spectra. Thus the information obtained by SREM represents 15 differently weighted integrals of the incident particle fluxes.

One of the key ingredients to the interpretation of the detector signals is the response functions which in case of SREM have been deduced by Monte Carlo simulations including mass models of the detector and the host satellite. Implementation of mass models of satellites can be a time consuming task but should not be neglected. The shielding power of the satellite can be important and significantly alter the response of the standalone instrument. The nominal aperture of the SREM detectors e.g. is rather narrow. But high energetic particles can also penetrate from outside the aperture and reach the sensitive detector parts even after traversing satellite material. To narrow down the acceptance angle of an instrument, and with this to minimize the influence of surrounding materials, stacks of detectors can be applied and operated in coincidence. In SREM there are a few coincidence channels. But most channels rely on the signal of one detector only.

The problem of the deconvolution of SREM count-rates into particle fluxes has been discussed before [1] and shall not be repeated here. However, the process is involved and only approximate solutions can be obtained. Especially in environments with equally important contributions from electrons and protons the de-convolution is related with some uncertainties. For the deconvolution of the SREM data it is assumed that the fluxes are isotropic. The response of SREM indeed depends on the angle of incidence [8]. But the resolving power is small and response functions integrated over 4π are applied.

Nevertheless, as it is shown in Technical Note 1, despite these shortcomings, omnidirectional fluxes deduced with SREM compare well with measurements from scientific level datasets. In cases however, where fluxes are not isotropic (e.g. protons in inner radiation belt) the SREM measured fluxes might be inaccurate.

In summary it is noted, that given the applied technology (silicon detectors) and the small number of sensitive elements (3) SREM performs well in measuring simultaneously omnidirectional particle spectra of electrons and protons. This is partly related to the carefully designed detector shieldings and selection of shielding materials (Aluminum and Tungsten) and partly to the dedicated deconvolution methods developed including extensive simulations of the instrument to determine the response functions. SREM provides no angular information.

Recommendations for future radiation monitoring activities in the magnetosphere and heliosphere

7 SREM units have been operated in space aboard satellites in various different orbits. They have been given 'piggy-back' rides on the host satellites and were never considered as primary payload. Hence the hosts were not primarily selected with respect to scientific arguments but rather according to the availability of resources. SREMs were thus flying in orbits covering the Earth's radiation belts (Strv-1c, PROBA-1, GIOVE-B, Integral) but also on missions at L2 (Herschel, Planck) and a mission into deep space (Rosetta)

SREM has been built and optimized to operate in the Earth's radiation belts. It is best operated in space regions with significant fluxes of electrons and protons. It was however not designed to be good in measuring cosmic radiation. Many of the orbits into which SREMs have been launched are exclusively or during significant parts of the time outside of the radiation belts and primarily exposed to cosmic rays. That is not to say, that the SREM data from Rosetta, Herschel, and Planck are not valuable. E.g. the solar cycle variations of the cosmic rays can be nicely traced with this data. In addition, solar proton fluxes measurements away from 1 AU may provide significant information regarding the propagation of solar protons. But for such missions a radiation monitor with better detection characteristics for cosmic rays would certainly be more suited.

In the magnetosphere the high energetic charged particles trapped in the radiation belts are the primary source of radiation hazards for space born missions. The outer radiation belt is notoriously difficult to map due to the large and rapid temporal and spatial variations of the trapped electron fluxes. Measurements at one point do not easily allow the prediction of radiation levels in other places. Thus multi-point observations would be desirable, as many as possible. However with - let's say - 4 monitors placed in orbits covering the outer radiation belt at different latitudes (one at the equator and the other ones in equal steps at higher latitudes) would allow to continuously map the outer belt with some time resolution in B and L. Such data could be used to study the dynamics of the radiation belts and to update/improve radiation belt modeling activities.

The inner radiation belt is far more stable than the outer electron belt. This is especially true for the protons which vary only on yearly time scales. The electron population can differ largely at different points in time. However the changes are slower than in the outer radiation belt. The challenge in this case is the measurement and evaluation of the trapped protons flux anisotropy and the extraction of both proton and electron fluxes from simultaneous measurements. A detailed measurement of the anisotropy seems challenging and probably calls for a dedicated mission with a satellite carrying an instrument with enhanced angular resolution or several radiation instruments with different viewing angles. The concurrent occurrence of electrons and protons leads to contamination in detector channels by either particle species which – if not properly treated – can lead to false measurements. In order to solve this properly, an instrument with effective particle separation over a large energy range is needed.

For radiation monitoring and the study of the ionizing particle populations in the magnetosphere and heliosphere a combination of missions with dedicated instruments and missions with simpler, monitoring like instruments seems suitable. Only with light and economical instruments a long-term continuous monitoring of the space radiation environment is feasible.

